Nemanja M. Zdravkovic

Performance analysis for industrial wireless networks

Thesis for the Degree of Philosophiae Doctor

Trondheim, June 2017

Norwegian University of Science and Technology
Faculty of Information Technology and Electrical Engineering
Department of Electronic Systems

NTNU
Norwegian University of
Science and Technology

NTNU
Norwegian University of Science and Technology

Thesis for the Degree of Philosophiae Doctor

Faculty of Information Technology and Electrical Engineering
Department of Electronic Systems

ISBN 978-82-326-2200-9 (printed ver.)
ISBN 978-82-326-2201-6 (electronic ver.)
ISSN 1503-8181

IMT-report 2017:64

Doctoral theses at NTNU, 2017:64

Printed by NTNU Grafisk senter

Norwegian University of Science and Technology
Faculty of Information Technology
and Electrical Engineering

University of Niš
Faculty of Electronic Engineering

Nemanja M. Zdravković

Performance analysis for industrial wireless networks

Thesis for the degree of Philosophiae Doctor

Norwegian University of Science and Technology
Faculty of Information Technology and
Electrical Engineering
Department of Electronic Systems

Thesis for the degree of Doctor of Science

University of Niš
Faculty of Electronic Engineering
Department of Telecommunications

This thesis is the result of the project "Norwegian, Bosnian, and Serbian cooperation platform for university and industry ICT R&D – NORBAS".

Trondheim, June 2017

Norveški univerzitet za nauku i tehnologiju
Fakultet informacionih tehnologija i elektrotehnike

Univerzitet u Nišu
Elektronski fakultet

Nemanja M. Zdravković

Analiza performansi za industrijske bežične mreže

Doktoska disertacija

Norveški univerzitet za nauku i tehnologiju
Fakultet informacionih tehnologija i elektrotehnike
Katedra za elektronske sisteme

Doktoska disertacija

Univerzitet u Nišu
Elektronski fakultet
Katedra za telekomunikacije

Ova disertacija je rezultat projekta "Norwegian, Bosnian, and Serbian cooperation platform for university and industry ICT R&D – NORBAS".

Trondhajm, jun 2017

"We will always be so much more human than we wish to be."

– *Daniel Gildenlöw*

Thesis data

Supervisors:
Professor Kimmo Kansanen, Norwegian University of Science and Technology (NTNU),
Faculty of Information Technology and Electrical Engineering,
Department of Electronic Systems
Professor Goran T. Đorđević, University of Niš, Faculty of Electronic Engineering,
Department of Telecommunications

Title:
Performance analysis for industrial wireless networks

Abstract:
Industrial wireless networks operate in harsher and noisier environments compared to traditional wireless networks, while demanding high reliability and low latency. These requirements, combined with the constant need for better coverage, higher data rates and overall seamless user experience call for a paradigm shift in communication in regards to the previous generations of technologies used. Cooperative diversity is one such approach.

The main focus of this thesis is on the performance analysis of cooperative wireless networks set in industrial environments – where the network, apart from additive white Gaussian noise, is subject to multipath fading and shadowing, and/or temporary random blockage effects. In these scenarios, in order to achieve specific performance metrics such as error rates or outage probabilities, existing cooperative strategies are aided by protocols in the channel between the cooperating nodes. Moreover, pair-wise analysis investigates the correlation of multiple data flows.

Building upon existing repetition protocols, outage performance of a network subject to fading and shadowing is observed, and the effects of fading and shadowing severity, network dimension, average signal-to-noise ratio values and packet length are discussed. Special cases are also observed, in which the composite fading channel is reduced to several familiar propagation environments, unifying the analysis.

Afterwards, the analysis of more complex protocols is presented, taking into account

random blockage in the channels between cooperating nodes. A novel, threshold-based internode protocol is introduced, which improves performance by listening to the transmissions and choosing whether to send a packet immediately or after a waiting period. As these two periods are close, the effect of temporal correlation is also investigated. Apart from the exact outage probability expressions, simpler asymptotic expressions, with and without blockage, are derived as well, giving a better insight on the network behaviour at high average signal-to-noise ratio regimes.

Both outage probability and packet error rate can be also improved by adding automatic repeat request schemes in the channel between cooperating nodes, which again utilize the internode channels by re-sending data until it can be successfully decoded. Error-free communication can be achieved, but at a delay cost. Nevertheless, a trade-off between performance gains and delays remains, and can therefore be used for designing wireless networks with different requirements – error-free or low-latency.

Finally, joint outage performance is investigated. Using a generic approach, which can be applied to any sort of data where multiple sources are communicating over wireless networks, pair-wise behaviour is investigated. As a result, any multi-route diversity type of scheme will have this sort of behaviour, since particular point-to-point relay links are being shared by source nodes. This in turn means that the performance of those flows will be correlated. For higher layers, there is a difference in the behaviour, meaning that when errors are correlated, data flows start behaving correlated as well. As a result, negative acknowledgements may start to correlate as well. All of this contributes to the network behaving in a correlated way, i.e., when something happens, it tends to happen to more than one data flow.

Scientific Field:
Electrical Engineering and Computer Science
Scientific Discipline:
Telecommunications
Keywords:
cooperative communications, decode-and-forward relaying, error rate analysis, fading channels, outage probability, shadowing, wireless networks
UDC:
(621.391+621.395.38):519.724
CERIF Classification:
T180

Podaci o doktorskoj disertaciji

Menotri:
Prof. dr Kimmo Kansanen, Norveški univerzitet za nauku i tehnologiju (NTNU),
Fakultet informacionih tehnologija i elektrotehnike,
Katedra za elektronske sisteme
Prof. dr Goran T. Đorđević, Univezitet u Nišu, Elektronski fakultet,
Katedra za telekomunikacije

Naslov:
Analiza performansi za industrijske bežične mreže

Rezime:
Industrijske bežične mreže zahtevaju rad u težim i bučnijim uslovima u odnosu na tradicionalne bežične mreže, dok takođe zadržavaju zahteve visoke pouzdanosti i malog kašnjenja. Ovi zahtevi, zajedno sa konstantnom potrebom za većim propusnim opsegom, boljom pokrivenošću, većom brzinom prenosa podataka i generalno boljom i neprekidnom vezom poziva na promenu paradigme u komunikaciji u odnosu na tehnologije ranijih generacija. Kooperativni diverziti predstavlja jedan pristup kojim je to moguće postići.

Glavna tema ove disertacije jeste analiza performansi kooperativnih bežičnih mreža smeštenih u industrijskom okruženju – gde je mreža, pored aditivnog Gausovog šuma podložna i fedingu usled višestruke propagacije, efektima senki i/ili privremenim slučajnim efektima blokade. U ovakvim scenarijima, da bi se postigle određene perfomanse, izražene preko verovatnoće greške ili verovatnoće prekida, postojećim kooperativnin strategijama pomažu i protokoli u kanalu između kooperirajućih čvorova. Takođe, analiza para čvorova govori nam o korelaciji više tokova podataka.

Polazeći od postojećih protokola koji koriste ponavljanje paketa, posmatra se verovatnoća prekida čvora u bežičnoj mreži koja je podložna efektima fedinga i senki, i istražuje se uticaj efekata dubine fedinga i senke, dimenzije mreže, srednjeg odnosa signal-šum, kao i dužine paketa na verovatnoću prekida. Posmatraju se takođe i specijalni slučajevi, kada se kompozitni feding kanal svodi na nekoliko poznatih propagacionih modela, i na taj način se analiza upotpunjuje.

Nakon toga, predstavljena je analiza kompleksnijeg protokola, koja uzima u obzir blokadu u kanalu između kooperirajućih čvorova. Uveden je novi protokol u komunikaciji između čvorova baziran na pragu odlučivanja, koji poboljšava performanse tako što osluškuje kanal, i na osnovu stanja kanala šalje svoj paket ili odmah, ili posle čekanja. Budući da su ova dva vremenska intervala bliska, efekat vremenske korelacije je takođe razmatran. Pored izvedenih tačnih izraza za verovatnoću prekida, jednostavniji asimptotski izrazi su takođe izvedeni za slučajeve sa i bez blokade, dajući bolji uvid u ponašanje mreže u režimu velikog odnosa signal-šum.

Performanse kao što su verovatnoća prekida i verovatnoća greške po paketu se takođe mogu poboljšati uvođenjem procedura automatske retransmisije, tako što se u kanalu između čvorova ponovo šalju paketi dok se uspešno ne dekoduju. Komunikacija bez greške se može ostvariti ali po ceni većeg kašnjenja. U svakom slučaju, kompromis između performansi i kašnjenja se može ostvariti, i može se iskoristiti za projektovanje bežičnih mreža različitih namena – mrežama sa komunikacijom bez grešaka ili sa malim kašnjenjem.

Konačno, istražena je istovremena verovatnoća prekida više čvorova. Koristeći jednostavan pristup koji se može primeniti na bilo koji tip komunikacije sa više čvorova unutar bežične mreže, istraženo je ponašanje grupe od dva čvora. Bilo koji tip diverziti šeme sa više putanja pokazaće ovakvo ponašanje, jer više izvorišnih čvorova dele pojedinačne linkove od tačke do tačke. To znači da će performanse tokova podataka koji potiču od ovih izvorišnih čvorova biti korelisane. Na višim slojevima, javlja se promena u ponašanju mreže, jer kada su greške korelisane, onda i tokovi podataka od različitih izvorišnih čvorova postaju korelisani. Sve ovo doprinosi da se mreža ponaša korelisano, tj. kada se nešto desi, desiće se istovremeno za više tokova podataka.

Naučna oblast:
Elektrotehnika i računarstvo
Naučna disciplina:
Telecomunikacije
Ključne reči:
bežične mreže, kooperativne mreže, decode-and-forward rejelni sistemi, efekti senke, kanali za fedingom, verovatnoća greške, verovatnoća prekida,
UDK:
(621.391+621.395.38):519.724
CERIF klasifikacija:
T180

Preface

This dissertation is submitted in partial fulfilment of the requirements for the degree of *philosophiae doctor* (Ph.D.) at the Norwegian University of Science and Technology (NTNU), and for the degree *doctor of science* at the University of Niš (UNiš). My main supervisor has been Professor Kimmo Kansanen at the Department of Electronics Systems at NTNU, while my supervisor has been Professor Goran T. Đorđević from the Department of Telecommunications at UNiš, Faculty of Electronic Engineering.

The studies have been carried out at NTNU and UNiš in the period from October 2012 to October 2016.

This work has been funded by the Norwegian Ministry for Foreign Affairs through the HERD program under the project "Norwegian, Bosnian, and Serbian cooperation platform for university and industry ICT R&D – NORBAS".

Acknowledgements

Many thanks to my supervisors, Professor Kimmo Kansanen at NTNU, and Professor Goran T. Đorđević at UNiš, who followed my studies every step and pointed me in the right directions. I will miss our weekly Skype meetings, where many research ideas were born.

I would like to extend a particular thanks to the NORBAS project coordinator, Tore Jørgensen, who made sure that all of the Ph.D. students that were involved in the NORBAS project "lived like kings" while staying in Trondheim.

I would also like to thank the thesis assessment committee members, who took their time to carefully evaluate this thesis, and for their valuable feedback and suggestions.

Thanks to everybody at the Signal Processing group at NTNU, who made every day during my stay in Trondheim a real pleasure. Also, thanks to the lovely people from Lab 304 at the Faculty of Electronic Engineering in Niš, who made me feel at home.

Finally, my gratitude goes to my loving family and close friends, who have always believed in me. I wouldn't have made it this far if it wasn't for their support. This thesis is dedicated to them as a token of my gratitude.

Nemanja Zdravković
June 2017, Niš

Contents

List of Figures

List of Tables

Abbreviations

ACK	Acknowledgement
AF	Amplify and Forward
ARQ	Automatic Repeat reQuest
AWGN	Additive White Gaussian Noise
BER	Bit Error Rate
BPSK	Binary Phase Shift Keying
BS	Base Station
CDF	Cumulative Distribution Function
CDMA	Code Division Multiple Access
CF	Compress and Forward
CoF	Compute and Forward
CSI	Channel State Information
DAF	Decode-Amplify-Forward
DF	Decode and Forward
DSSS	Direct-Sequence Spread Spectrum
EF	Estimate and Forward
FDMA	Frequency Division Multiple Access
FEC	Forward Error Correction
FSO	Free-Space Optics
i.i.d.	Independent Identically Distributed
LDPC	Low Density Parity Check
LF	Linear-Process and Forward
LoS	Line-of-Sight
MAC	Medium Access Control

Abbreviations

MGF	Moment Generating Function
MIMO	Multiple-Input Multiple-Output
mm-Wave	Millimetre-Wave
MPSK	M-ary Phase Shift Keying
MQAM	M-ary Quadrature Amplitude Modulation
MRC	Maximal Ratio Combiner
MS	Mobile Station
NAK	Negative Acknowledgement
nLF	Nonlinear-Process and Forward
OFDM	Orthogonal Frequency Division Multiplexing
OP	Outage Probability
P2P	Point-to-Point
PDF	Probability Density Function
PER	Packet Error Rate
PF	Purge and Forward
PMF	Probability Mass Function
RF	Radio Frequency
RS	Relay Station
RV	Random Variable
SC	Selection Combiner
SNR	Signal-to-Noise Ratio
SR-ARQ	Selective Repeat Automatic Repeat reQuest
TDMA	Time Division Multiple Access
WiMAX	Worldwide Interoperability for Microwave Access
WSN	Wireless Sensor Network

Chapter 1

Introduction

1.1 The industrial wireless network

In recent years, industrial centres are incorporating wireless communication systems in their production processes. Companies that own large industrial plants face growing demands to improve their efficiency, meet environment regulations and cost objectives [1,2]. With the increase of the industrial manufacturing market, intelligent communication systems are required to improve productivity [3]. Machines such as production or assembly lines in man-made installations and factories are often moved. As a result, workspaces within these industrial environments change over time, and wired communication requires frequent routing of cables, which can be costly and time consuming. Industrial organizations such as ZigBee Alliance and the HART Foundation have been active in introducing wireless solutions such as ZigBee [4] and WirelessHART [5] for automation in industrial environments. Compared to traditional wireless networks, industrial wireless networks operate in harsher and noisier environments [6]. Industrial wireless networks have more demanding requirements in terms of reliability and low-latency. The quality of control may be severely degraded if data packets are delayed or not transmitted correctly.

The main motivation in this thesis is to analyse and improve performance in industrial wireless networks through the use of the effects of spatial diversity. The propagation channel in industrial environments behaves differently from the channel found in other closed-space environments such as office space [1]. These environments have a more open layout, consist of large machines, and there is a presence of concrete and highly reflective materials such as metal. In these environments, apart from the fading phenomena, the macroscopic changes in the propagation environment are also accounted, e.g., moving large objects which block Line-of-Sight (LoS) paths, and other obstacles [1,7,8]. Within these types of industrial environments, network source nodes are also subject to dynamic shadowing and outage events occur due to propagation phenomena, which are not static

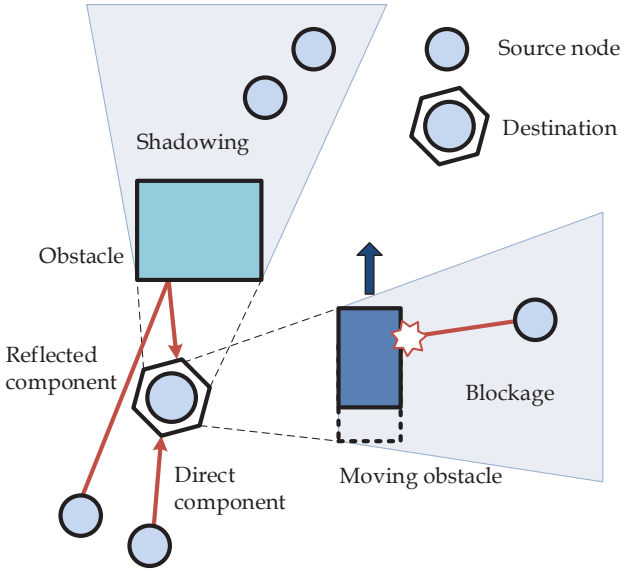

Figure 1.1: Wireless network in an industrial environment.

but are slower than short-term fading. Industrial wireless networks typically require low and deterministic latency. When wireless networks are used for process control, any missing or delayed data can severely degrade the quality of control [6]. If Wireless Sensor Networks (WSNs) are used in an industrial environment, any potential equipment problems and failures can be avoided and replacement costs can be prevented with an early notification system [2]. In these operating regimes Outage Probability (OP), which can be defined as the probability that the instantaneous error probability exceeds a specified value, is the correct performance indicator [9]. Note that alongside OP, average throughput and error rate are equally good performance indicators; however, throughout the thesis OP is the primary performance metric used.

A typical wireless network set in industrial environment is shown in Fig. 1.1. In this thesis, the applications of cooperative relaying in industrial wireless network scenarios are investigated. Dynamic shadowing is modelled with a simple node or link blockage model, where in the former any node can be totally blocked from its environment [9]. This simple blockage case is used for modelling macroscopic, dynamic link attenuation, where in the worst case scenario any node can be totally blocked from its environment. It is also useful in modelling situations where some nodes are randomly eliminated due to battery depletion or other reasons causing device failures. The fading and shadowing phenomena are statistically modelled as a composite fading channel [10–12], combining the effects of multipath fading and shadowing.

Cooperative communication systems have developed as an upgrade to existing cellular network architectures. In the wireless community, a paradigm shift has risen from single-hop systems to two- and multi-hop systems [13]. In industrial wireless networks, the deployment of cooperative multi-hop relaying communication systems adds performance gains when compared to a traditional, single-hop system. Due to the broadcast nature of the wireless medium, when a transmitting node sends its data to the destination, other nodes in the vicinity can pick up these transmissions as well, and relay them to the destination. The destination can combine all the received independently faded signals and obtain diversity gains. Diversity obtained through multi-hop transmissions in literature is usually referred as cooperative diversity. Furthermore, cooperative systems provide fast communication with little overhead, obtaining diversity gains which in turn provide low OP. The high reliability and low-latency requirements in industrial wireless networks are addressed through the utilization of cooperative diversity. Two-hop networks are considered, as a two-hop network is the simplest non-trivial case, which exposes basic macro-diversity behaviour and propagation effects.

1.2 Background on cooperative diversity

The concept of using relays to enhance a communication link from a source to a destination is not new. In fact, the protocols encountered in modern relay-assisted and cooperative communications have been known in part by the satellite community for half a century [14–18]. However, the main use of relays was to improve coverage and range problems typical for satellite communications.

The capacity and performance benefits of cooperative relaying protocols under realistic channel and system conditions are responsible for returning cooperative communication as a “hot topic” in modern communication systems [19].

In cooperative communications, a user’s communication link is enhanced in a supportive manner by other users in the network acting as relays [19]. In traditional (supportive) relaying, a relay node is placed between the source node and the destination, extending the source node’s communication range by forwarding its data to the destination. On the other hand, in cooperative relaying multiple source nodes act as each other’s relays simultaneously, enhancing communications links to all active source nodes. Supportive relaying and cooperative relaying schemes are shown in Fig. 1.2.

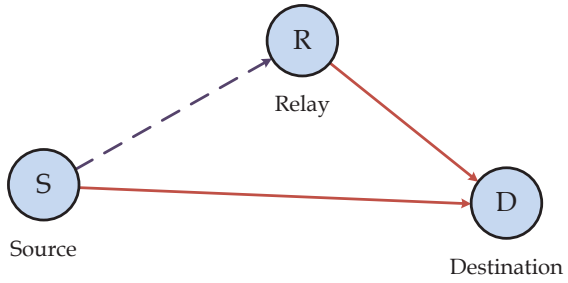

(a) Supportive relaying.

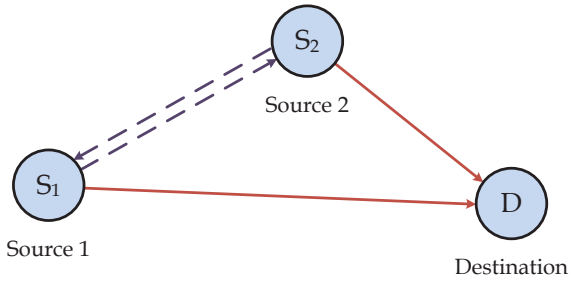

(b) Cooperative relaying.

Figure 1.2: Types of relaying.

1.2.1 Supportive relaying

The simplest form of cooperative communications, termed supportive relaying has been introduced by van der Meulen in [20, 21], and also studied in [22]. However, the first information theoretic analysis of the relay channel was published by Cover in [23,24]. In supportive relaying, a source Mobile Station (MS) communicates both directly with the destination and over the Relay Station (RS). The achievable communication rate was derived for the cases with and without feedback to either the MS or RS or both, and the main conclusions were that the capacity of a communication system with a relay improves the capacity of a single, direct link. These early works presented results for Gaussian channels only – no channel fading was taken into account. The idea of utilizing relays to improve capacity of wireless networks was revisited at the last decade of the 20th century [25], where the emphasis was on the use of relays in cellular systems [26–29].

1.2.2 Cooperative relaying

The concept of cooperative relaying, in which at least two users help each other to improve both users' performance has been pioneered by Sendonaris *et al.* in [30]. The

authors studied a simple cooperation protocol which improved capacity and reduced OP at a given rate. The same authors extended [30] in [31, 32], where more sophisticated cooperative schemes were proposed.

Based on [30], Laneman *et al.* gave the mathematical framework for energy-efficient multiple-access cooperative strategies in [33–36]. These strategies, based on Amplify and Forward (AF) and Decode and Forward (DF) relaying, achieve significant diversity and outage gains when compared to a non-cooperative single link case [19].

1.2.3 Pros, cons, and trade-offs of cooperative relaying

The main advantages, disadvantages and trade-offs of cooperative communication in wireless systems are presented below. The key points are taken from [19]. To design a system that would take full advantage of cooperation, one must ensure that by applying cooperative schemes, overall system performance does not deteriorate.

Advantages of cooperative relaying

The main advantages of applying cooperative schemes in wireless communication systems can be given as follows:

- **Performance improvement**. End-to-end improvement of performance metrics such as error rates and OP can be achieved when using cooperative schemes compared to traditional direct link systems. These improvements are a result of diversity and coding gains and allow higher capacity and better coverage.
- **Balanced Quality of Service**. In traditional systems nodes that are in shadowed areas, in coverage holes or on a cell edge, suffer from coverage or capacity problems. With the use of relays, these performance issues are balanced.
- **Less infrastructure**. The use of nodes as relays results in no infrastructure investments to an existing system.
- **Reduced cost**. Compared to a pure cellular approach, the use of relays is a more efficient solution w.r.t. costs.

Disadvantages of cooperative relaying

The main disadvantages of applying cooperative schemes in communication systems can be summarized as follows:

- **More complex scheduling**. A system with a large number of users and relays can require complex scheduling mechanisms. The gains achieved at the physical layer can be negligible if not properly addressed at higher layers.

- **Increased overhead**. A system employing cooperative schemes requires handovers, additional security and tight synchronization when compared to a non-cooperative scheme.
- **Increased interference**. The use of relaying will increase the total number of transmissions in the wireless medium, resulting in more both inter- and intra-cell interference.
- **Synchronization**. In a cooperative network, synchronization needs to be tight to maintain seamless data flow between cooperating nodes and between the nodes and the destination [37, 38].
- **Increased end-to-end latency**. Relaying typically involves the reception and decoding of the entire data packet before it can be re-transmitted. If delay-sensitive services are being supported, such as voice or multimedia, then the latency induced by the decoding may become detrimental. Latency also increases with the number of relays. To prevent the increase of latency, either simple transparent relaying or novel decoding methods need to be used.
- **Power consumption**. If cooperating nodes are not powered by mains, the power consumption can be prime design driver. It determines battery recharging cycles and costs. Additionally, in a dynamic cooperative network, power consumption is not deterministic, which remains a challenge for many industrial applications.

Trade-offs

The main trade-offs in designing a system with cooperative schemes are

- **Coverage versus capacity**. This is the equivalent to the diversity-multiplexing trade-off [39]. Relays can help to improve the system capacity or increase network coverage – increasing one diminishes the other.
- **Software versus hardware complexity**. Relays usually have low hardware complexity, and are a cost-effective solution compared to installing new Base Stations (BSs) to increase capacity or coverage. However, the algorithm complexity increases, as cooperative schemes require more scheduling, overhead and synchronization.
- **Interference versus performance**. The gains obtained by using cooperative schemes can be used to reduce transmission power per node and therefore reduce the level of interference in the network. The use of same transmission power in a non-cooperative scheme results in an increase of capacity or coverage; however, relaying generates more overall traffic, which itself is a source of more interference.

1.2.4 Types of cooperative protocols

Cooperative protocols can be divided into two main protocols and their derivations – Amplify and Forward (AF) and Decode and Forward (DF) [19]. The simplest protocol is AF, where the signal received by the relay node is amplified, frequency translated and retransmitted. Amplification is performed by either a fixed or variable gain. In DF, the relay detects the signal, decodes it, re-encodes and only then retransmits it. These protocols require more hardware and are more complex in processing terms compared to AF.

Apart from AF and DF, additional cooperative protocols are listed in the following paragraph. These protocols are not used in this thesis in the performance analysis of industrial networks, and are therefore only briefly mentioned.

In addition to the AF and DF cooperative protocols, the combination of these two approaches resulted in the Decode-Amplify-Forward (DAF) protocol [40, 41]. The DAF protocol combined the benefits of both AF and DF protocols. With the Linear-Process and Forward (LF) protocol, the relaying node, besides amplification, performs simple linear operations on the received signal. These operations, such as phase shifting, are performed in the analogue domain after amplification. Similarly, Nonlinear-Process and Forward (nLF) performs nonlinear operations on the received signal before retransmission, such as end-to-end error rate minimization. Utilizing the Estimate and Forward (EF) protocol at the relay, the analogue signal is firstly amplified and down-converted to baseband. Afterwards, detection algorithms try to recover the original signal, and then the relay retransmits the signal. When a relay node retransmits to the receiver a compressed version of the detected signal, it uses a Compress and Forward (CF) protocol. Usually, these protocols apply source coding on the sampled signal.

Modern wireless communication networks that consist of many nodes are usually treated as interference-limited rather than noise-limited. Therefore, a group of protocols that are interference-aware are developed as well. In cooperative systems, Purge and Forward (PF) protocols eliminate as much interference as possible at each relaying node, while in Compute and Forward (CoF) protocols, relays decode linear functions of transmitted messages according to their observed channel coefficients rather than ignoring the interference as noise [42, 43].

1.2.5 Decode-and-Forward protocols

In this thesis, the protocols presented are based on DF, as this protocol is known to be a performance optimum w.r.t. metrics such as error rates or OP [19]. Moreover, DF protocols are implementable with current orthogonal Medium Access Control (MAC) systems. Channel orthogonality can be achieved by using various modes of multiple access, i.e.,

time/frequency/code division multiple access (TDMA/FDMA/CDMA). However, when considering DF protocols with the utilization of Orthogonal Frequency Division Multiplexing (OFDM) results in an unavoidable processing delay of at least one OFDM symbol, because OFDM symbols cannot be demodulated before they are completely received [44].

Medium access control

Throughout the thesis, DF protocols utilizing orthogonal MAC are investigated. Similar to many existing systems like wireless LAN and cellular networks, the available bandwidth is divided into orthogonal channels, which are allocated to the nodes in the cooperative network [36]. By utilizing orthogonal MAC, interference issues between the cooperating nodes are avoided. Collisions are avoided as well, resulting overall lower latency. As a result, receiver algorithms are simplified, as well as the outage analysis.

A problem in DF schemes is that relay node can forward data from the source to the destination only if the data is fully decoded at the relay. When the channel is poor (i.e., under heavy fading and/or shadowing) the relay cannot fully decode a packet and therefore it does not forward it. The destination in turn may lose synchronization with the network unless it has a packet distinguishing mechanism or the transmitted data has more overhead.

Some of the disadvantages of DF protocols are arising from the lack of full-duplex operation, i.e., transmitting and receiving at the same time in the same frequency band. Full-duplex relaying has been investigated in [44–49], and while this relaying mode does indeed increase the spectral efficiency, it is echieved at the expense of self-interference. Interference-aware cooperative protocols like CoF utilize simultaneous transmissions [42], but these protocols are more complicated and are beyond the scope of this thesis.

Decode and Forward literature overview

Chatzigeorgiou *et al.* have introduced repetition schemes in their works, ensuring the destination will always receive the same amount of data per node [50–52].

In [50], M nodes operate either cooperatively or selfishly. Namely, in the high Signal-to-Noise Ratio (SNR) regime in the channel between nodes all data is successfully decoded, and all nodes relay each others' data to the destination. On the other hand, if any node fails to decode a packet, the whole network drops cooperation and each node sends its packets another $(M-1)$ times. Either way, the destination receives M packet copies per cooperation frame.

Although the destination receives the same amount of packet copies per cooperation

frame, the whole network suffers if one of the packets is not successfully decoded, since in that case cooperation is dropped and every node re-sends its packets. This issue is avoided in [51] where only those packets which are not successfully decoded are re-sent. Additionally, besides exact OP expressions over Rayleigh fading, in [52] asymptotic expressions are derived as well, giving more insight on the interplay between the channel conditions.

An extension to Nakagami-m fading is presented in [53], where the effects of fading severity and LoS and non-LoS environments were taken into account. Furthermore, the effects of unequal SNR and node blockage were investigated in [9].

Besides the repetition protocols, Ikki and Ahmed have investigated the best-relay and incremental-best-relay selection schemes, respectively, in [54, 55]. In the former, instead of using all nodes in the network as relays, only the "best" one is used for forwarding data, i.e., the relay with the highest uplink SNR to the destination. In the latter, this relay is used only if the destination provides a negative acknowledgement via feedback messages. With the use of these schemes, only two channels are needed – the source node uplink channel and the best relay uplink channel.

When data-link layer performance is investigated, a more natural metric to wireless packet transmission when compared to physical layer Bit Error Rate (BER) performance is Packet Error Rate (PER) [56]. PER analysis was performed in [56] by applying several Automatic Repeat reQuest (ARQ) feedback schemes from the destination to cooperating nodes. Three protocols that apply ARQ mechanisms at the relay and/or destination are presented in [57]. In [58], the authors proposed an ARQ-based Low Density Parity Check (LDPC) coded cooperative system that provides an improvement in both error rate and throughput.

1.2.6 Application to modern communication systems

Cooperative communications have a large set of applications in communication systems, ranging from cellular systems, ad-hoc networks, vehicular systems and WSNs. A brief overview is given below, demonstrating the benefits of cooperative systems. Afterwards, an example of how cooperative communication can be utilized in industrial wireless networks is presented.

Cellular systems

In a cellular system, the communication network is composed of cells, each containing its BS serving multiple MSs which communicate directly to their BS. Cellular networks suffer from capacity, coverage and interference problems [19], and often these problems are not independent. By adding a RS to a cellular system, significant gains can be

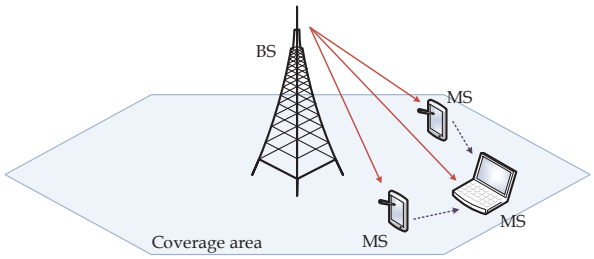

(a) Improving capacity.

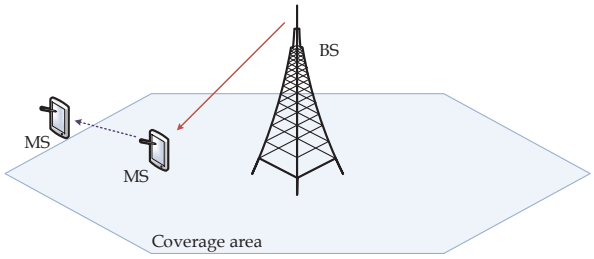

(b) Improving coverage.

Figure 1.3: Application in cellular systems.

achieved.

Firstly, those MSs within the coverage area can gain additional capacity. Namely, MSs acting as relays reduce the propagation path, allowing the BS to use higher modulation orders, improving capacity, as shown in Fig. 1.3(a).

Secondly, coverage can be extended for those MSs beyond the cell edge receiving poor signal, shown in Fig. 1.3(b). Furthermore, in urban and industrial environments, coverage holes can be covered.

Thirdly, these capacity and coverage gains result in less transmission power needed, reducing the interference in the whole system.

Ad-hoc networks

In wireless ad-hoc networks, apart from interference, fading, and shadowing, nodes frequently join and leave the decentralized network. This dynamic behaviour of an ad-hoc network causes an additional design issue [59]. By forming node pairs, the two transmitting nodes and the two receiving nodes can mutually cooperate, forming two-by-two Multiple-Input Multiple-Output (MIMO) channel, but retaining a single antenna per node, as shown in Fig. 1.4.

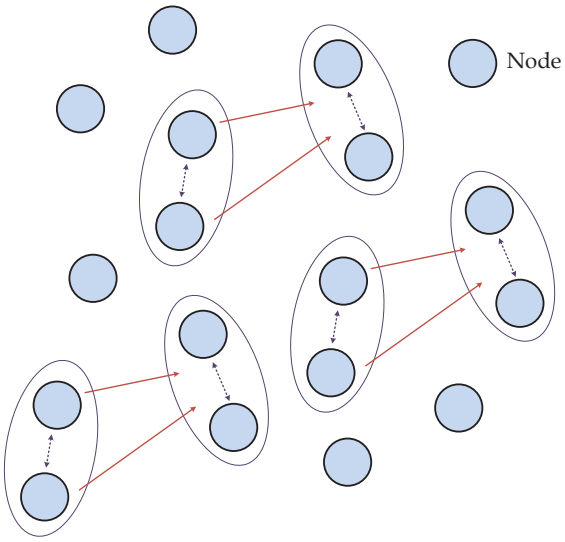

Figure 1.4: Application in ad-hoc networks.

Vehicular systems

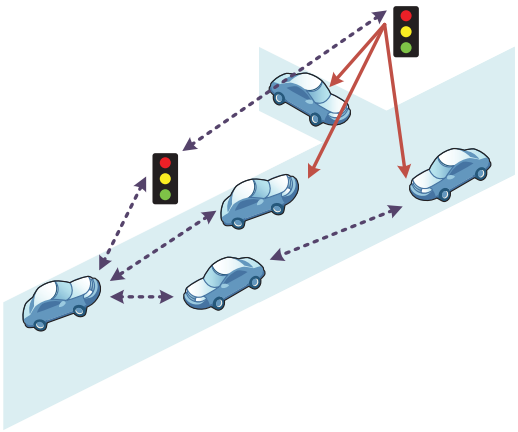

Figure 1.5: Application in vehicular systems.

Novel vehicular systems will include in-vehicle Internet access, vehicle-to-vehicle and vehicle-to-infrastructure communication [60–65]. Vehicle collision avoidance, traffic routing due to congestion can all benefit from cooperation within a vehicular communication system, as shown in Fig. 1.5.

Wireless sensor networks

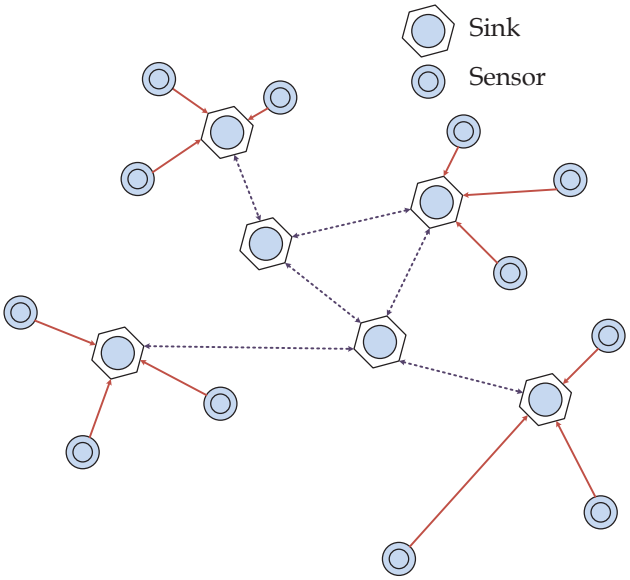

Figure 1.6: Application in wireless sensor networks.

In WSNs, battery consumption poses an limiting issue in network design [66–70]. One must optimize the network lifetime w.r.t. reliable communication between the sensors themselves, as well as between the sensors and sinks. With the use of cooperative strategies, shown in Fig. 1.6, coverage gaps can be avoided, redundant links can be established, overall network reliability can be improved, and network life expectancy can be prolonged.

Industrial wireless networks

Utilizing cooperative diversity in an industrial network is shown in Fig. 1.7. Each network cluster can have a local destination node and a number of corresponding local cooperating nodes. Each node cooperates with other nodes in its cluster and sends data to its local destination. The destination nodes can be static, and therefore interconnected either by a microwave link or a wired connection. Whereas traditional WSNs have in general different latency requirements, industrial wireless networks have the low-latency constraint. Two-hop communication within a cluster provides low-latency while maintaining the diversity benefits of cooperative schemes. Throughout the thesis, the performance of a single network cluster is investigated.

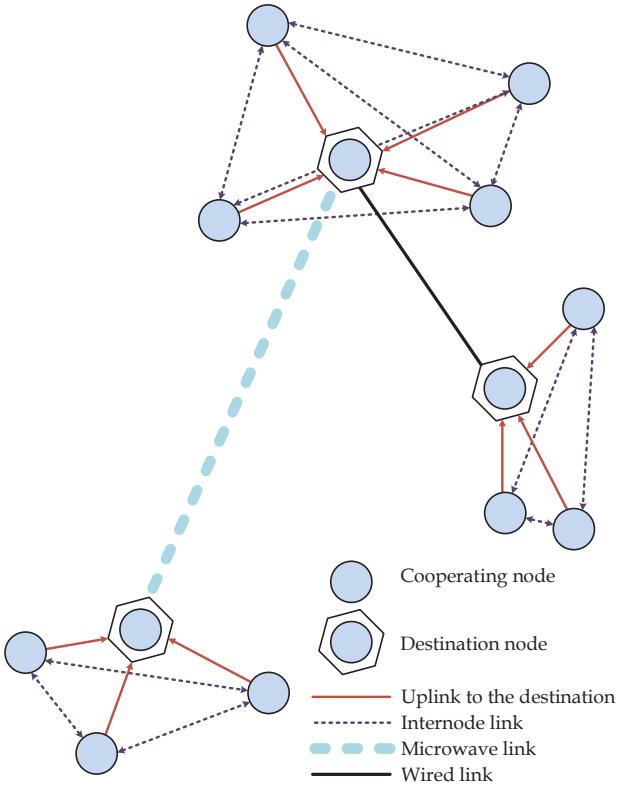

Figure 1.7: Application in industrial wireless networks.

1.3 The industrial wireless channel

Wireless communication on Radio Frequency (RF) is a complex phenomenon which is characterized by various degrading effects such as multipath fading, shadowing and noise [71]. These effects are modelled statistically. Throughout the vast literature on wireless communications, there exist statistical fading channel models for different communication scenarios and propagation environments.

Multipath fading is a consequence of constructive and destructive combination of randomly delayed, reflected, scattered, and diffracted signal components [71]. This type of short-term signal variations is also termed short-term fading, which occurs at the spatial scale of the order of the carrier wavelength [72]. Depending on the nature of the propagation channel, several models used for describing the statistical behaviour of multipath fading, which are used throughout the thesis are presented.

Furthermore, when regarding the analysis of signal transmission over wireless RF links, it is certainly important to take into account the consequences of possible moving

obstacles in the propagation path and in the destructive Fresnel zones [73]. This dynamic shadowing can cause temporary communication interruption between the transmitter and the receiver – blockage. The blockage caused by densely located buildings in urban areas was analysed in [74]. Based on random shape theory, the authors have modelled buildings as a line segment processes and have computed coverage probability of wireless network with link blockage. Moreover, in [75] the outage probability of macro diversity with multiple base stations in Millimetre-Wave (mm-Wave) communications was evaluated.

In wireless communication systems, the received amplitude of the signal is modulated by the random fading amplitude X, which has a mean-square value of $\Omega = \mathrm{E}[X^2]$, with $\mathrm{E}[\cdot]$ denoting the expectation operator. Upon passing through the fading channel, the signal is degraded at the receiver by Additive White Gaussian Noise (AWGN). The noise, characterized by one-sided power spectral density N_0 W/Hz is usually assumed to be statistically independent of the fading amplitude X. Denote the instantaneous received SNR per symbol with $\gamma = X^2 E_S/N_0$, with E_S denoting symbol energy. The average SNR per symbol is therefore $\bar{\gamma} = \Omega E_S/N_0$. With a known Probability Density Function (PDF) of the fading envelope $p_X(x)$, the PDF and Cumulative Distribution Function (CDF) of the instantaneous SNR, denoted with $p_\gamma(\gamma)$ and $P_\gamma(\gamma_0)$, respectively, are obtained as [71, 76]

$$p_\gamma(\gamma) = \frac{1}{2\sqrt{\gamma\bar{\gamma}/\Omega}} \times p_X\left(\sqrt{\Omega\gamma/\bar{\gamma}}\right) \tag{1.1}$$

and

$$P_\gamma(\gamma_0) = \int_0^{\gamma_0} p_\gamma(\gamma)\,\mathrm{d}\gamma. \tag{1.2}$$

Throughout the thesis, the performance metric used is OP. In terms of the output SNR, this is the probability that γ will fall below a certain outage threshold, γ_0. Using the CDF expressions for various fading channels presented in the following subsections, OP, denoted with $P_O(\bar{\gamma};\gamma_0)$ is obtained as

$$P_O(\bar{\gamma};\gamma_0) \equiv P_\gamma(\gamma_0). \tag{1.3}$$

Note that the expressions for OP and CDF are identical, but in OP the threshold is parameter, whereas in the CDF expression γ_0 is the argument.

At high SNR, (1.3) can be approximated by a first order Taylor series, which can be expressed in terms of coding and diversity gain [77]. This asymptotic OP can therefore be written as

$$P_{O_{\text{asy}}}(\bar{\gamma};\gamma_0) = (\mathcal{G}_c\bar{\gamma})^{-\mathcal{G}_d} \tag{1.4}$$

with $\mathcal{G}_c$ denoting the coding gain, and $\mathcal{G}_d$ the diversity gain. This approximation is done in order to simplify the analysis of the system at high SNR.

1.3.1 Common channel models

In this subsection, the PDFs of the fading envelope and instantaneous SNR at the receiver for fading channels presented throughout the thesis are presented. Furthermore, the expressions for the CDF of the SNR are also given, as they are used as the basis for the performance analysis.

Rayleigh channel

When the received signal consists of a large number of multipath components, from the central limit theorem, the received envelope is treated as complex Gaussian process [78]. The in-phase and quadrature components are Independent Identically Distributed (i.i.d.), and the magnitude of the received envelope has a Rayleigh distribution. Hence, the most commonly used fading model for non-LoS communications is Rayleigh fading, and the PDF of the envelope is given as [71]

$$p_X(x) = \frac{2x}{\Omega} \exp\left(-\frac{x^2}{\Omega}\right), \quad x \geq 0. \tag{1.5}$$

The PDF of the instantaneous SNR is given as [71]

$$p_\gamma(\gamma) = \frac{1}{\bar{\gamma}} \exp\left(-\frac{\gamma}{\bar{\gamma}}\right), \quad \gamma \geq 0 \tag{1.6}$$

and the CDF is given as

$$P_\gamma(\gamma_0) = 1 - \exp\left(-\frac{\gamma_0}{\bar{\gamma}}\right). \tag{1.7}$$

Nakagami-m channel

Replacing the Rayleigh distribution with the Nakagami-m distribution [79] allows the analysis of fading conditions that can have a direct component, as well as severe fading, even severer than Rayleigh, depending on the fading parameter m, $m \geq 0.5$. For instance, for $m = 0.5$, the distribution reduces to the one-sided Gaussian distribution, while for $m = 1$ the Rayleigh distribution is obtained. Furthermore, as $m \to \infty$, the fading channel converges to the non-fading AWGN channel [71]. The PDFs for the envelope X and instantaneous SNR γ are respectively given as

$$p_X(x) = \frac{2}{\Gamma(m)} \left(\frac{m}{\Omega}\right)^m x^{2m-1} \exp\left(-\frac{mx^2}{\Omega}\right), \quad x \geq 0 \tag{1.8}$$

and

$$p_\gamma(\gamma) = \frac{1}{\Gamma(m)} \left(\frac{m}{\bar{\gamma}}\right)^m \gamma^{m-1} \exp\left(-\frac{m\gamma}{\bar{\gamma}}\right), \quad \gamma \geq 0, \tag{1.9}$$

where $\Gamma(\cdot)$ is the Gamma function defined in [80, eq. (1.1)]. For arbitrary m, the CDF is obtained as

$$P_\gamma(\gamma_0) = 1 - \frac{1}{\Gamma(m)}\Gamma_i\left(m, \frac{m\gamma_0}{\bar{\gamma}}\right), \tag{1.10}$$

with $\Gamma_i(\cdot,\cdot)$ denoting the incomplete Gamma function, defined in [80, eq. (8.350.2)].

However, when m is an integer, using the series expansion of the Gamma functions in [80, eq. (8.352.2)], (1.10) is reduced to

$$P_\gamma(\gamma_0) = 1 - \exp\left(-\frac{m\gamma_0}{\bar{\gamma}}\right)\sum_{\kappa=0}^{m-1}\frac{1}{\kappa!}\left(\frac{m\gamma_0}{\bar{\gamma}}\right)^\kappa. \tag{1.11}$$

Log-normal shadowing

The wireless channel is degraded not only by short-term multipath fading, but also by a long-term fading, i.e., shadowing [11, 71]. Depending on the properties of the propagation channel, multipath fading has been described by various statistical models [71]. As for shadowing effects, the log-normal distribution has empirically shown to be acceptable [81–87]. The PDF of the instantaneous SNR is given as

$$p_\gamma(\gamma) = \frac{\xi}{\sqrt{2\pi}\sigma_{SH}\gamma}\exp\left(-\frac{\left(10\log_{10}\gamma - \mu_{SH}\right)^2}{2\sigma_{SH}^2}\right), \tag{1.12}$$

where $\xi = \frac{10}{\ln 10}$, μ_{SH} is the mean, and σ_{SH} is the shadowing spread.

However, this model is not appropriate for further mathematical manipulations, and therefore shadowing effects are often modelled by the Gamma distribution.

Composite fading channel – the Generalized-$\mathcal{K}$ channel

Replacing the log-normal distribution with the Gamma distribution, with appropriate parameter substitutions a more desirable form for modelling the effects of both multipath fading and shadowing is obtained [11]. The Rayleigh-gamma, denoted as the $\mathcal{K}$-distribution [88], can be used for modelling diverse scattering phenomena in wireless and in optical communications. The composite Nakagami-m-gamma model found in literature under the name generalized-$\mathcal{K}$ ($\mathcal{K}_G$) model was proposed [10, 12] as a general fading/shadowing model for describing simultaneous effects of multipath fading and shadowing. The multipath portion of the compound fading channel is described by the Nakagami-m distribution, while the shadowing portion is described with the Gamma distribution. The PDF of a $\mathcal{K}_G$ fading envelope is given as [10]

$$p_X(x) = \frac{4m^{\frac{k+m}{2}}x^{k+m-1}}{\Gamma(m)\Gamma(k)\Omega_{SH}^{\frac{k+m}{2}}}K_{k-m}\left(2\sqrt{\frac{m}{\Omega_{SH}}}x\right) \quad x \geq 0, \tag{1.13}$$

where k and m are the shadowing and fading severity parameters, respectively, Ω_{SH} is the mean power defined as $\Omega_{SH} = \mathrm{E}\left[X^2\right]/k$. Furthermore, $K_\nu(\cdot)$ is the ν-th order modified Bessel function of the second kind, defined in [80, eq. (8.432)]. A variety of channel models can be obtained by setting certain values of the fading and shadowing severity parameters. The shadowing severity parameter k is related to the shadowing spread parameter σ_{SH} in log-normal shadowing as [12, 89]

$$\sigma_{SH}\,[\mathrm{dB}] = \frac{10}{\ln 10}\sqrt{\psi'(k)}, \tag{1.14}$$

where $\psi\prime(\cdot)$ is the first derivative of the digamma function, defined in [80, eq. (8.360)]. The PDF of the received SNR is obtained using a random variable transform as [10]

$$p_\gamma(\gamma) = \frac{2\Xi^{\frac{k+m}{2}}}{\Gamma(m)\,\Gamma(k)}\gamma^{\frac{k+m}{2}-1}K_{k-m}\left(2\sqrt{\Xi\gamma}\right), \quad \gamma \geq 0 \tag{1.15}$$

with $\Xi = km/\bar{\gamma}$ and $\bar{\gamma} = k\Omega E_S/N_0$. The CDF of γ, can be obtained in closed-form as [10, 90]

$$P_\gamma(\gamma_0) = \frac{1}{\Gamma(m)\,\Gamma(k)}G_{1,3}^{2,1}\left(\Xi\gamma_0\,\middle|\,\begin{matrix} & 1 & \\ m, & k, & 0\end{matrix}\right), \tag{1.16}$$

where $G(\cdot)$ is the Meijer's G-function, defined in [80, eq. (9.301)]. It should be noted that the CDF is expressed in terms of the Meijer's G-function, which is built-in function in Mathematica software package [91]. Moreover, Meijer's G-functions can be transformed to more familiar hypergeometric functions [80, eq. (9.41.1)] by applying the relation [91, eq. (07.34.26.0004.01)]. Hypergeometric functions are build-in software packages such as MATLAB or Maple.

Alternatively, the Generalized-$\mathcal{K}$ composite fading envelope can be presented as a product of two Nakagami-m distributed Random Variables (RV)s, one for the multipath portion, and another for the shadowing portion [90, 92, 93]

$$x_{\mathcal{K}_G} = x_m x_{SH}, \tag{1.17}$$

where both x_m and x_{SH} follow (1.8). This approach is relevant in simulating $\mathcal{K}_G$ variates, as one can easily generate two Nakagami-m variates with appropriate parameters in MATLAB for instance, and then take their product to obtain variates that would have the desired distribution.

Fig. 1.8 shows simulated fading envelope variations over time for the multipath, shadowing and composite fading envelopes, respectively [94, 95]. The mobile terminal velocity is set to $v = 5.4$ km/h, resulting in maximum Doppler frequency f_d of 10 Hz, as shown in Fig. 1.8(a). The duration of a shadow fade lasts for multiple seconds or minutes, and hence occurs at a much slower time-scale compared to multipath fading.

Usually, shadowing is modelled to be 10 or 100 times slower compared with multipath fading, and Fig. 1.8(b) shows the shadowing envelope which is 10 times slower than multipath fading, with a shadowing spread of $\sigma_{SH} = 3$ dB. Finally, 1.8(c) shows the combined multipath and shadowing envelopes, resulting in the composite envelope.

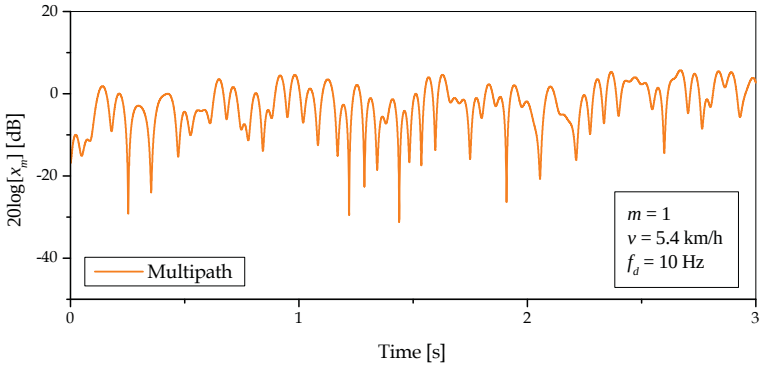

(a) Multipath envelope.

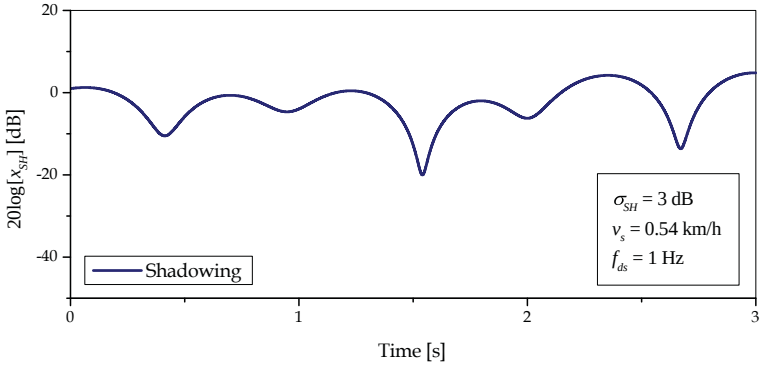

(b) Shadowing envelope.

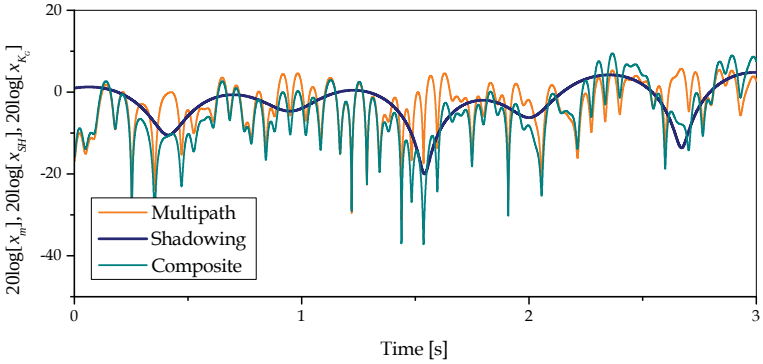

(c) Composite envelope.

Figure 1.8: Composite fading envelope and its components.

The extended Generalized-$\mathcal{K}$ channel

As an even more general distribution, Yilmaz and Alouini have utilized the so-called extended generalized-$\mathcal{K}$ (EGK) distribution in [96,97], which includes the fading and shadowing shaping parameters as novel parameters in describing propagation entities. This distribution unifies, as its special or limiting cases, almost every distribution in literature for interpreting fading/shadowing widely encountered channel conditions [96, Table I]. It is suggested as suitable for modelling composite fading channels in mm-Wave communications, as well as Free-Space Optics (FSO) channels [96, 98]. Additionally, this statistical model can be utilized in very heavy shadowing conditions, at high RF frequencies (60 GHz or above). These mm-Wave bands were suggested for next generation cellular systems because of a wide bandwidth, supporting high data rates.

The PDF of the EGK fading envelope is given as [96, eq. (2), correcting one typo]

$$p_X(x) = \frac{2\xi}{\Gamma(k)\Gamma(m)}\left(\frac{\beta_s\beta}{\Omega}\right)^{m\xi} x^{2m\xi-1} \times \Gamma_{ei}\left(k - m\frac{\xi}{\xi_s}, 0, \left(\frac{\beta_s\beta}{\Omega}\right)^{\xi} x^{2\xi}, \frac{\xi}{\xi_s}\right), \tag{1.18}$$

where m and k are the severity parameters of short-term fading and shadowing, respectively, ξ and ξ_s are the fading and shadowing shaping factors, respectively, $\Omega = \mathrm{E}[X^2]$ is the average power of the fading envelope. The remaining terms are defined as follows

$$\beta = \frac{\Gamma\left(m + \frac{1}{\xi}\right)}{\Gamma(m)}, \tag{1.19}$$

$$\beta_s = \frac{\Gamma\left(k + \frac{1}{\xi_s}\right)}{\Gamma(k)}, \tag{1.20}$$

and

$$\Gamma_{ei}(\alpha, y, b, \beta) = \int_y^{\infty} t^{\alpha-1}\exp\left(-t - bt^{-\beta}\right)\mathrm{d}t \tag{1.21}$$

is the extended incomplete Gamma function, defined in [99, eq. (6.2)].

Using the representation of the extended incomplete Gamma function through Fox's H function [99, eq. (6.22)], the PDF of the signal envelope is given by

$$p_X(x) = \frac{2}{\Gamma(k)\Gamma(m)x} H_{0,2}^{2,0}\left(\frac{\beta_s\beta x^2}{\Omega}\middle| \begin{matrix} -,- \\ (k, 1/\xi_s), (m, 1/\xi) \end{matrix}\right). \tag{1.22}$$

From (1.22), the PDF of the received SNR can be obtained as

$$p_\gamma(\gamma) = \frac{1}{\Gamma(k)\Gamma(m)\gamma} H_{0,2}^{2,0}\left(\frac{\beta_s\beta}{\bar{\gamma}}\gamma\middle| \begin{matrix} -,- \\ (k, 1/\xi_s), (m, 1/\xi) \end{matrix}\right). \tag{1.23}$$

1.4 Cooperative system model

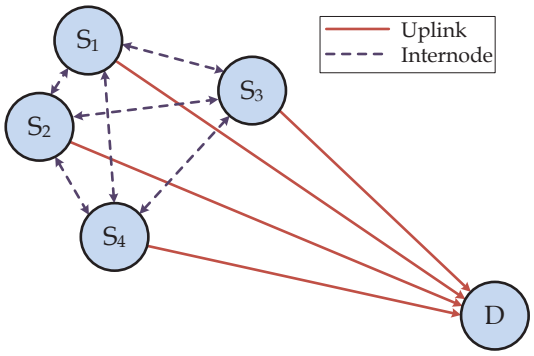

(a) Source nodes are grouped together.

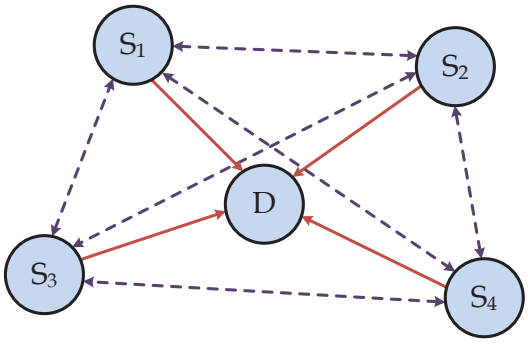

(b) Source nodes are positioned around the destination.

Figure 1.9: Positioning of source nodes and the destination node.

Throughout the thesis, a cooperative wireless network under investigation is comprised of M nodes. The source nodes are denoted by $\mathrm{S}_i, i \in \{1, \ldots, M\}$, with the destination denoted with D. The destination can detect data from each node individually due to orthogonal channels. Time periods allocated for reception and transmission are assumed to be equal. The nodes cooperate and communicate with each other and the destination over a frequency-flat channel subject to multipath fading and/or shadowing, temporary random blockage and AWGN. The channel between a source node and the destination is denoted as the uplink channel, while the channels between cooperating nodes are denoted as internode channels.

Cooperation consists of two stages. In the first stage, each node sends its own packet to the destination and to the other nodes. In the second stage, each node acts as a relay, re-encodes and forwards the received packet. The destination then applies combining

techniques of the received copies of the packet. In this thesis, the destination applies a linear combination on the received packets, namely Maximal Ratio Combiner (MRC) is applied, which is in general a sub-optimal combiner. A more optimal combining scheme at high SNR would be jointly encoding the packets that are transmitted from the source nodes, and jointly decoding at the destination. However, this type of combining is more complicated to analyse, while MRC remains mathematically tractable and close to optimal at low SNR.

Unless otherwise stated, symmetric networks are considered, meaning that average uplink SNRs are equal, and the same holds for the average internode SNR. Performance metrics such as OP and error rates of a single node can be applied for any other node in the network. With this assumption, basic behaviour is still exposed and the same conclusions are made as in a more general, non-symmetric case [9]. In general, two types of positioning of the source and destination nodes are encountered, as shown in Fig. 1.9. Each following chapter utilizes a variation of the general cooperative system model.

1.5 Contribution

The main contributions of this thesis can be summarized in the following main points

Outage performance of DF cooperative wireless networks over composite fading
Chapter 2 focuses on OP analysis of a DF wireless cooperative network, subject to multipath fading and shadowing. Nodes choose either to fully cooperate, relaying all data, or act selfishly, retransmitting their own packets to the destination. Closed-form expressions for OP of a single node are derived. Moreover, special cases are observed, in which the generalized fading channel is reduced to several familiar propagation environments. The work presented in Chapter 2 is published in [100–102].

Improving performance in DF cooperative wireless networks by introducing the threshold-based protocol
Chapter 3 introduces the internode threshold-based protocol. Source nodes monitor the instantaneous internode SNR by listening to the transmissions of other nodes. Depending on the internode channel state, each node sends its packet to other cooperating nodes if channel conditions are favourable or, regardless of the channel state, sends in another time period. Besides exact expressions, simpler and more tractable asymptotic expressions are derived as well, for the regimes of high average internode and uplink SNR, respectively. The effects of temporal internode channel correlation, network size and the interplay of average uplink and internode SNR values on OP are investigated.

Initial results, over Rayleigh fading channels, are published in [103], while the effects of temporal correlation, link blockage, as well as asymptotic results, are published in [104].

Improving performance in DF cooperative wireless networks with implementing SR-ARQ protocols

Chapter 4 deals with performance improvement by adding Selective Repeat Automatic Repeat reQuest (SR-ARQ) in the internode communication. Apart from Rayleigh fading, Nakagami-m fading channels are also investigated. Besides OP analysis, PER performance is studied as well using a tight PER approximation. The impact of fading severity, average SNR values, number of retransmission attempts and coding schemes on performance is investigated. Moreover, a comparison between the previously introduced threshold-based protocol is made. Results obtained in Chapter 4 are published in [105].

Outage correlation in DF cooperative wireless networks

In Chapter 5, the focus is on the joint outage performance of nodes in a two-hop DF network where each source forwards each others' data. System-wide error patterns that arise due to link sharing in low-latency networks are studied. All links experience independent Rayleigh fading, and the destination utilizes MRC for packet copies. Extending the well-known Moment Generating Function (MGF) approach for performance analysis to the multidimensional case, approximate expressions for simultaneous outage of any pair of nodes at high SNR are derived, as well as asymptotic expressions for diversity and coding gains. The expression for conditional outage, i.e., the OP given that another node is already in outage is also derived. Moreover, by applying an iterative approach, the analysis is extended to arbitrary number of nodes. The simultaneous outage dependence on network dimension and average SNR is investigated. The results of Chapter 5 are summarized in [106].

Summary and future research

Finally, a summary for each of the chapters and future research directions are presented in Chapter 6.

Unified simulation tools

All derived expressions are confirmed by running independent Monte-Carlo simulations using MATLAB. The scripts used for simulations are presented in the Appendix. Fading samples which are distributed according to a certain PDF are generated independently. The simulated average OP and average PER are obtained over a significantly large time period, i.e., over a large number (10^7) generated samples per plot point. These scripts are for single-link cases only, when no cooperation is present and no combining

at the receiver is used. However, these scripts served as a basis for writing Monte-Carlo simulations presented throughout the thesis.

1.6 Papers not included in the Thesis

In addition to the publications that this thesis is based on, the author has also contributed to the following papers, either as a first author or a co-author, as mentioned briefly in the following.

a.1 **N. Zdravković**, "Outage analysis of low-latency cooperative wireless networks with threshold-based protocol over composite fading," *Facta Universitatis, series Automatic Control and Robotics*, vol 16, no. 1, pp. 37-48, 2017. [107]

a.2 **N. Zdravković**, M. Petković, G. T. Đorđević, and K. Kansanen, "Outage analysis of mixed FSO/WiMAX link," *IEEE Photonics Journal*, vol. 8, no. 1, pp. 1-14, Feb. 2016. [108]

a.3 **N. Zdravković**, A. Cvetković, D. Milić, and G. T. Đorđević, "Packet error rate analysis of decode-and-forward free-space optical cooperative networks in the presence of random link blockage," *Journal of Modern Optics* (Accepted, available online). [109]

a.4 J. Anastasov, **N. Zdravković**, and G. T. Đorđević, "Outage capacity evaluation of extended generalized-$\mathcal{K}$ fading channel in the presence of random blockage," *Journal of the Franklin Institute*, vol. 352, no. 10, pp. 4610–4623, Oct. 2015. [98]

a.5 A. Cvetković, J. Anastasov, and **N. Zdravković**, "Outage performance of satellite-terrestrial multiuser networks with fixed gain AF relay," in *Proceedings of LI International Scientific Conference on Information, Communication and Energy Systems and Technologies (ICEST)*, Ohrid, FYR of Macedonia, Jun. 2016, pp. 131-134. [110]

Chapter 2

Outage performance analysis of a cooperative wireless network with channels subject to composite fading

In this chapter the OP analysis of a cooperative wireless network subject to composite fading is presented. Closed-form analytical expression for OP is derived when the destination node selects either the signal output of the MRC circuit, combining signals arriving from the nodes acting as relays, or a repeated signal from the originating source node, depending on the reliability of the internode channel. While in literature one can find similar protocols [50], performance analysis was examined only under Rayleigh multipath fading conditions. Therefore, in this chapter, the effects of multipath fading and shadowing are taken into account. Special cases are derived as well, in which the generalized-$\mathcal{K}$ fading channel is reduced to several familiar propagation environments, unifying the analysis. Analytical results are further confirmed by Monte-Carlo simulations.

The effects of multipath fading and shadowing severity parameters, average SNR values, network dimension, and packet length on outage performance are discussed. Performance is dominantly degraded by heavy shadowing, even when a LoS component is present between a source node and cooperating node and/or destination. Furthermore, for a fixed average uplink SNR, increasing the average internode SNR improves performance only to a certain point, upon which an unavoidable outage floor is reached.

2.1 System model

The nodes communicate with the destination and cooperate with each other over a composite fading channel. The network consists of M source nodes, denoted with $\mathrm{S}_i, \quad i = 1, \ldots, M$, and the destination node denoted with D. The network topology is

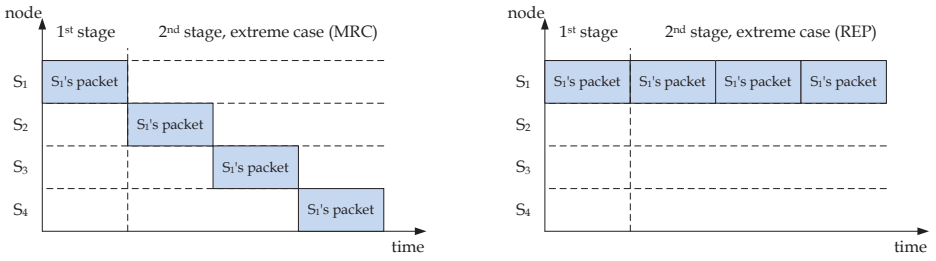

(a) Extreme case 1 – all packets are forwarded. **(b)** Extreme case 2 – all packets are repeated.

Figure 2.1: Packet scheduling in the two stages of cooperation.

shown in the previous chapter in Fig. 1.9. Cooperation between the nodes is performed in two stages. In the first stage, each node broadcasts its own data packet to the destination via the uplink channel, and to the other nodes via the internode channels. In the second stage of cooperation, if the internode channel is reliable, each node will forward a packet that has been successfully decoded to the destination. For those packets a node has failed to decode, it will re-send its own data packets. The second stage is performed over a total of $(M–1)$ time slots, ensuring the energy of the whole cooperation frame per source node remains constant. It is assumed that each channel condition remains unchanged during one cooperation frame, but has independent changes from frame to frame, i.e., the network is subject to quasi-static fading. Owing to system simplicity, all average uplink SNRs are considered to be the same. Similarly, the same follows for average internode SNRs. Internode channel reciprocity is assumed, allowing an internode channel realization in the direction from node S_i to S_j, to be the same as in the opposite direction, namely from S_j to S_i.

Nodes transmit their data packets on orthogonal channels allowing the destination to detect each node individually. If the instantaneous internode SNR is above a predetermined threshold, cooperating nodes will be able to fully decode packets from a source node, forwarding them to the destination. If this is not the case, cooperation is dropped and the source node will re-send it's own packet the remaining $(M–1)$ times to the destination. This kind of node behaviour has been dubbed "selfish" in literature [50].

The destination applies MRC on the relayed packet copies with the initial packet (which was received in the first stage of cooperation). If all packet copies are arriving from a single source node, the destination views these packets as a single copy with a power gain equal to the number of repetitions. These are the two extreme cases in the so-called "selfish" protocol – when there are no retransmissions as in Fig. 2.1(a), and when there are no relayed packets as shown in Fig. 2.1(b).

2.2 Outage probability analysis

Node S_i can successfully decode the whole packet if the instantaneous internode SNR, denoted by γ_{int}, is greater than the optimal SNR threshold γ_0. This optimal threshold γ_0, which the authors of [111, 112] have termed the "waterfall" threshold, divides the range of SNR into a high SNR and low SNR region, respectively. At low SNR an error event is all but unavoidable; conversely, at high SNR error events are negligible. This approach can also be used when approximating PER, and is given in more detail in Chapter 4.

The decoding probability for one node pair can therefore be expressed as

$$p_{\text{dec}} = \int_{\gamma_0}^{\infty} p\left(\gamma_{\text{int}}\right) d\gamma_{\text{int}} = 1 - P_{\gamma}\left(\gamma_0\right), \tag{2.1}$$

where $P_{\gamma}\left(\gamma_0\right)$ is given by (1.16). Since all internode channels from S_i to the remaining $(M-1)$ nodes are independent, the probability of decoding all packets will simply be p_{dec}^{M-1}. When node S_i is unable to decode packets, it replaces them with its own packets and re-sends them to the destination. One can treat the repeated copies as a single copy with M times the average uplink SNR. The resulting PDF $p_{\text{rep}}(\gamma)$ and CDF $P_{\text{rep}}(\gamma_0)$ in this repetition mode will have the same expressions as (1.15) and (1.16), respectively, substituting $\bar{\gamma}$ with $M\bar{\gamma}$, and are given as

$$p_{\text{rep}}\left(\gamma\right) = \frac{2\Xi_{\text{rep}}^{\frac{k+m}{2}}}{\Gamma\left(m\right)\Gamma\left(k\right)} \gamma^{\frac{k+m}{2}-1} K_{k-m}\left(2\sqrt{\Xi_{\text{rep}}\gamma}\right) \tag{2.2}$$

and

$$P_{\text{rep}}\left(\gamma_0\right) = \frac{1}{\Gamma\left(m\right)\Gamma\left(k\right)} G_{1,3}^{2,1}\left(\Xi_{\text{rep}}\gamma_0 \left| \begin{matrix} & 1 & \\ m, & k, & 0 \end{matrix} \right.\right) \tag{2.3}$$

with $\Xi_{\text{rep}} = km/\left(M\bar{\gamma}\right)$.

For reliable internode channels, the destination applies MRC at the $(M-1)$ relayed packet copies alongside the initial packet copy from the originating node. It has been shown in [89] that the PDF of the received SNR γ_{mrc} is of an M-branch MRC receiver obtained by substituting the fading severity parameter m in (1.15) with Mm. Note that the multipath fading is independent for all paths, while shadowing effects remain the same for all paths. The resulting PDF is therefore given as

$$p_{\gamma_{\text{mrc}}}\left(\gamma_{\text{mrc}}\right) = \frac{2\Xi_{\text{mrc}}^{\frac{k+Mm}{2}}}{\Gamma\left(Mm\right)\Gamma\left(k\right)} \gamma_{\text{mrc}}^{\frac{k+Mm}{2}-1} K_{k-Mm}\left(2\sqrt{\Xi_{\text{mrc}}\gamma_{\text{mrc}}}\right), \tag{2.4}$$

where $\Xi_{\text{mrc}} = km/\bar{\gamma}$.

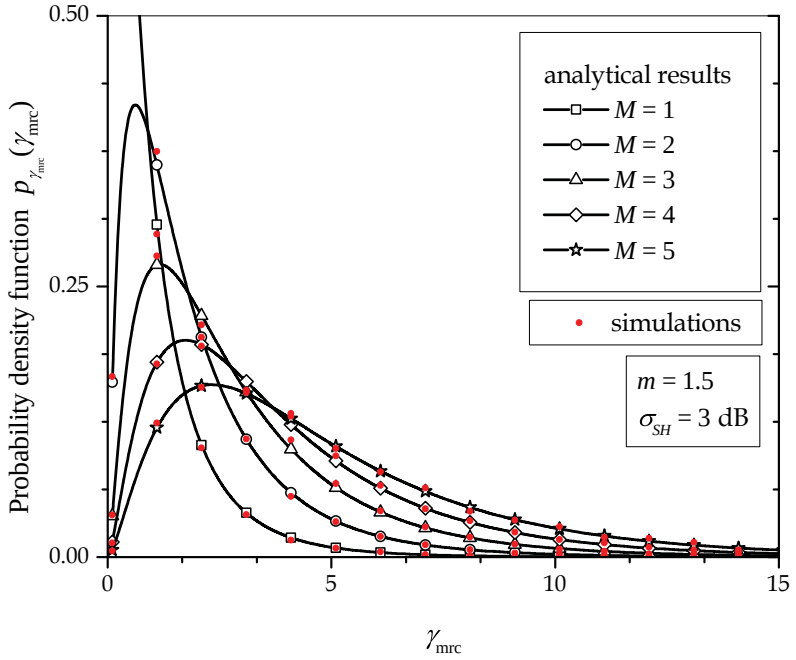

Figure 2.2: Probability density function of the combined SNR γ_{mrc} for different number of branches.

Fig. 2.2 shows the PDF of γ_{mrc} for different number of independent branches. All PDFs are one-tailed, and as the number of branches increases, the tail of the distribution becomes shorter.

The CDF of γ_{mrc}, will have the same expression as in (1.16) with argument γ_0, and by substituting m with Mm and γ with γ_{mrc}

$$P_{\mathrm{mrc}}(\gamma_0) = \frac{1}{\Gamma(Mm)\,\Gamma(k)} G_{1,3}^{2,1}\left(\Xi_{\mathrm{mrc}}\gamma_0 \,\middle|\, \begin{matrix} 1 \\ Mm, \quad k, \quad 0 \end{matrix}\right). \tag{2.5}$$

The destination will receive either the MRC-combined signal, relayed over M independently multipath faded paths, or the M-times stronger signal, from the originating node.

Finally, the OP can be expressed in terms of the CDFs as a piecewise function, depending on the number of repeated packets as

$$P_O(\bar{\gamma};\gamma_0) = \begin{cases} P_{\mathrm{mrc}}(\gamma_0), & \gamma_{\mathrm{int}} \geq \gamma_0, \\ P_{\mathrm{rep}}(\gamma_0), & \gamma_{\mathrm{int}} < \gamma_0. \end{cases} \tag{2.6}$$

In terms of the decoding probability p_{dec}, (2.6) can be expressed as

$$P_O(\bar{\gamma};\gamma_0) = p_{\mathrm{dec}}^{M-1} P_{\mathrm{mrc}}(\gamma_0) + \left(1 - p_{\mathrm{dec}}^{M-1}\right) P_{\mathrm{rep}}(\gamma_0). \tag{2.7}$$

Table 2.1: Special cases for the Generalized-$\mathcal{K}$ fading channel.

Envelope distribution	m	k
$\mathcal{K}$-Distribution	1	k
Nakagami-m	m	∞
Rayleigh	1	∞

2.3 Special cases

In this section, the analytical expressions for the CDF in "mrc" and "rep" mode, respectively given in (2.3) and (2.5), are reduced for the cases of some commonly used fading models, indicating the generality of the presented outage analysis. The reduced versions of CDF expressions presented in the following subsections account for the outage probability of specific fading and/or shadowing conditions, as given in Table 2.1. As in (2.7), the expressions are weighted the probability of decoding from all nodes, and afterwards summed in order to obtain the final OP expression. The probabilities of successful decoding for each special case can be obtained directly from the derived corresponding "rep" expressions as $p_{\text{dec}} = 1 - P_{\text{rep}}(\gamma_0)$, replacing $M\bar{\gamma}$ with $\bar{\gamma}_{\text{int}}$.

2.3.1 $\mathcal{K}$ fading channel

By setting $m = 1$ in (2.3) and (2.6) we obtain the so-called $\mathcal{K}$ fading channel, where the multipath component reduces from Nakagami-m to Rayleigh distribution, while the shadowing component remains Gamma distributed. The CDF expressions can be expressed therefore as [101]

$$P_{\text{mrc}}^{(\mathcal{K}\text{ - dist})}(\gamma_0) = \frac{1}{\Gamma(M)\Gamma(k)} G_{1,3}^{2,1}\left(\frac{k\gamma_0}{\bar{\gamma}}\middle|\begin{matrix} & 1 & \\ M, & k, & 0 \end{matrix}\right) \tag{2.8}$$

and

$$P_{\text{rep}}^{(\mathcal{K}\text{ - dist})}(\gamma_0) = \frac{1}{\Gamma(k)} G_{1,3}^{2,1}\left(\frac{k\gamma_0}{M\bar{\gamma}}\middle|\begin{matrix} & 1 & \\ 1, & k, & 0 \end{matrix}\right). \tag{2.9}$$

2.3.2 Nakagami-m channel

The $\mathcal{K}_G$ channel reduces to the Nakagami-m channel by letting $k \to \infty$, diminishing the shadowing component. By exploiting the permutation symmetry property of the Meijer's G-function [91, eq. (07.34.04.0004.01)] and with the help of [91, eq.

(07.34.25.0007.01)] we take the limit

$$\lim_{k\to\infty} P_{\text{mrc}}(\gamma_0) = \frac{1}{\Gamma(Mm)} G_{1,2}^{1,1}\left(\frac{m\gamma_0}{\bar{\gamma}}\middle|\begin{matrix}1\\ Mm,\ 0\end{matrix}\right). \tag{2.10}$$

Furthermore, this form of the G-function in (2.10) can be further reduced with the use of [91, eq. (07.34.03.0275.01)] to obtain

$$P_{\text{mrc}}^{(\text{naka})}(\gamma_0) = \frac{1}{\Gamma(Mm)} \Gamma_{gi}\left(Mm, 0, \frac{m\gamma_0}{\bar{\gamma}}\right), \tag{2.11}$$

where $\Gamma_{gi}(\cdot,\cdot,\cdot)$ is the generalized incomplete Gamma function, defined in [91, eq. (06.07.02.0001.01)]. Finally, with the use of [91, eqs. (06.07.27.0002.01), (06.06.03.0002.01)], the CDF for the "mrc" mode over Nakagami-m fading takes the familiar form [71]

$$P_{\text{mrc}}^{(\text{naka})}(\gamma_0) = 1 - \frac{1}{\Gamma(Mm)} \Gamma_i\left(Mm, \frac{m\gamma_0}{\bar{\gamma}}\right). \tag{2.12}$$

Moreover, for integer values of the fading severity parameter m, the Gamma functions in (2.12) reduces to a finite series applying [91, eq. (06.06.03.0009.01)] as

$$P_{\text{mrc}}^{(\text{naka})}(\gamma_0) = 1 - \exp\left(-\frac{m\gamma_0}{\bar{\gamma}}\right) \sum_{\kappa=0}^{Mm-1} \frac{1}{\kappa!}\left(\frac{m\gamma_0}{\bar{\gamma}}\right)^{\kappa}. \tag{2.13}$$

Following the same steps, the CDF expression for "rep" mode over Nakagami-m channels for non-integer and integer values of m are given respectively as

$$P_{\text{rep}}^{(\text{naka})}(\gamma_0) = 1 - \frac{\Gamma_i\left(m, m\gamma_0/(M\bar{\gamma})\right)}{\Gamma(m)} \tag{2.14}$$

and

$$P_{\text{rep}}^{(\text{naka})}(\gamma_0) = 1 - \exp\left(-\frac{m\gamma_0}{M\bar{\gamma}}\right) \sum_{\kappa=0}^{m-1} \frac{1}{\kappa!}\left(\frac{m\gamma_0}{M\bar{\gamma}}\right)^{\kappa}. \tag{2.15}$$

2.3.3 Rayleigh channel

Finally, by setting $m = 1$ in (2.13) and (2.15), the CDF expressions are obtained when the network is subject to Rayleigh fading. The expressions for "mrc" and "rep" mode are therefore given respectively as [71]

$$P_{\text{mrc}}^{(\text{ray})}(\gamma_0) = 1 - \exp\left(-\frac{\gamma_0}{\bar{\gamma}}\right) \sum_{\kappa=0}^{M-1} \frac{1}{\kappa!}\left(\frac{\gamma_0}{\bar{\gamma}}\right)^{\kappa} \tag{2.16}$$

and

$$P_{\text{rep}}^{(\text{ray})}(\gamma_0) = 1 - \exp\left(-\frac{\gamma_0}{M\bar{\gamma}}\right). \tag{2.17}$$

Table 2.2: Values pairs for σ_{SH} and k.

σ_{SH} [dB]	k	σ_{SH} [dB]	k	σ_{SH} [dB]	k
1	19.35680	6	0.904356	11	0.429599
2	5.197760	7	0.739634	12	0.389289
3	2.557350	8	0.625900	13	0.356020
4	1.614560	9	0.542808	14	0.328086
5	1.162320	10	0.479475	15	0.304288

2.4 Numerical results

The derived OP expressions are used to efficiently evaluate numerical results for any practical values of fading and shadowing severity parameters, average uplink and internode SNR and network cluster size. The outage threshold and the decoding threshold are set to be same value, which depends on average SNR, packet length L, as well as fading and shadowing parameters m and k, respectively.

The optimal threshold values for uncoded signals using Binary Phase Shift Keying (BPSK) is calculated numerically applying a technique similar to the one in [111]. Although the authors of [111] applied this technique to Rayleigh fading, numerical threshold evaluation is also valid other types of fading, including scintillation in FSO systems [109].

Upon evaluating the threshold value for various packet lengths, fading and shadowing conditions, results have shown that the optimal threshold is highly dependent only on packet length, and for $L = 256$, 512 and 1024 bits, the decoding threshold γ_0 will have values 5.87 dB, 6.534 dB and 7.113 dB, respectively [101,102]. All analytical results are confirmed by Monte-Carlo simulations.

The mapping of the shadowing spread σ_{SH} to the k parameter is given in (1.14), and performed using Mathematica software package, with the code is given below. Table 2.2 shows specific value pairs of σ_{SH} and k.

Code 2.1: Evaluating σ_{SH} for given k.

```
sSH[k_] := 10/Log[10]*Sqrt[PolyGamma[1, k]];
```

Code 2.2: Evaluating k for given σ_{SH}.

```
k[x_] :=  sSH /. FindRoot[10/Log[10]*Sqrt[PolyGamma[1, sSH]] == x, ...
    {sSH, 0.001}];
```

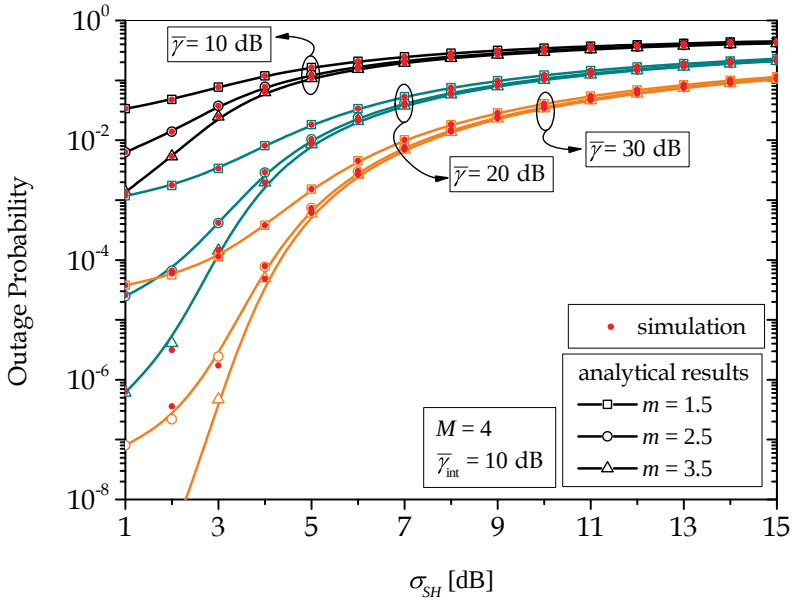

Figure 2.3: Outage probability dependence on shadowing spread for different values of fading severity and average uplink SNR.

Fig. 2.3 shows OP dependence on shadowing spread for different values of multipath fading severity and average uplink SNR. As expected, by increasing the shadowing spread σ_{SH}, OP grows. This effect is more evident when the uplink channel is more reliable. At high average uplink SNR and low shadowing, the OP can be very small. By increasing the shadowing severity, OP can increase by several orders of magnitude. For instance, for $m = 2.5$ at $\bar{\gamma} = 10$ dB, OP grows only 15.21 times as shadowing spread increases from 3 dB to 12 dB. However, for reliable uplink channels, at $\bar{\gamma} = 30$ dB, this increase is even 1.38×10^5 times greater.

The effects of multipath fading severity is shown in Fig. 2.4. In addition to light and heavy shadowing conditions, two curves corresponding to the case when no shadowing is present (i.e., Nakagami-m fading) are shown. In heavy shadowing, for $\sigma_{SH} = 12$ dB, OP stays above 10^{-2}, regardless of the multipath fading severity parameter variations.

Moreover, in severe fading, OP is not smaller than 0.016, even when no shadowing is present. In favourable fading conditions, i.e., $m = 2.5$ and for $\bar{\gamma} = 30$ dB, outage can by even lower than 10^{-8} when no shadowing is present, and around 10^{-6} for $\sigma_{SH} = 3$ dB.

Fig. 2.5 shows OP dependence on average internode SNR for different average uplink SNR and fading severity in moderate shadowing conditions. As average internode SNR increases, OP decreases at up to reaching an outage floor. Further increasing of average internode SNR has no effect on performance. For instance, the outage floor of

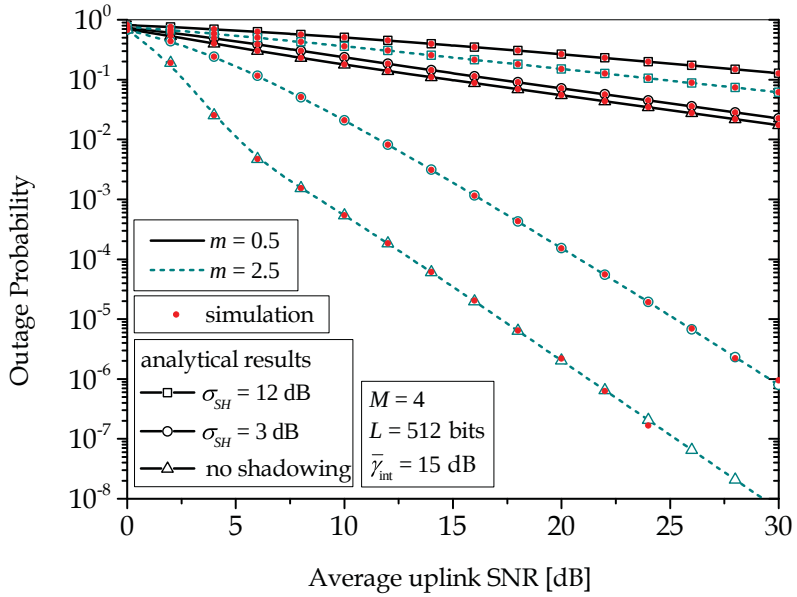

Figure 2.4: Outage probability dependence on average uplink SNR for different shadowing spread and fading severity.

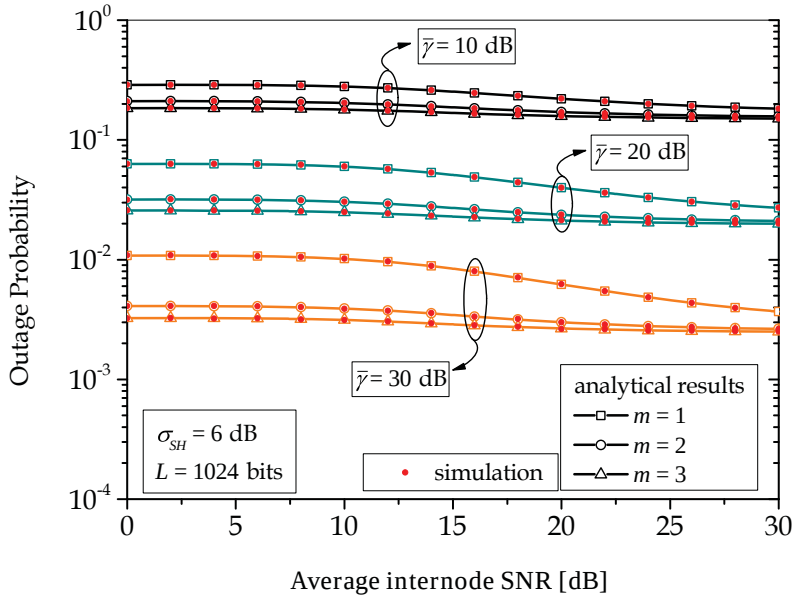

Figure 2.5: Outage probability dependence on average internode SNR for different fading severity and average uplink SNR.

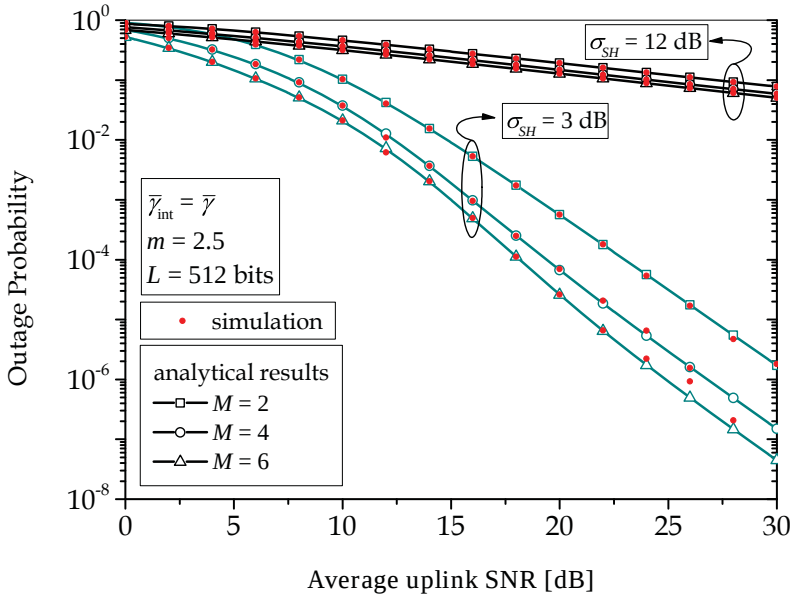

Figure 2.6: Outage probability dependence on average uplink SNR for different network sizes and shadowing spread.

$P_O(\bar{\gamma};\gamma_0) = 0.02$, when $\bar{\gamma} = 20$ dB appears at around $\bar{\gamma}_{\text{int}} = 24$ dB for both $m = 2$ and $m = 3$.

Finally, Fig. 2.6 shows OP dependence on average uplink SNR for different network sizes and shadowing severity. Additionally, average internode SNR increases simultaneously with average uplink SNR. As in the previous figures, heavy shadowing will limit OP regardless of channel reliability and network size. With the decrease of shadowing severity, the gain in adding more nodes to the network can be seen. For instance, at $\sigma_{SH} = 3$ dB, to reach an outage of 10^{-5}, for $M = 2$ the average SNR needs to be 26.9 dB, and only 21.27 dB for $M = 6$. Furthermore, the slope of the outage curves is also dominated by the degree of shadowing.

2.5 Conclusion

In this chapter, the outage probability of a DF cooperative wireless network affected by Nagakami-m multipath fading and Gamma shadowing has been analysed. The focus has been set on making a selection between relayed and repeated data packets, which is based on successful decoding at the relays. Closed-form outage probability expressions have been derived and confirmed by Monte-Carlo simulations. Additionally, these expressions derived for the generalized-$\mathcal{K}$ fading and shadowing channel have been reduced to $\mathcal{K}$,

Nakagami-m and Rayleigh fading environments. The impact of uplink and internode channel realizations, shadowing spread and multipath fading severity, as well as network size have been discussed.

The effects of shadowing on OP have shown to be dominating, acting as a limiting performance factor regardless of the multipath fading severity variations. The diversity order of the observed system has also been affected by the level of shadowing, and higher diversity gains have been obtained for lighter shadowing. Moreover, by increasing the number of nodes in the network, only a coding gain has been detected. By increasing the average internode SNR, outage performance has improved until reaching an outage floor.

Chapter 3

Threshold-based internode protocol

In this chapter, a threshold-based protocol in the internode communications part of the network is introduced in order to further improve overall performance. This protocol is based on monitoring instantaneous internode SNR, and choosing to send a packet immediately, or after a delayed period. Firstly, closed-form OP expressions are derived in the case when the network is subject just to Rayleigh fading, with independent SNR instances in the initial and delayed transmission. This is further expanded by including temporal fading correlation in these two instances. The effects of dynamic shadowing are modelled as internode blockage events, for which OP expressions are also derived. All exact results are confirmed by independently run Monte-Carlo simulations.

Moreover, apart from the exact expressions, derived asymptotic results give a better insight into outage performance at high average SNR.

The results illustrate that the internode protocol improves outage performance in the whole range of average uplink SNR. Internode channel correlation has a significant effect on the OP in the range of low average internode SNR. With increasing correlation, the OP increases up to an order of magnitude. The results also show that link blockage has a dominating effect on outage performance. The finite probability of all internode links being blocked reduces network performance to a single-link scenario, regardless of using the threshold-based protocol.

3.1 System model

As in the general model presented in Section 1.4, the wireless network is comprised of M nodes with nodes denoted with $\mathrm{S}_i, \quad i \in \{1, \ldots, M\}$, and the destination D, with channel orthogonality assumed. The network is subject to frequency-flat Rayleigh fading and AWGN.

Without loss of generality, we focus on the internode links from a single node, for example S_i. Due to various obstacles like mobile obstructions, an internode link from S_i to

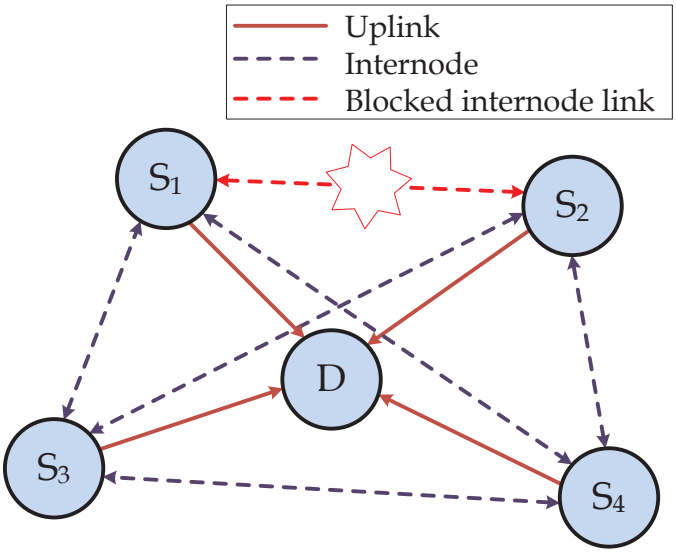

Figure 3.1: System model with internode link blockage.

S_j, denoted with $(i \to j)$ can be blocked with probability b_{ij}, $\quad j \in \{1, \ldots, M\}, \quad j \neq i$, as shown in Fig 3.1. When $(i \to j)$ is blocked, node S_j is cut off from the network from the point of view of S_i, and S_j continues to cooperate with the remaining nodes. Internode links are reciprocal; therefore, if $(i \to j)$ is blocked, $(j \to i)$ is blocked as well. We assume that the environment from nodes to the destination is such that direct links, from S_i to D, cannot be blocked, and communication from a node to the destination is always possible and all average uplink SNRs are equal.

Cooperation consists of two stages. In the first stage, each node sends its own packet to the destination and to the other nodes. In the second stage, each node acts as a relay, re-encodes and forwards the received packet.

At the end of the first stage, each node has received $(M-1)$ coded packets from other nodes. Out of those received coded packets, p packets are not successfully decoded. Hence, a node which fails to decode p packets has decoded $(M-p-1)$ packets successfully. During the second stage of cooperation, each node acts as a relay and re-encodes and forwards the $(M-p-1)$ packets to the destination. To maintain constant cooperation frame energy, the p packets which the node failed to decode are replaced with p copies of its own packet.

At the end of the second stage of cooperation, node S_i has transmitted $(p+1)$ copies of its own packets over the uplink channel. In addition to these packets, $(M-p-1)$ copies of the same packet are transmitted to the destination over other cooperating

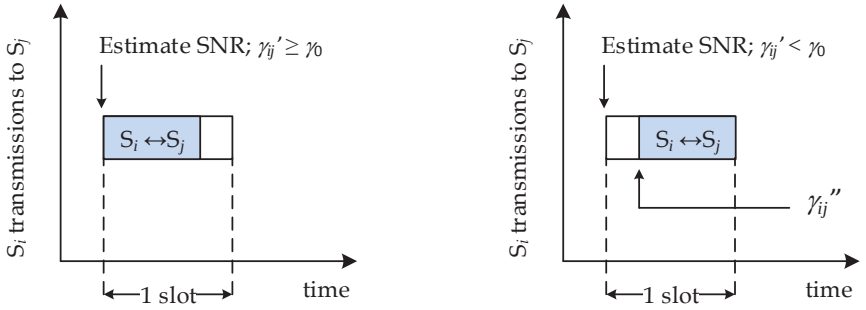

(a) Estimated SNR is greater than the threshold – node S_i sends its packet immediately.

(b) Estimated SNR is less than the threshold – node S_i sends its packet after a delay.

Figure 3.2: SNR estimation and packet transmission using the threshold-based protocol.

nodes. The destination then applies MRC of the M copies of the packet. If we observe the OP from node S_i, the number of cooperating nodes will depend on the network size, i.e., the number of unblocked links to S_i. We assume that link blockages are statistically independent. n_b denotes the number of blocked links to node S_i. The probability of N_b links being blocked is given by

$$\mathbb{P}[n_b = N_b] = \mathbb{P}[N_b] = \sum_{\substack{B_b \subseteq B_i \\ |B_b| = N_b}} \prod_{\nu \in B_i} b_{i\nu} \prod_{\mu \in B_i \setminus B_b} (1 - b_{i\mu}), \tag{3.1}$$

with $\mathbb{P}[\cdot]$ denoting probability, $N_b = 1, 2, \ldots, M-1$, B_i denoting the set of internode links from S_i, B_b the subset of blocked links, $|B_b|$ the cardinality of the set with different combinations of N_b elements, which are in the set B_i, and b_{ij} denoting the probability of the link $(i \to j)$ being blocked.

If all blockage probabilities are equal (i.e., $b_{ij} = b_i$), then (3.1) reduces to a binomial distribution

$$\mathbb{P}(N_b) = \binom{M-1}{N_b} b_i^{N_b} (1 - b_i)^{M - N_b - 1}. \tag{3.2}$$

3.2 Protocol description

As in the previous chapter, in the 1st stage of cooperation, node S_i sends to other nodes and to the destination. Note that each packet transmission time is shorter than the dedicated time slot, allowing the use of the internode protocol.

Each node monitors and estimates the instantaneous internode SNR to a non-blocked link. Depending on the internode Channel State Information (CSI), each node sends

its packet to other cooperating nodes if the internode SNR is above a predetermined threshold, as shown in Fig. 3.2(a). If this is not the case, regardless of the CSI, each node sends its packet after a waiting period, as in Fig. 3.2(b). Two cases are considered – when the internode SNR instances of the initial and delayed transmissions are independent, and when they are correlated.

3.2.1 Uncorrelated internode SNRs

At first, the instantaneous SNR instance of the delayed transmission is uncorrelated with the initial estimated SNR value. The Random Variable (RV) associated with the instantaneous internode SNR in the initial transmission is denoted with γ'_{ij}, while the RV in the delayed transmission is denoted with γ''_{ij}. It is assumed that the PDFs of the instantaneous SNRs in the two transmissions are identical.

Namely, the two PDFs are

$$p_{\gamma'_{ij}}\left(\gamma'_{ij}\right) = p_{\text{ray}}\left(\gamma'_{ij}\right) \tag{3.3}$$

and

$$p_{\gamma'_{ij}}\left(\gamma''_{ij}\right) = p_{\text{ray}}\left(\gamma''_{ij}\right), \tag{3.4}$$

where $p_{\text{ray}}\left(\gamma_{\text{ray}}\right)$ is exponentially distributed and given in (1.6) [71].

If the instantaneous SNR in the internode channel is greater than or equal to protocol threshold, i.e., $\gamma'_{ij} \geq \gamma_{\text{th}}$, the source node sends its packet through the internode channel immediately. However, if the instantaneous SNR in the internode channel is less than the threshold ($\gamma'_{ij} < \gamma_{\text{th}}$), the source node sends its packets after a delay, regardless the value of instantaneous SNR, γ''_{ij}.

The event that γ'_{ij} is greater than or equal to γ_{th} is denoted with A, while the event that γ'_{ij} is less than γ_{th} is denoted with B. It holds that $\mathbb{P}\left[A\right] = \Pr\left[\gamma'_{ij} \geq \gamma_{\text{th}}\right]$ and $\mathbb{P}\left[B\right] = \Pr\left[\gamma'_{ij} < \gamma_{\text{th}}\right] = 1 - \mathbb{P}\left[A\right]$.

Let γ_{int} denote the RV corresponding to the instantaneous SNR observed at the receiver node. The PDF of the resulting instantaneous PDF is determined by

$$p_{\gamma_{\text{int}}}\left(\gamma_{\text{int}}\right) = \mathbb{P}\left[A\right] p_{\gamma'_{ij}|A}\left(\gamma_{\text{int}}|A\right) + \mathbb{P}\left[B\right] p_{\gamma''_{ij}|B}\left(\gamma_{\text{int}}|B\right). \tag{3.5}$$

From (3.5), the first conditional PDF, $p_{\gamma'_{ij}|A}\left(\gamma_{\text{int}}|A\right)$ can be determined by using the Bayesian rule

$$\mathbb{P}\left[A\right] p_{\gamma'_{ij}|A}\left(\gamma_{\text{int}}|A\right) = \mathbb{P}\left[A|\gamma'_{ij} = \gamma_{\text{int}}\right] p_{\gamma'_{ij}}\left(\gamma_{\text{int}}\right). \tag{3.6}$$

From (3.6) it follows

$$p_{\gamma'_{ij}|A}\left(\gamma_{\text{int}}|A\right) = \frac{\mathbb{P}\left[A|\gamma'_{ij} = \gamma_{\text{int}}\right] p_{\gamma'_{ij}}\left(\gamma_{\text{int}}\right)}{\mathbb{P}\left[A\right]}. \tag{3.7}$$

The conditional probability $\mathbb{P}\left[A|\gamma'_{ij}=\gamma_{\text{int}}\right]$ is given by

$$\mathbb{P}\left[A|\gamma'_{ij}=\gamma_{\text{int}}\right]=\begin{cases}0, & \gamma_{\text{int}}<\gamma_{\text{th}}\\ 1, & \gamma_{\text{int}}\geq\gamma_{\text{th}}\end{cases}. \tag{3.8}$$

The second conditional PDF in (3.5) is just

$$p_{\gamma''_{ij}|B}\left(\gamma_{\text{int}}|B\right)=p_{\text{ray}}\left(\gamma_{\text{int}}\right). \tag{3.9}$$

Combining (3.7) and (3.9) in (3.5), the resulting PDF of γ_{int} is obtained by applying the total probability theorem as

$$\begin{aligned}p_{\gamma_{\text{int}}}\left(\gamma_{\text{int}}\right)&=\mathbb{P}\left[A\right]\frac{\mathbb{P}\left[A|\gamma'_{ij}=\gamma_{\text{int}}\right]p_{\text{ray}}\left(\gamma_{\text{int}}\right)}{\mathbb{P}\left[A\right]}+\mathbb{P}\left[B\right]p_{\text{ray}}\left(\gamma_{\text{int}}\right)\\&=\mathbb{P}\left[A|\gamma'_{ij}=\gamma_{\text{int}}\right]p_{\text{ray}}\left(\gamma_{\text{int}}\right)+\mathbb{P}\left[B\right]p_{\text{ray}}\left(\gamma_{\text{int}}\right).\end{aligned} \tag{3.10}$$

The probability that a cooperating node S_j will successfully decode the packet from source node S_i through an internode channel is the probability that the instantaneous internode SNR is greater than the given outage threshold γ_0, i.e., $p_{\text{dec}_{ij}}=\Pr\left[\gamma_{\text{int}}\geq\gamma_0\right]$, and in the case of Rayleigh fading, this probability takes the form

$$p_{\text{dec}_{ij}}=\exp\left(-\frac{\gamma_{\text{th}}}{\bar{\gamma}_{\text{int}}}\right)\times\left(2-\exp\left(-\frac{\gamma_0}{\bar{\gamma}_{\text{int}}}\right)\right). \tag{3.11}$$

Note that we have two thresholds – the protocol threshold γ_{th} and the outage threshold γ_0. If the protocol threshold is set below the outage threshold, not all packets could be decoded even if the channel quality is good. On the other hand, if γ_{th} is set above the γ_0, packets could be successfully decoded even if the channel is of poorer quality. Therefore, an optimum threshold γ_{th} which minimizes OP exists, and is equal to γ_0 [71].

3.2.2 Correlated internode SNRs

For the case when γ'_{ij} and γ''_{ij} are both are correlated, they have a joint PDF given as [71]

$$p_{\gamma'_{ij}\gamma''_{ij}}\left(\gamma'_{ij},\gamma''_{ij}\right)=\frac{1}{\left(1-\rho\right)\bar{\gamma}_{\text{int}}^2}\exp\left(-\frac{\gamma'_{ij}+\gamma''_{ij}}{\left(1-\rho\right)\bar{\gamma}_{\text{int}}}\right)I_0\left(\frac{2\sqrt{\rho\gamma'_{ij}\gamma''_{ij}}}{\left(1-\rho\right)\bar{\gamma}_{\text{int}}}\right), \tag{3.12}$$

where ρ is the correlation coefficient, assumed to be the same for all links and $I_\nu\left(\cdot\right)$ is the ν-th order modified Bessel function of the first kind.

In the case of correlated Rayleigh fading, successful decoding probability takes the form

$$p_{\text{dec}_{ij}}=1-\int_0^{\gamma_0}\int_0^{\gamma_0}p_{\gamma'_{ij}\gamma''_{ij}}\left(\gamma'_{ij},\gamma''_{ij}\right)\mathrm{d}\gamma'_{ij}\mathrm{d}\gamma''_{ij}. \tag{3.13}$$

Table 3.1: Convergence to the 6-th significant digit of the sum in (3.19).

$\gamma_0 = -0.441$ dB	$\rho = 0.2$	$\rho = 0.4$	$\rho = 0.6$	$\rho = 0.8$	$\rho = 0.9$
$\bar{\gamma}_{\text{int}} = 0$ dB	3	4	6	10	12
$\bar{\gamma}_{\text{int}} = 5$ dB	2	2	4	5	7
$\bar{\gamma}_{\text{int}} = 10$ dB	1	1	1	2	4
$\bar{\gamma}_{\text{int}} = 15$ dB	1	1	1	1	2

Integration over the variable γ'_{ij}, presented in [71, eq. (9.279)] and [113] results in a closed-form expression that includes the Marcum-Q function, defined in [114, eq. (2-1-122)]. Integration over the second variable does not yield a closed-form expression.

To get a more desirable solution, the following derivation uses a series expansion of the 0-th order modified Bessel function of the first kind [80, eq. (447.1)]

$$I_0(z) = \sum_{\kappa=0}^{\infty} \frac{1}{(\kappa!)^2} \left(\frac{z}{2}\right)^{2\kappa}, \tag{3.14}$$

and the joint PDF in (3.12) can be rewritten as

$$p_{\gamma'_{ij}\gamma''_{ij}}\left(\gamma'_{ij}, \gamma''_{ij}\right) = \frac{1}{(1-\rho)\,\bar{\gamma}_{\text{int}}^2} \exp\left(-\frac{\gamma'_{ij} + \gamma''_{ij}}{(1-\rho)\,\bar{\gamma}_{\text{int}}}\right) \times \sum_{\kappa=0}^{\infty} \frac{1}{(\kappa!)^2} \left(\frac{\rho\gamma''_{ij}\gamma''_{ij}}{(1-\rho)^2\bar{\gamma}_{\text{int}}^2}\right)^{\kappa}. \tag{3.15}$$

Substituting (3.12) with (3.15), (3.13) can be written in the form

$$p_{\text{dec}_{ij}} = 1 - \sum_{\kappa=0}^{\infty} \frac{\rho^{\kappa}}{(\kappa!)^2(1-\rho)^{2\kappa+1}\bar{\gamma}_{\text{int}}^{2\kappa+2}} \times \mathcal{I}_1\mathcal{I}_2, \tag{3.16}$$

with

$$\mathcal{I}_1 = \int_0^{\gamma_0} \left(\gamma'_{ij}\right)^{\kappa} \exp\left(-\frac{\gamma'_{ij}}{(1-\rho)\,\bar{\gamma}_{\text{int}}}\right) \mathrm{d}\gamma'_{ij} \tag{3.17}$$

and

$$\mathcal{I}_2 = \int_0^{\gamma_0} \left(\gamma''_{ij}\right)^{\kappa} \exp\left(-\frac{\gamma''_{ij}}{(1-\rho)\,\bar{\gamma}_{\text{int}}}\right) \mathrm{d}\gamma''_{ij}. \tag{3.18}$$

The integrals can be directly solved using [80, eq. (3.351)]; hence, the probability that a cooperating node will successfully decode a data packet from the node S_i is derived in the form of

$$p_{\text{dec}_{ij}} = 1 - (1-\rho)\sum_{\kappa=0}^{\infty} \rho^{\kappa}\left(1 - \frac{1}{\kappa!}\Gamma_i\left(\kappa+1, \frac{\gamma_0}{(1-\rho)\,\bar{\gamma}_{\text{int}}}\right)\right)^2. \tag{3.19}$$

The infinite sum in (3.19) converges very rapidly, as shown in Table 3.1.

The expression in (3.19) gives exact numerical results using only a few terms in the infinite sum. For instance, to achieve accuracy at the 6-th significant digit, only three terms are required for $\rho = 0.2$, and 12 terms for $\rho = 0.9$ when average internode SNR is $\bar{\gamma}_{\text{int}} = 0$ dB. As $\bar{\gamma}_{\text{int}}$ increases, less terms give accurate results, and for $\bar{\gamma}_{\text{int}} = 15$ dB, just one term is sufficient for $\rho = 0.2$ and two terms for $\rho = 0.9$.

3.3 Outage probability analysis

In order to determine the OP in the system, the cases of full and partial cooperation are respectively analysed. Full cooperation is the ideal case, and it assumes that node S_i has successfully decoded all packets from the other cooperating nodes, i.e., error-free communication. The other case, denoted as partial cooperation, models the real-world system behaviour. In partial cooperation, node S_i can fail to decode some of the packets from other nodes due to insufficient received SNR. Node S_i will therefore re-send its own packet copies to the destination, replacing the packets from other nodes it has failed to decode. Furthermore, the overall OP will depend on the number of successfully decoded packets as well as the number of cooperating nodes (nodes which links are not blocked).

As in the previous chapter, p denotes the number of packet copies that the destination receives directly from node S_i in the second stage of cooperation. Similar to (3.1), p is determined by

$$\mathbb{P}[p] = \sum_{\substack{\mathrm{B}_c \subseteq \mathrm{B}_i \\ |\mathrm{B}_c| = n}} \prod_{\lambda \in \mathrm{B}_i} (1 - p_{\mathrm{dec}_{i\lambda}}) \prod_{\eta \in \mathrm{B}_i \setminus \mathrm{B}_c} p_{\mathrm{dec}_{i\eta}}, \tag{3.20}$$

with $p = 0, 1, \ldots, M-1$. Similar to (3.1), B_c, the subset of B_i, denotes the number of packet copies that node S_i re-sends in the second stage of cooperation, and $|\mathrm{B}_c|$ is the cardinality of the set with different combinations of p elements. For the case when all $p_{\mathrm{dec}_{ij}}$ are equal, i.e., $p_{\mathrm{dec}_{ij}} = p_{\mathrm{dec}} \quad \forall i, j \in \{1, \ldots, M\}, \quad i \neq j$, (3.20) has a binomial distribution

$$\mathbb{P}[p] = \binom{M-1}{p} (1 - p_{\mathrm{dec}})^p p_{\mathrm{dec}}^{M-p-1}. \tag{3.21}$$

The instantaneous SNR at the MRC receiver output at the destination is denoted as γ_{mrc}. To determine the OP of the network in the full and partial cooperation cases, it is required to find the individual OPs $P_{\mathcal{F}}(\bar{\gamma}; \gamma_0 | M)$ and $P_{\mathcal{P}}(\bar{\gamma}; \gamma_0 | M, p)$, where $\mathcal{F}$ and $\mathcal{P}$ denote full and partial cooperation, respectively. The full and partial OPs are conditioned on the number of nodes, which in the case of link blockage has a probability given by (3.1). In the case of full cooperation, node S_i has decoded all the packets from other nodes. In this case, the destination combines M copies of the packet, and also, it

holds that $p = 0$. Similar to [71, eq. (9.5)], the conditional OP is

$$P_{\mathcal{F}}\left(\bar{\gamma};\gamma_0|M\right) = 1 - \frac{1}{(M-1)!}\Gamma_i\left(M, \frac{\gamma_0}{\bar{\gamma}}\right). \tag{3.22}$$

In the case of partial cooperation, the number of packets which node S_i transmits in the second stage is $p > 0$. In this case, just from node S_i, the destination receives $p+1$ copies of the packet, where each packet has an average SNR of $\bar{\gamma}$. The destination then applies MRC on the $p+1$ copies (which can be written as a single copy at an SNR value of $(p+1)\bar{\gamma}$) with the remaining $M-p-1$ copies from other cooperating nodes. The OP, conditioned on M and p, can be derived from the MGF of γ_{mrc}. Using partial fractions [69,80] and taking the inverse Laplace transform, the expression for the conditional OP for partial cooperation, similar to [52, eq. (6)], can be written as

$$\begin{aligned} P_{\mathcal{P}}\left(\bar{\gamma};\gamma_0|M,p\right) = 1 &- \exp\left(-\frac{\gamma_0}{(p+1)\,\bar{\gamma}}\right)\left(\frac{p+1}{p}\right)^{M-p-1} \\ &+ \exp\left(-\frac{\gamma_0}{\bar{\gamma}}\right)\sum_{\kappa=0}^{M-p-2}\frac{1}{\kappa!}\left(\left(\frac{p+1}{p}\right)^{M-p-\kappa-1} - 1\right). \end{aligned} \tag{3.23}$$

A piecewise general expression for the OP can be expressed as [52, eq. (7)]

$$P_O(\bar{\gamma};\gamma_0|M,p) = \begin{cases} P_{\mathcal{F}}\left(\bar{\gamma};\gamma_0,M\right), & p = 0, \\ P_{\mathcal{P}}\left(\bar{\gamma};\gamma_0|M,p\right), & p > 0. \end{cases} \tag{3.24}$$

The overall OP for a network of M nodes without link blockage can be obtained by averaging (3.24) over the number of packets received by the destination directly from node S_i in the second stage of cooperation as

$$P_O\left(\bar{\gamma};\gamma_0\right) = \sum_{p=0}^{M-1}\mathbb{P}\left[p\right]P_O\left(\bar{\gamma};\gamma_0|M,p\right). \tag{3.25}$$

Furthermore, taking into account the number of internode links being blocked, N_b, the OP for the blocked case is obtained by averaging (3.25) over the distribution of number of blocked links as

$$P_O\left(\bar{\gamma};\gamma_0\right) = \sum_{N_b=0}^{M-1}\sum_{p=0}^{M-N_b-1}\mathbb{P}\left(N_b\right)\mathbb{P}\left(p\right)P_O\left(\bar{\gamma};\gamma_0|M-N_b,p\right). \tag{3.26}$$

3.4 Asymptotic analysis

We analyse the asymptotic behaviour of the network at high average SNR to gain a better insight on outage performance. As both average uplink and average internode SNR increase, the relation of $\bar{\gamma}$ and $\bar{\gamma}_{\text{int}}$ is examined and presented are OP approximations for two distinct cases, the former being high average internode ($\bar{\gamma}_{\text{int}} \gg \bar{\gamma}$), and the latter being the high average uplink ($\bar{\gamma} \gg \bar{\gamma}_{\text{int}}$) regime. In addition, as the average uplink SNR goes to infinity, asymptotic OP, expressed through coding and diversity gains, given in (1.4), is observed. First, the OP, coding and diversity gains are derived for the non-blocked case, and then extend to the blocked case by averaging over the number of blocked links.

The approximate asymptotic expressions for full and partial conditional outage probabilities when $\bar{\gamma} \gg \gamma_0$, which hold for both cases, are given, respectively, as [52, eq. (15)]

$$P_{\mathcal{F}_{\text{asy}}}\left(\bar{\gamma};\gamma_0|M\right) = \frac{1}{M!}\left(\frac{\gamma_0}{\bar{\gamma}}\right)^M, \tag{3.27}$$

and [52, eq. (16)]

$$P_{\mathcal{P}_{\text{asy}}}\left(\bar{\gamma};\gamma_0|M,p\right) = \frac{1}{(M-p-1)!\,(p+1)}\left(\frac{\gamma_0}{\bar{\gamma}}\right)^{M-p}. \tag{3.28}$$

We utilize the expressions above in the derivation of the asymptotic results.

3.4.1 Case I: Asymptotic internode regime

In the first case, we assume that the average internode SNR is greater than the average uplink SNR (i.e., $\bar{\gamma}_{\text{int}} \gg \bar{\gamma}$), and internode communication is fully reliable. There are no delayed transmissions in the internode protocol. This in turn also results that in the second phase of cooperation, node S_i does not re-send its own packets.

The dominating term in the expression for successful decoding in the internode channel in (3.19) is the first term in the sum, and we can write

$$p_{\text{dec}_{\text{asy}}} = 1 - (1-\rho)\left(1 - \Gamma_i\left(1, \frac{\gamma_0}{(1-\rho)\,\bar{\gamma}_{\text{int}}}\right)\right)^2. \tag{3.29}$$

Furthermore, from $\bar{\gamma}_{\text{int}} \gg \bar{\gamma} \gg \gamma_0$, the approximation $\frac{1}{N!}\Gamma_i\left(N+1,z\right) \approx 1 - \frac{z^{N+1}}{\Gamma(N+2)}$ is applied, and after some mathematical manipulations, the approximation for successful internode decoding is obtained as

$$p_{\text{dec}_{\text{asy}}} = 1 - \frac{1}{(1-\rho)}\left(\frac{\gamma_0}{\bar{\gamma}_{\text{int}}}\right)^2. \tag{3.30}$$

By inserting (3.27) and (3.30) into (3.25), the expression for asymptotic OP without link blockage can therefore be written as

$$P_{O_{\text{asy}}}(\bar{\gamma};\gamma_0) = \frac{1}{M!}\left(\frac{\gamma_0}{\bar{\gamma}}\right)^M \left(1 - \frac{1}{(1-\rho)}\left(\frac{\gamma_0}{\bar{\gamma}_{\text{int}}}\right)^2\right)^{M-1}. \tag{3.31}$$

As $\bar{\gamma}$ goes to infinity, we observe the coding and diversity gains. Directly from (3.31), and using $\bar{\gamma}_i \gg \gamma_0$, the gains are obtained as

$$\mathcal{G}_{c_i} = \frac{(M!)^{1/M}}{\gamma_0}, \quad \mathcal{G}_{d_i} = M. \tag{3.32}$$

Next, we will be examining the impact of link blockage. Averaging the OP (3.31) over the number of blocked links we obtain the OP in the high average internode regime in the case of link blockage as

$$\begin{aligned} P_{O_{\text{asy}}}(\bar{\gamma};\gamma_0) = \sum_{N_b=0}^{M-1} \mathbb{P}[N_b] \frac{1}{(M-N_b)!}\left(\frac{\gamma_0}{\bar{\gamma}}\right)^{M-N_b} \\ \times \left(1 - \frac{1}{(1-\rho)}\left(\frac{\gamma_0}{\bar{\gamma}_{\text{int}}}\right)^2\right)^{M-N_b-1}. \end{aligned} \tag{3.33}$$

Bearing in mind that there exists a finite probability that all internode links are blocked, outage performance will be dominated by the case when the only active link is the direct link from node S_i to the destination. Diversity gain is therefore reduced to one, and the coding gain is obtained from (3.33) when $N_b = M-1$, i.e., when all internode links are blocked. The gains are therefore

$$\mathcal{G}_{c_i} = \frac{1}{\gamma_0 b_i^{M-1}}, \quad \mathcal{G}_{d_i} = 1. \tag{3.34}$$

3.4.2 Case II: Asymptotic uplink regime

In the second case, the average uplink SNR is greater than the average internode SNR ($\bar{\gamma} \gg \bar{\gamma}_{\text{int}}$). Performance is determined by the case when all internode channels fail, and nodes cannot successfully decode packets originating from node S_i. In this case, all packets are re-sent directly from the initial node S_i in the second stage of cooperation. This behaviour can be analytically expressed as, when calculating the OP, the only term in the sum w.r.t. n in (3.25) is the last, $(M-1)$-st term. The outage probability can therefore be calculated inserting (3.28) into (3.25) for $p = M-1$, without blockage, as

$$P_{O_{\text{asy}}}(\bar{\gamma};\gamma_0) = \frac{1}{M}\left(\frac{\gamma_0}{\bar{\gamma}}\right)\left(1 - p_{\text{dec}_{\text{asy}}}\right)^{M-1}. \tag{3.35}$$

It is worth noting that, in the expression above, $p_{\text{dec}_{\text{asy}}}$ cannot be approximated to the first term as in (3.30), as the ratio between $\bar{\gamma}_{\text{int}}$ and γ_0 can be arbitrary. The

approximation for successful internode packet decoding from (3.30) is accurate only for $\bar{\gamma}_{\text{int}} \gg \gamma_0$. Rather, the exact probability of successful packet decoding in (3.19) is used.

In a similar fashion to the internode regime, from (3.35) the coding and diversity gains for high average uplink SNR regime, when $\bar{\gamma} \to \infty$, are given respectively, as

$$\mathcal{G}_{c_u} = \frac{M}{\gamma_0 \left(1 - p_{\text{dec}_{\text{asy}}}\right)^{M-1}}, \quad \mathcal{G}_{d_u} = 1. \tag{3.36}$$

However, for the ratio $\bar{\gamma}_{\text{int}} \gg \gamma_0$, in accordance with Table 3.1, only the first term in (3.19) is sufficient, and we can apply the approximation for successful internode channel decoding (3.29). For this case, $\mathcal{G}_{d_u}$ remains equal to one, but one can see more clearly the impact of the correlation coefficient ρ on $\mathcal{G}_{c_u}$ as

$$\mathcal{G}_{c_u} = \frac{M}{\gamma_0 \left(\frac{1}{(1-\rho)} \left(\frac{\gamma_0}{\bar{\gamma}_{\text{int}}} \right)^2 \right)^{M-1}}, \quad \mathcal{G}_{d_u} = 1. \tag{3.37}$$

Finally, when we take into account the probability of link blockage, we can write the asymptotic expression for the high average uplink SNR regime, from (3.35), as

$$P_{O_{\text{asy}}}\left(\bar{\gamma}; \gamma_0\right) = \sum_{N_b=0}^{M-1} \mathbb{P}\left[N_b\right] \frac{1}{(M - N_b)} \left(\frac{\gamma_0}{\bar{\gamma}} \right) \left(1 - p_{\text{dec}_{\text{asy}}}\right)^{M-N_b-1}. \tag{3.38}$$

From (3.38), the coding and diversity gains for the high average uplink SNR regime with link blockage can be directly obtained as

$$\mathcal{G}_{c_u} = \frac{1}{\gamma_0 \sum\limits_{N_b=0}^{M-1} \mathbb{P}\left[N_b\right] \frac{\left(1-p_{\text{dec}_{\text{asy}}}\right)^{M-N_b-1}}{(M-N_b)}}, \quad \mathcal{G}_{d_u} = 1. \tag{3.39}$$

3.5 Numerical results

The expressions derived in the previous section are used to efficiently compute numerical values of OP for any practical value of average SNRs over internode and uplink channels, correlation coefficient and network dimension. The threshold for successfully decoding packets depends on the coding scheme used and on the packet length L, as derived in [111]. The optimum threshold is set to $\gamma_0 = -0.441$ dB, which describes a network where each node encodes a packet of length $L = 512$ bits using a convolutional coding scheme with 1/2 code rate with octal generator polynomials $(1, 17/15)$, [111]. In addition, average internode SNRs are assumed to be equal due to simpler mathematical tractability, except in Fig. 3.7, where average internode SNRs follow an exponential power profile [115]. All exact results are confirmed by independently run Monte-Carlo simulations.

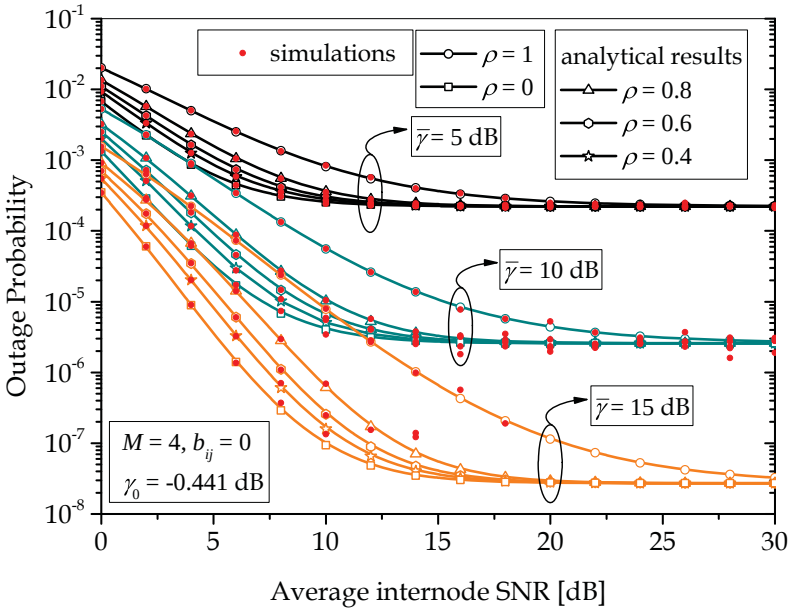

Figure 3.3: Outage probability dependence on average internode SNR for different values of correlation coefficient ρ and average uplink SNR.

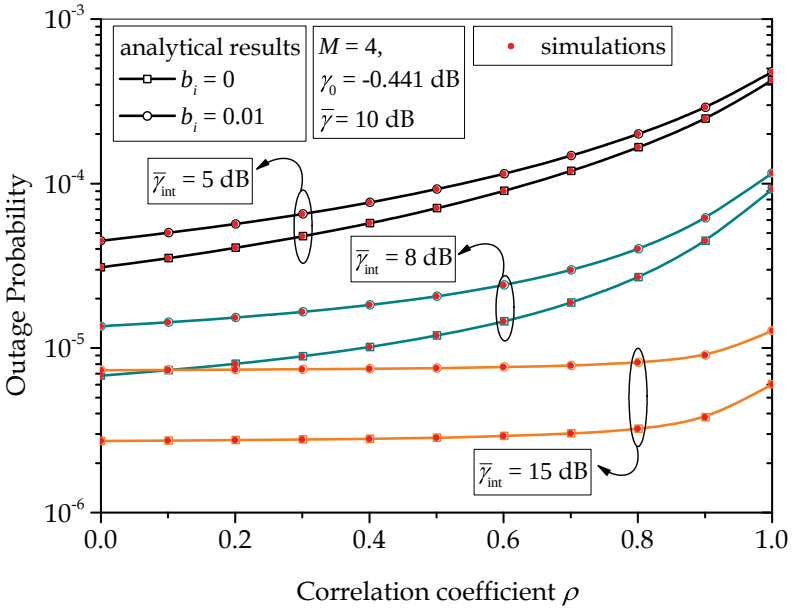

Figure 3.4: Outage probability dependence on correlation coefficient for different values of average internode SNR $\bar{\gamma}_{\mathrm{int}}$.

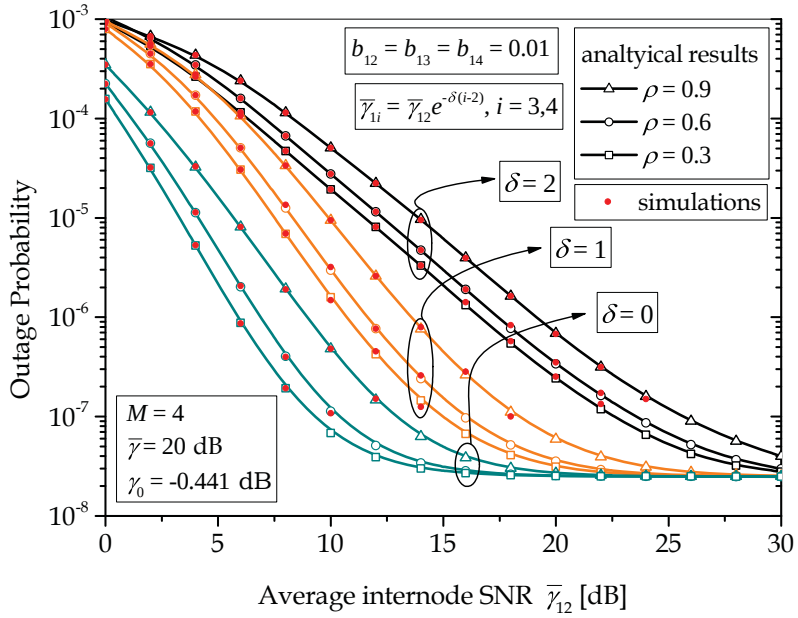

Figure 3.5: Outage probability dependence on average internode SNR $\bar{\gamma}_{12}$ for different δ.

Fig. 3.3 shows the OP as a function of average internode SNR, for various values of average uplink SNR and correlation coefficient ρ. The results for the full correlation limiting case coincide with the results when the threshold-based protocol is not used, as presented in [52]. This additional curve from [52], alongside the curve when internode SNR instances are uncorrelated act as upper and lower bounds, for the limiting cases when ρ approaches one (full correlation) and zero (no correlation), respectively. For higher average internode SNR, on the average, internode channel state will be above the threshold. This results in less packet errors between the nodes, obtaining better performance until a floor is reached. The impact of correlation is dominant in the low average internode SNR regime. For instance, for $\bar{\gamma}_{\text{int}} =$ 10 dB, when ρ increases from 0 to 1, P_0 increases 85.1 times for $\bar{\gamma} = 15$ dB, and only 3.5 times for $\bar{\gamma} = 5$ dB. For greater values of $\bar{\gamma}_{\text{int}}$ correlation does not have an impact on OP. All curves corresponding to different values of ρ tend to an outage floor that does not depend on ρ.

Fig. 3.4 further shows outage probability dependence on the correlation coefficient for different values of average internode SNR for a network without and with link blockage. As expected, increasing the correlation between fading samples in internode communication, outage performance is degraded. However, by increasing $\bar{\gamma}_{\text{int}}$ the probability of delayed internode packet transmissions decreases, and the impact of correlation on the system performance becomes less significant. The difference in OP when link blockage exists, when compared to the non-blocked case, is more apparent for higher $\bar{\gamma}_{\text{int}}$.

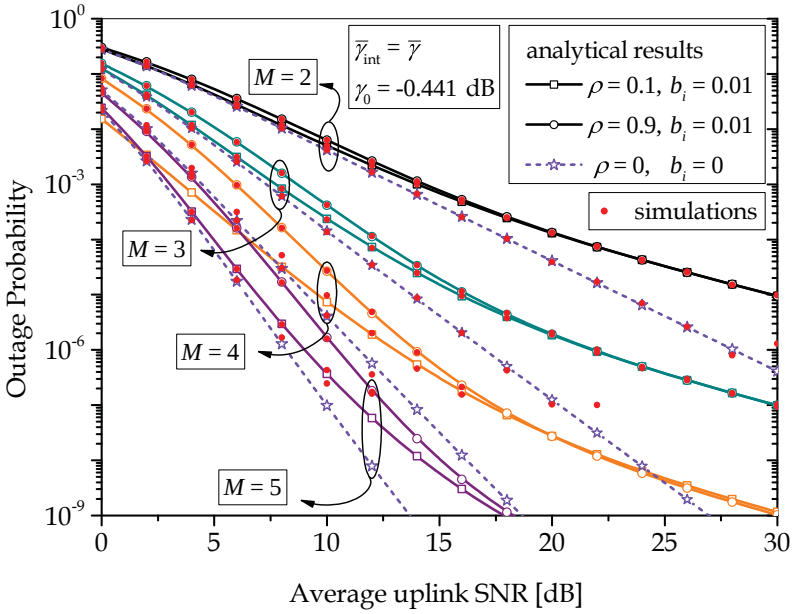

Figure 3.6: Outage probability dependence on average uplink SNR $\bar{\gamma}$ for different number of nodes and different ρ.

In Fig. 3.5, average internode SNRs are unequal and follow the exponential power profile [115], given as $\bar{\gamma}_{1j} = \bar{\gamma}_{1i}\exp\left(-\delta\left(j-2\right)\right)$, where $i, j = 1, \ldots, M$, $i \neq j$ and δ is an non-negative integer. Increasing δ, outage saturation is reached at higher $\bar{\gamma}_{12}$. For $\delta = 0$, all internode SNRs are equal and the outage floor is reached at $\bar{\gamma}_{12} = 20$ dB. Outage probability increases with increasing δ, and the required $\bar{\gamma}_{12}$ to reach the floor shifts from 20 dB to 28 dB as δ goes from 0 to 1.

Fig. 3.6 shows outage probability dependence on average uplink SNR for different number of nodes M and correlation coefficient ρ. Average internode SNRs increase simultaneously with the average uplink SNRs. The impact of correlation is stronger at lower average SNR, and is more pronounced for higher network dimension. For instance, at $\bar{\gamma} = 5$ dB, as ρ decreases from 0.9 to 0.1 OP drops only 1.266 times for $M = 2$, while for $M = 5$, outage is 4.83 times lower. When the blockage probability is different from zero, in the high average SNR regime correlation has no impact on outage for any network size. Additionally, the finite blockage probability causes the slope of the outage curves to approach diversity order one at high SNR for any number of nodes (because the node's uplink channel is always available), and diverge from the non-blocked case, presented by the dashed curves. Note that in the non-blocked case, outage curves have diversity order M.

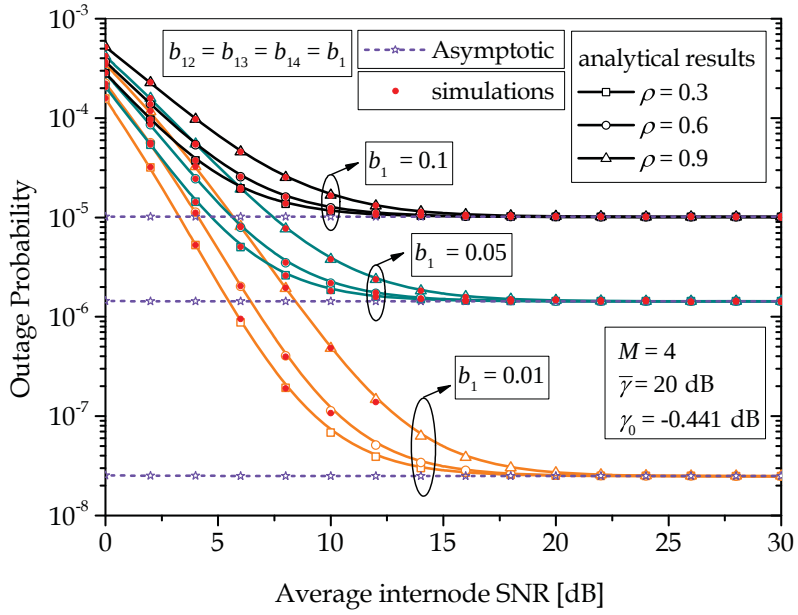

Figure 3.7: Outage probability dependence on average internode SNR for different blockage probabilities b_i.

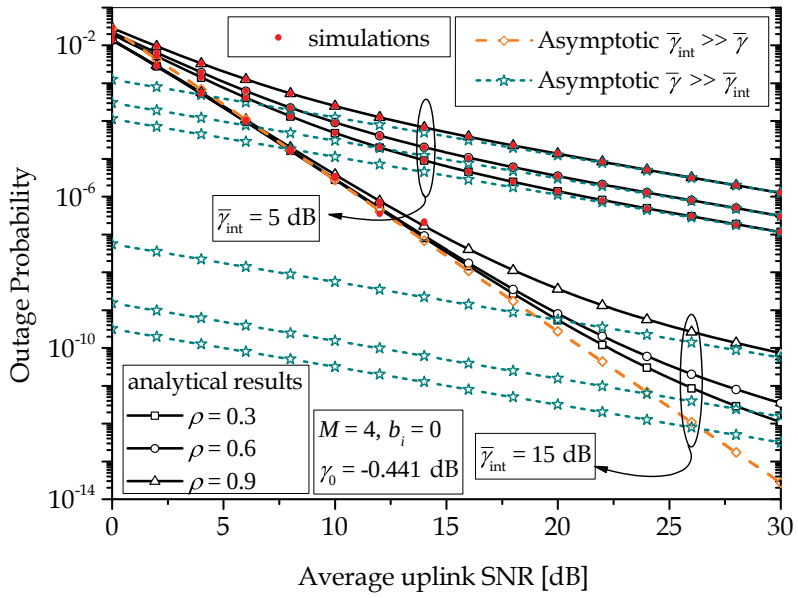

Figure 3.8: Outage probability dependence on average uplink SNR for different values of correlation coefficient ρ.

The effects of different blockage probabilities are shown in Fig. 3.7. Even for high average uplink SNR $\bar{\gamma}$, the impact of link blockage is dominant. As b_{ij} increases, the floor is reached at a smaller value of OP. For instance, at $b_{ij} = 0.01$ the outage floor of 2.6×10^{-8} is reached at about $\bar{\gamma} = 20$ dB, while at $b_{ij} = 0.1$, the floor of 10^{-5} is reached at $\bar{\gamma} = 15$ dB. In the asymptotic average internode SNR regime with fixed average uplink SNR, one can notice that the outage does not depend on internode communication. The value of the outage floor can be obtained using (3.27), as

$$P_{\text{FLOOR}}\left(\bar{\gamma};\gamma_0\right) = \sum_{N_b=0}^{M-1} \mathbb{P}\left[N_b\right] P_{\mathcal{F}_{\text{asy}}}\left(\bar{\gamma};\gamma_0|M\right). \tag{3.40}$$

When plotting the OP dependence on average uplink SNR in Fig. 3.8, the effect of correlation in the internode communication protocol can be observed. Asymptotic expressions for both high average internode and average uplink SNR are plotted as well. Orange curves represent the high average internode regime, and are plotted for $\bar{\gamma}_{\text{int}} = 15$ dB, and are a good match for the exact curves until $\bar{\gamma} = 12$ dB, as expected. On the other hand, for $\bar{\gamma}_{\text{int}} = 5$ dB, the teal curves, for the high average uplink regime, are a good match beyond $\bar{\gamma} = 16$ dB, and for $\bar{\gamma}_{\text{int}} = 15$ dB beyond $\bar{\gamma} = 30$ dB.

One can also notice the diversity and coding gains on the asymptotic curves. As expected, at high average internode SNR, the diversity gain is determined by the slope of the orange curve, and is equal to M, while for high average uplink SNR, all teal curves are diversity order one. Coding gain in the high average internode regime does not depend on the correlation in the internode protocol (all three orange curves are overlapping), while ρ has a significant impact in the high average uplink SNR regime.

Finally, Fig. 3.9 shows OP dependence on average uplink SNR for different values of node blockage b_i. Exact and asymptotic results are presented. As b_i increases, OP converges to a single-link case (with no cooperation). The additional, single-link curve is plotted as well for comparison. Furthermore, asymptotic results, in both the high average internode SNR from (3.33), and high average uplink SNR from (3.38), converge to the exact value of the OP as b_i increases. The slope of the $\bar{\gamma}_{\text{int}} \gg \bar{\gamma}$ asymptotic curves changes from being very high at low $\bar{\gamma}$, but reduces to first order diversity as $\bar{\gamma}$ increases. For instance, for $b_i = 0.01$, the slope tends to full order diversity, (as in Fig. 3.8, with no blockage) for $\bar{\gamma} < 15$ dB. However, due to link blockage, this slope tends to first order diversity as $\bar{\gamma}$ goes above 15 dB. As b_i decreases, the slope turning point tends to the fixed value of the average internode SNR.

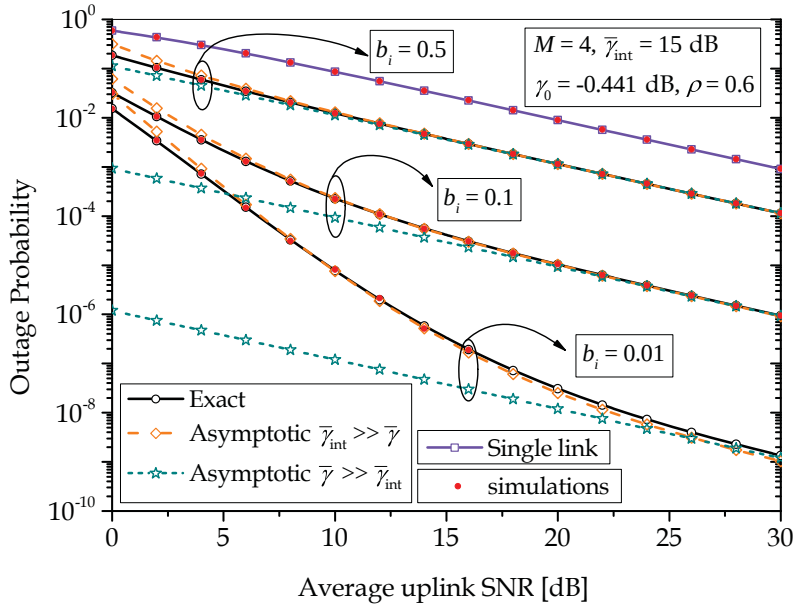

Figure 3.9: Outage probability dependence on average uplink SNR for different blockage probabilities b_i.

3.6 Conclusion

In this chapter, a DF cooperative wireless network prone to link blockage over temporally correlated Rayleigh fading between nodes has been investigated, and novel exact and asymptotic expressions for OP have been derived. Based on these expressions, the OP dependence on different channel and network parameters, as are link blockage probability, number of nodes in the network, average SNR over uplink and internode channels, as well as temporary fading correlation have been analysed. Asymptotic results demonstrate the interplay of high average uplink and internode SNRs on outage performance. The derived asymptotic expressions, which are more tractable from an engineering point of view, emphasize network behaviour at high average SNR regimes.

The presented numerical results demonstrate that fading correlation over the internode channels has a stronger influence on outage for greater values of average uplink SNR, and at low ranges of average internode SNR. At high average internode SNR, the impact of correlation even diminishes. Moreover, as the network size increases, correlation has greater impact on OP.

The results have shown that the presence of finite link blockage causes significant performance degradation, reducing the diversity order of the system to a single-link case with diversity order one. This non-negligible performance loss is present regardless of

the correlation coefficient in the threshold-based internode protocol. Furthermore, by increasing link blockage probability by one order of magnitude, the OP is increased by several orders of magnitude.

Chapter 4

Performance analysis of DF cooperative wireless networks with internode SR-ARQ

Whereas in the previous chapter only OP was used as a performance metric, in this chapter, both OP and PER of a DF wireless cooperative network are analysed. Firstly, in order to compare results presented in the previous chapter, outage analysis which utilizes SR-ARQ in internode communication is performed over a network subject to Rayleigh fading. In the observed system, only source node pairs exchange Acknowledgement (ACK)/Negative Acknowledgement (NAK) messages, retaining the focus on improving internode communication. Afterwards, an extension to Nakagami-m fading channels is presented, in order to examine the impact of fading severity on outage performance. Finally, using a simple but tight PER approximation, end-to-end PER performance is investigated. Closed-form exact analytical results are derived and confirmed by Monte-Carlo simulations. The impact of average SNR values, network dimension and number of retransmission attempts is discussed.

When the SR-ARQ scheme is used with maximally one retransmission attempt, results are comparable with the ones obtained with the threshold-based protocol. Increasing the number of maximum retransmission attempts, OP can be lowered, but with a price – each time a source node re-sends its data packet to another node, a delay of one time slot is added.

Furthermore, both source nodes and the destination require more complexity. A feedback message mechanism has to be implemented at the source nodes, and a combining mechanism, which can account for variable cooperation frame size. The choice of internode protocols can be considered a trade-off between low-latency (threshold-based) and no data loss (SR-ARQ) communication.

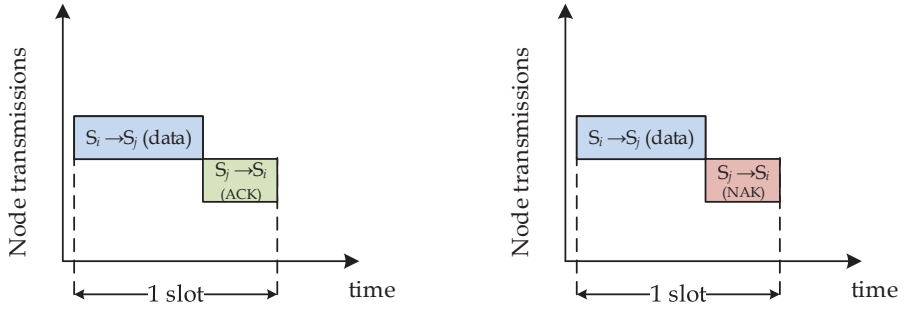

(a) Node S_i receives an ACK from S_j and no retransmissions are included.

(b) Node S_i receives a NAK from S_j and sends its packet again in the next time slot.

Figure 4.1: Feedback mechanism and packet retransmission using the SR-ARQ scheme.

4.1 System model

The system model in this chapter is the same as in the general model. Source nodes S_i, $i \in \{1, \ldots, M\}$ send their data over the uplink channel to the destination D, and cooperate among themselves over internode channels. Both node positioning cases can be considered; nodes can be grouped together as in Fig. 1.9(a) or placed around the destination as in Fig. 1.9(b). The whole network is subject to Rayleigh fading. Blockage is not taken into account in this chapter, but without loss of generality it can be modelled as in Chapter 3. Adding blockage will only add one level of averaging on the derived OP or PER expressions, as the number of active nodes will become a RV with Probability Mass Function (PMF) given in either (3.1) or (3.2).

With internode channel reciprocity assumed, a source node that forwards a partner's data packet will have its own packet forwarded by that node as well. Each node transmits on orthogonal channels, hence no interference is present. However, channel orthogonality can also be a limiting factor – the number of nodes cannot exceed the number of available orthogonal channels. In practical systems, such as Ultra wideband IEEE 802.15.3a specification, orthogonality is achieved using OFDM in the 2.4 GHz and 5 GHz bands [116]. Additionally, ZigBee, which follows the IEEE 802.15.4 standard and uses Direct-Sequence Spread Spectrum (DSSS) [4], can operate in the 868 MHz band as well.

Node cooperation is done in a two-stage approach.

In the first stage, source nodes broadcast their packets to the destination and to the other nodes in the network. After the initial broadcast, each node will try to decode packets received from other nodes. If a packet is successfully decoded, an ACK packet is

sent to the corresponding node, while a NAK is sent otherwise. Since channel reciprocity is assumed, the exchange of ACK/NAK messages is carried out only in one direction between a node pair, i.e., if S_i succeeds or fails in decoding a packet from S_j, then S_i assumes that in turn, its own packet has also been respectively decoded or dropped by S_j. Both cases are shown in Fig. 4.1.

In the second stage, if a node decodes a partner's packet, it will forward that packet to the destination. The ACK from the partner node guarantees that in return, the partner node will do the same. However, if a node receives a NAK, it will send its own packet to that node in the next, independently faded time slot, which creates a one-slot time delay. This process continues until an ACK is received, or until the maximum number of retransmission attempts is reached. Upon receiving a NAK after the maximum number of retransmissions, the node will simply drop cooperation and re-send its packet directly to the destination. This process is repeated for every partner node. By adding more time slots caused by retransmissions, the whole cooperation frame is no longer constant. It is assumed that the feedback packets containing ACK/NAK messages are always transmitted correctly, which can be achieved by powerful Forward Error Correction (FEC) codes.

Unless otherwise stated, a maximum of one retransmission attempt is used throughout the chapter, which is a valid assumption for real-time communication [56].

4.2 Outage probability analysis

At the beginning of cooperation, source node S_i broadcasts its packet to all other nodes and the destination, and receives packets from other nodes. Out of $(M-1)$ packets, S_i fails to decode p packets from other nodes. Owing to simplicity, the probability of p unsuccessfully decoded packets has a binomial distribution, given in (3.21). However, whereas in Chapter 3 the decoding probability is based on monitoring the instantaneous internode SNR, a simple *on-off* rule is used in this chapter. Namely, a packet is fully decoded if the instantaneous internode SNR is greater than the threshold γ_0 [51,52,111]. For Rayleigh fading, this can be written as

$$p_{\text{dec}} = \exp\left(-\frac{\gamma_0}{\bar{\gamma}_{\text{int}}}\right). \tag{4.1}$$

With the ARQ scheme applied, out of (M–1) possible partners in the network, node S_i has failed to decode p packets and sends p NAK packets. Due to internode channel reciprocity, it will also receive a total of p NAK packets from other nodes. It will then re-transmit its own packet to the nodes that have sent NAKs, anticipating successful decoding from other nodes. In addition, the packets that S_i has failed to decode are retransmitted by other nodes to node S_i.

After the retransmissions, node S_i still has sent and received a total of $p_{[1]} \leq p$ NAK packets. With no further retransmission attempts, node S_i will send its own packet to the destination another $p_{[1]}$ times. The probability that the destination will receive the $p_{[1]}$ packets from node S_i has also a binomial distribution

$$\mathbb{P}\left[p_{[1]}\right] = \binom{p}{p_{[1]}}(1-p_{\text{dec}})^{p_{[1]}}{p_{\text{dec}}}^{p-p_{[1]}}, \quad p_{[1]} \in \{0., \ldots, p\}. \tag{4.2}$$

Ideally, internode channels are fully reliable and no retransmissions are needed. In practice, nodes will operate in partially cooperate based on the ACK/NAK feedback from other nodes, and choose which packets to forward, and how many copies of its own packets to re-send to the destination.

When all nodes have successfully decoded and forwarded the packets originating from node S_i, D combines M copies of the packet received through M independent paths. The OP of the combined SNR for this case is the OP for the full cooperation mode $P_{\mathcal{F}}\left(\bar{\gamma}; \gamma_0 | M\right)$, given in (3.22).

Similar to the partial cooperation case in the previous chapter, after the maximum number of retransmission attempts is reached, the destination combines the $\left(p_{[1]}+1\right)$ repeated copies sent directly from node S_i, with the $(M–p_{[1]}–1)$ relayed copies from other nodes. The conditional OP for the partial case, $P_{\mathcal{P}}\left(\bar{\gamma}; \gamma_0 | M, p_{[1]}\right)$ will have the same expressions as (3.23), with p replaced with $p_{[1]}$. The resulting expression for OP will be similar to (3.24),

$$P_O(\bar{\gamma}; \gamma_0 | M, p_{[1]}) = \begin{cases} P_{\mathcal{F}}\left(\bar{\gamma}; \gamma_0, M\right), & p_{[1]} = 0, \\ P_{\mathcal{P}}\left(\bar{\gamma}; \gamma_0 | M, p_{[1]}\right), & p_{[1]} > 0. \end{cases} \tag{4.3}$$

Finally, the OP is obtained by averaging (4.3) over the number of received packets directly from node S_i in the second stage of cooperation after the retransmission, i.e., averaging is performed over both p and $p_{[1]}$, given in (3.21) and (4.2) respectively, obtaining

$$P_O\left(\bar{\gamma}; \gamma_0\right) = \sum_{p=0}^{M-1} \mathbb{P}\left[p\right] \sum_{p_{[1]}=0}^{p} \mathbb{P}\left[p_{[1]}\right] P_O\left(\bar{\gamma}; \gamma_0 | M, p_{[1]}\right). \tag{4.4}$$

Additionally, if the number of retransmission attempts increases, the number of averaging over binomially distributed RVs increases as well. For instance, for two retransmission attempts, the OP expression is given as

$$P_O\left(\bar{\gamma}; \gamma_0\right) = \sum_{p=0}^{M-1} \mathbb{P}\left[p\right] \sum_{p_{[1]}=0}^{p} \mathbb{P}\left[p_{[1]}\right] \sum_{p_{[2]}=0}^{p_{[1]}} \mathbb{P}\left[p_{[2]}\right] P_O\left(\bar{\gamma}; \gamma_0 | M, p_{[2]}\right), \tag{4.5}$$

where $p_{[2]} \in \{0, \ldots, p_{[1]}\}$ is the number of repeated packets from S_i after the second retransmission attempt.

In general, for $\kappa_{\max}$ retransmission attempts, (4.4) expands to

$$P_{\mathcal{O}}\left(\bar{\gamma};\gamma_0\right)=\sum_{p=0}^{M-1}\mathbb{P}\left[p\right]\prod_{\kappa=1}^{\kappa_{\max}}\sum_{p_{[\kappa]}=0}^{p_{[\kappa-1]}}\mathbb{P}\left[p_{[\kappa]}\right]P_{\mathcal{O}}\left(\bar{\gamma};\gamma_0|M,p_{[\kappa_{\max}]}\right), \tag{4.6}$$

where it holds that $p_{[0]}=p$.

4.3 Extension to Nakagami-m fading

Extending to the Nakagami-m fading, it is possible to analyse fading conditions that can have a LoS component, as well as severe fading, even more severe than Rayleigh. The analysis of cooperative networks with repetitive schemes was analysed in [9, 53], and in this section their results are improved by adding SR-ARQ.

Firstly, the probability of successful decoding, given in (4.1) for Rayleigh channels is from (1.10) given as

$$p_{\text{dec}}=\frac{1}{\Gamma\left(m\right)}\Gamma_i\left(m,\frac{m\gamma_0}{\bar{\gamma}_{\text{int}}}\right). \tag{4.7}$$

As in (1.11), the Gamma functions can be reduced to a finite sum for integer values of the fading parameter m.

When there are no repetitions, the destination applies MRC on the M packets arriving on i.i.d. Nakagami-m faded paths and the conditional OP is given as [71]

$$P_{\mathcal{F}}^{(\text{naka})}\left(\gamma;\gamma_0|M\right)=1-\frac{1}{\Gamma\left(Mm\right)}\Gamma_i\left(Mm,\frac{m\gamma_0}{\bar{\gamma}}\right). \tag{4.8}$$

For integer m (4.8) reduces to

$$P_{\mathcal{F}}^{(\text{naka})}\left(\bar{\gamma};\gamma_0|M\right)=1-\exp\left(-\frac{m\gamma_0}{\bar{\gamma}}\right)\sum_{\kappa=0}^{Mm-1}\frac{1}{\kappa!}\left(\frac{m\gamma_0}{\bar{\gamma}}\right)^{\kappa}. \tag{4.9}$$

Note that (4.8) and (4.9) are equal to the CDF expressions for the "mrc" mode in the special Nakagami-m case in Chapter 2, given in (2.12) and (2.13), respectively.

For the partial cooperation case, the conditional OP has been derived for the integer case as [53]

$$\begin{aligned}P_{\mathcal{P}}\left(\bar{\gamma};\gamma_0|M,p\right)=&\sum_{\kappa_1=1}^{m}\left(-1\right)^{-\kappa_1+1}\left(p_{[1]}+1\right)^{-\kappa_1+1}\left(\frac{p_{[1]}}{p_{[1]}+1}\right)^{-ml-\kappa_1+1}\\&\times\binom{ml+\kappa_1-2}{\kappa_1-1}\left(1-\frac{1}{(m-\kappa_1)!}\Gamma_i\left(m-\kappa_1+1,\frac{m\gamma_0}{\bar{\gamma}\left(p_{[1]}+1\right)}\right)\right)\\&+\sum_{\kappa_2=1}^{ml}\left(-1\right)^{-m}\left(p_{[1]}+1\right)^{-m}\left(\frac{p_{[1]}}{p_{[1]}+1}\right)^{-m-\kappa_2+1}\\&\times\binom{m+\kappa_2-2}{\kappa_2-1}\left(1-\frac{1}{(ml-\kappa_2)!}\Gamma_i\left(ml-\kappa_2+1,\frac{m\gamma_0}{\bar{\gamma}}\right)\right)\end{aligned} \tag{4.10}$$

where $l = (M - p_{[1]} - 1)$ is the number of packet copies arriving from source node S_i after the maximum number of retransmissions is reached. As in the Rayleigh case, OP is obtained averaging over $p_{[1]}$ and $p_{[0]}$.

4.4 Packet Error Rate analysis

The exact PER for uncoded packets, i.e., when no FEC codes are applied, for given instantaneous SNR can be expressed as [114]

$$P_e(\gamma) = 1 - (1 - P_b(\gamma))^L, \tag{4.11}$$

where $P_b(\gamma)$ is the BER and L is the packet length. Applying a block code with l-bit correction capability, PER is given as [114]

$$P_e(\gamma) = 1 - \sum_{\kappa=0}^{l} \binom{L}{\kappa} (P_b(\gamma))^{\kappa} (1 - P_b(\gamma))^{L-\kappa}. \tag{4.12}$$

Averaging (4.11) or (4.12) over γ with PDF $p_\gamma(\gamma)$, the expression for average PER becomes

$$P_E(\bar{\gamma}) = \int_0^{\infty} P_e(\gamma)\, p_\gamma(\gamma)\, \mathrm{d}\gamma. \tag{4.13}$$

Notice that (4.13) can be quite cumbersome to evaluate, and approximate expressions have been encountered in literature [111, 112, 117–119].

In this chapter, the expressions for OPs derived in the previous section are used to approximate average PER using methods described in [111, 112]. Note that although the analysis builds upon these approximations, the addition of the SR-ARQ scheme in internode communication further expands already published results.

For a given arbitrary threshold γ_0, (4.13) can be re-written as [111]

$$P_E(\bar{\gamma}) = \mathbb{P}[\text{error}|\gamma < \gamma_0]\, \mathbb{P}[\gamma < \gamma_0] + \mathbb{P}[\text{error}|\gamma \geq \gamma_0]\, \mathbb{P}[\gamma \geq \gamma_0]. \tag{4.14}$$

As stated in Section 2.2, the "waterfall" threshold, divides the range of SNR into a high and low SNR regions. In terms of probabilities, this can be written as [111, 120]

$$\mathbb{P}[\text{error}|\gamma < \gamma_0] \approx 1 \tag{4.15}$$

and

$$\mathbb{P}[\text{error}|\gamma \geq \gamma_0] \approx 0. \tag{4.16}$$

Subsittuting (4.15) and (4.16) in (4.14), the approximation for PER is obtained as [111]

$$P_E(\bar{\gamma}) \approx \mathbb{P}[\text{error}|\gamma < \gamma_0]\, \mathbb{P}[\gamma < \gamma_0] = \mathbb{P}[\gamma < \gamma_0] = P_\gamma(\gamma_0). \tag{4.17}$$

Table 4.1: Values of PER threshold for different coding schemes used.

Packet length	Uncoded	Convolutional coded	Turbo coded
$L = 256$ bits	5.782 dB	−0.983 dB	−4.401 dB
$L = 1024$ bits	7.083 dB	0.023 dB	−4.312 dB

As PER is approximated with the CDF of γ with argument γ_0, and using (1.3), PER is expressed in terms of OP, i.e.,

$$P_E\left(\bar{\gamma}\right) \simeq P_O\left(\bar{\gamma}; \gamma_0\right). \tag{4.18}$$

Applying the approximation in the equation above, end-to-end PER of a cooperative wireless network is obtained by setting the outage threshold value to the value of the "waterfall" threshold.

Besides evaluating PER threshold values for uncoded signals using BPSK at various packet lengths, the authors of [111] also obtained values for both convolutional coded and turbo coded signals. These threshold values, given in Table 4.1 are used when evaluating numerical results presented in the following section.

4.5 Numerical results

In this section, the results for OP when applying the SR-ARQ scheme are compared with those obtained in the previous chapter, using the internode threshold-based protocol. Afterwards, numerical results showing PER performance are presented.

Fig. 4.2 shows OP dependence on average uplink SNR for different number of nodes in the network, and different protocols used. Average internode SNR increases simultaneously with the uplink. With either of the protocols used, increasing network size will increase the diversity order of the network, and this also holds when no protocol is used. However, by implementing the threshold-based protocol, or SR-ARQ, a gain can be observed over all ranges of $\bar{\gamma}$.

Moreover, when a maximum of one retransmission attempt is used in the ARQ protocol, outage performance is, on average, comparable to the case when the threshold-based protocol is used. This is somewhat expected – although using different mechanisms, both protocols exploit the internode channel, either by monitoring the instantaneous SNR in the threshold-based case, or by re-sending a data packet if the internode channel was too poor for successful decoding.

However, by applying the SR-ARQ scheme, source node S_i may send its data packet in the initial stage twice, while only one transmission is used in the threshold-based

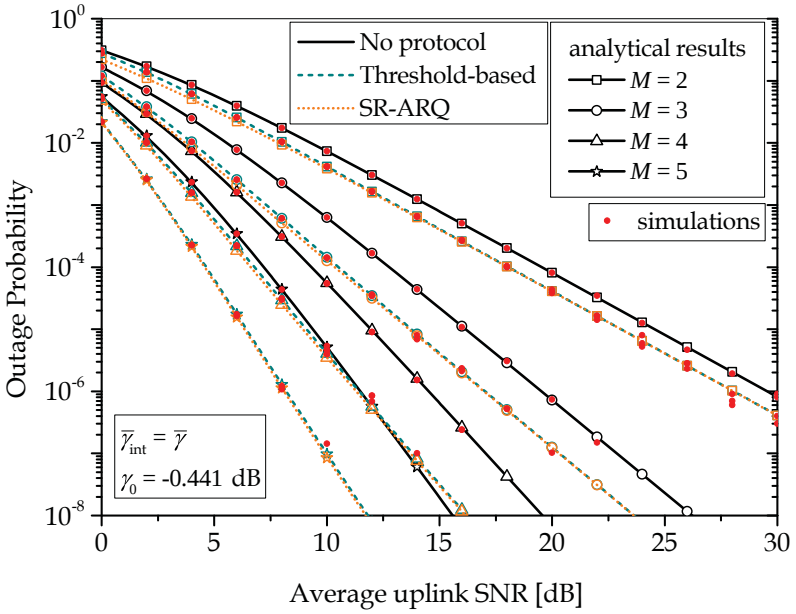

Figure 4.2: Outage probability dependence on average uplink SNR for different network size and different protocols used over Rayleigh fading.

approach. Furthermore, the energy and duration of a cooperative frame remains constant using the threshold-based protocol, while a time slot delay may be present in the SR-ARQ case along with more power dissipation. Finally, the combining mechanism at the destination node has to be more complex in the SR-ARQ case, as the destination needs to account for possible retransmissions and delays.

Outage probability dependence on average internode SNR for a network consisting of $M = 4$ is shown in Fig. 4.3, when the ARQ scheme is extended by increasing the number of maximum retransmission attempts to two. The gain in the low average SNR regime when the maximum number of retransmissions increases to two is lower when compared to the gain with just one retransmission attempt achieved over no ARQ added. The price that has to be paid for the performance gain in the low average internode SNR regime is adding another time slot delay. One can consider a trade-off between performance and delay, depending on system configuration requirements.

Figure 4.4 shows outage dependence on average uplink SNR for different values of $\bar{\gamma}_{\text{int}}$ and fading severity. As expected, as the fading parameter m increases, fading severity decreases and better performance is obtained. For instance, to achieve an OP of 1×10^{-5} at $\bar{\gamma}_{\text{int}} = 10$ dB, the required average uplink SNR is 14.44 dB at $m = 1$, 5.86 dB at $m = 2$ and only 3.09 dB at $m = 3$.

Finally, Fig. 4.5 shows the PER dependence on average uplink SNR with different

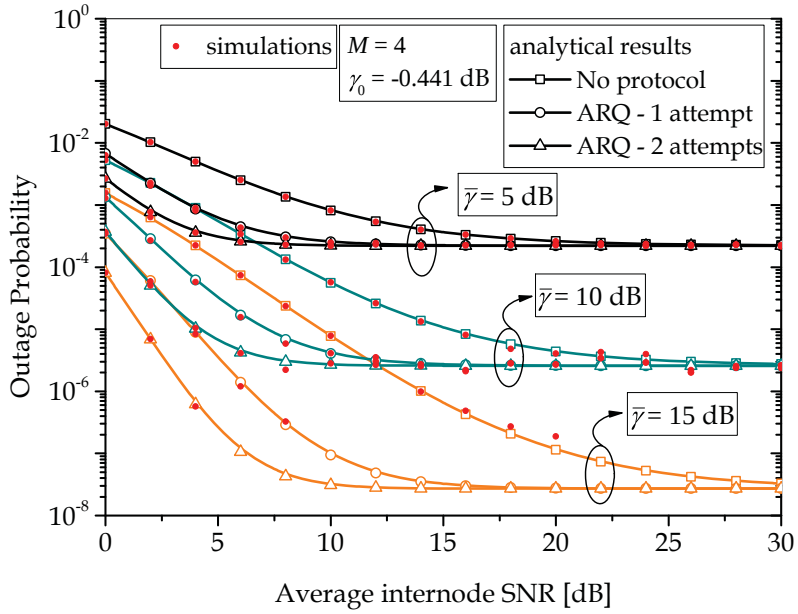

Figure 4.3: Outage probability dependence on average internode SNR for different number of retransmission attempts over Rayleigh fading.

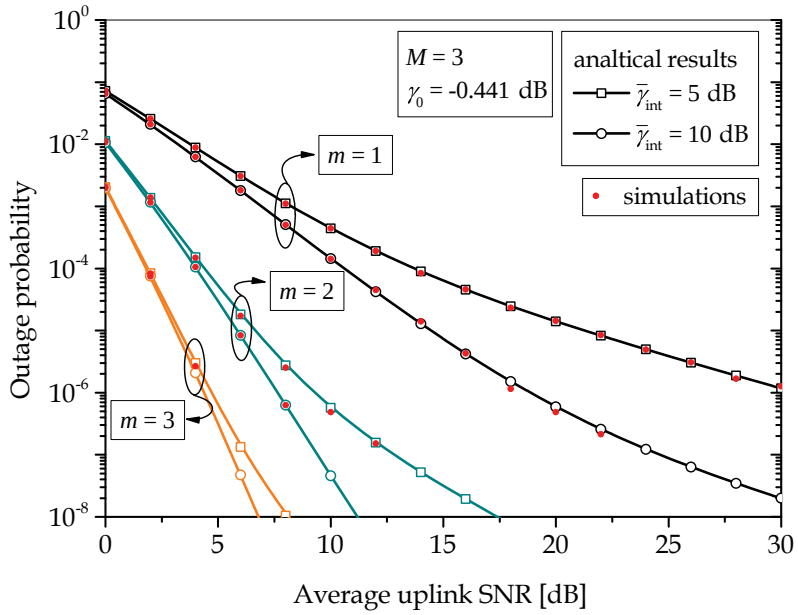

Figure 4.4: Outage probability dependence on average uplink SNR over Nakagami-m fading with different fading severity.

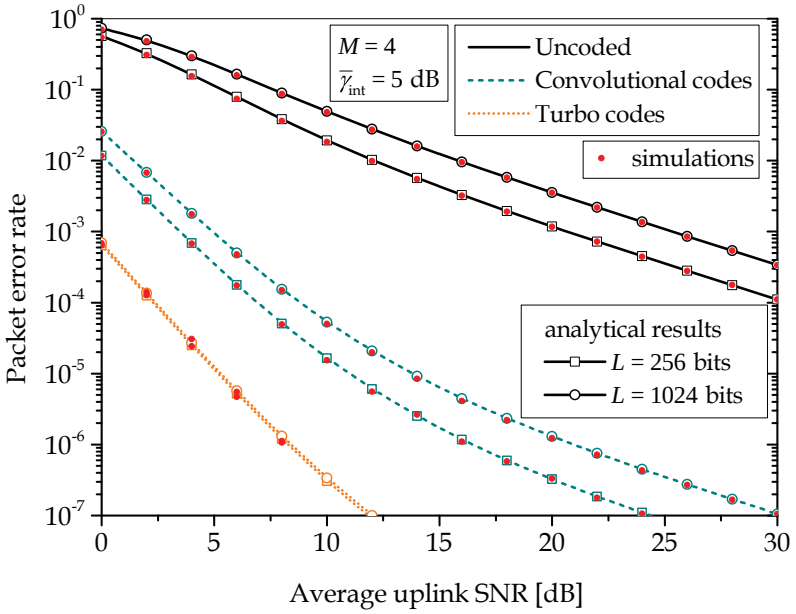

Figure 4.5: Packet error rate dependence on average uplink SNR for different packet length and coding schemes over Rayleigh fading.

outage thresholds used, depending on packet lengths and coding schemes, as given in Table 4.1. In addition uncoded BPSK transmission, convolutional codes with 1/2 code rate with octal generator polynomials $(1, 17/15)$, and turbo codes with a 1/3 code rate with generator polynomials $(1, 5/7, 5/7)$ [111]. With coding added, a significant increase in performance can be observed. It is noticeable that packet length does not play a noteworthy role in the determination of the decoding threshold when Turbo codes are applied.

4.6 Conclusion

This chapter analysed outage and packet error performance of a cooperative wireless network, subject to Rayleigh and Nakagami-m multipath fading, with SR-ARQ scheme applied in the internode communication, and closed-form analytical expressions were derived and confirmed by Monte-Carlo simulations. Additionally, results obtained are compared to those from the previous chapter, where the threshold-based protocol was applied in the internode communication.

When a maximum of one retransmission attempt is used in the ARQ scheme, results were similar to the threshold-based ones, although at a higher price. Namely, the combining complexity at the destination grows due to variable frame duration, and

more power is used for retransmissions. Moreover, a feedback mechanism to relay the ACK/NAK messages also has to be implemented. However, if the network requirements include communication with no loss of data, the use of SR-ARQ scheme is preferred over the threshold-based protocol.

Adding FEC greatly increases performance, and capacity reaching codes, such as Turbo codes, even make packet length negligible, as similar results are obtained for packets of lengths 256 and 1024 bits.

Chapter 5

Outage correlation in DF cooperative wireless networks

Whereas in previous chapters the emphasis was set on single-node performance, in this chapter the outage performance of multiple nodes simultaneously is studied. For low-latency networks, used e.g. as an industrial network, OP is the correct performance indicator [9]. The main motivation is to analyse the source of error correlation and the resulting error patterns when several source nodes share (reuse) point-to-point links to the destination. Usually link reuse is not addressed in existing literature, as it is not important when data flows are independent [121, 122]. In [123], the authors introduce a network state process describing a set of network configurations, with temporal correlation between links and investigate the stability for centralized time-varying Kalman filtering over a wireless sensor network. In this case, the data flows may be related even though the communication system is not designed to take this into account.

The aim of this chapter is to expose the underlying cause of this correlated behaviour and observe simultaneous OP performance of several source nodes that reuse transmission links. We firstly derive the simultaneous OP of any node pair. The analysis extends to determining the conditional outage, i.e., the probability that a node will be in outage given that the second node is already in outage. This analysis characterizes all pairwise behaviours. We then show how our approach can be easily extended for arbitrary number of nodes being simultaneously in outage, generalizing the analysis. The resulting insights are generic in that they expose a fundamental behaviour of collaborative networks, where links are reused for multiple data flows. Any multi-hop diversity type of scheme where multiple data flows are transmitted through shared links would have this behaviour, since particular point-to-point links are being shared by multiple data flows.

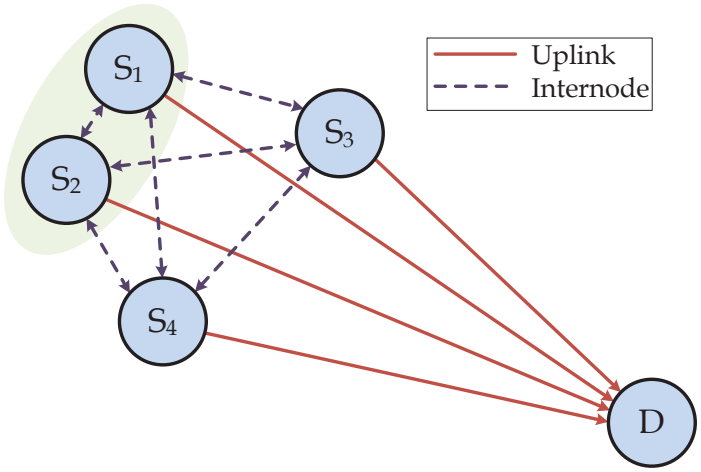

Figure 5.1: Block diagram of a network consisting of $M = 4$ nodes. Nodes S_1 and S_2 are those of interest.

5.1 System model

In this section, we first present the channel model, as well as the node cooperation scheme utilized. Afterwards, we present the decoding and forwarding matrices as a metric of describing decodings.

5.1.1 Channel model and node cooperation

A cooperative network consisting of M nodes, denoted with S_i, $i \in \{1, \ldots, M\}$, and the destination, denoted by D is observed. A block diagram of the considered network is shown in Fig. 5.1.

Each node sends its own data packet to D, and cooperates with each other in a DF manner in a two-stage cooperation frame. In the first stage, each node broadcasts its own packet to the other nodes over internode channels, and to D over its uplink channel. In addition, each node detects transmissions from the other node and attempts to decode the data. Data is successfully decoded if the instantaneous SNR of the internode channel is reliable, i.e., equal or above a predetermined decoding threshold [52]. In the second stage, a successfully decoded packet is forwarded to the destination, which then applies maximal MRC on the packets. Quasi-static fading (or block fading) channels are considered, in which each channel realization remains unchanged during one cooperation frame, but has independent changes from frame to frame. Each node is equipped with a single antenna, and all transmissions are orthogonal.

The transmission channel between a node and D is called the uplink channel, while

two nodes are linked with a pair of internode channels which are modelled to be independent, which means that the instantaneous channel realization from one node to the other is not the same in the opposite direction. All uplink channels are subject to i.i.d. Rayleigh fading, as well as AWGN. Therefore, the instantaneous uplink SNR, γ, has an exponential distribution given in (1.6).

5.1.2 Decoding and forwarding matrices

After the first stage of cooperation, node S_i has broadcast its data to the other nodes and to the destination. If an internode channel from S_i to another node is reliable, that node has decoded data originating from S_i, and can forward it in the next stage.

Let $d_{ij} \in \{0, 1\}$ denote the indicator variable stating if node S_j has successfully decoded data from node S_i. Since every source node has its own data at all times, it holds that $d_{ii} = 1 \quad \forall i$. The RV d_{ij} is therefore Bernoulli distributed with PMF

$$p\left(d_{ij}\right) = p_{\mathrm{dec}}^{d_{ij}}(1 - p_{\mathrm{dec}})^{1-d_{ij}} = \begin{cases} p_{\mathrm{dec}}, & d_{ij} = 1 \\ 1 - p_{\mathrm{dec}}, & d_{ij} = 0 \end{cases}, \tag{5.1}$$

where p_{dec} is the decoding probability, given as [52]

$$p_{\mathrm{dec}} = \exp\left(-\frac{\gamma_0}{\bar{\gamma}_{\mathrm{int}}}\right), \tag{5.2}$$

with γ_0 and $\bar{\gamma}_{\mathrm{int}}$ denoting the decoding threshold and average internode SNR, respectively.

For every node-to-node combination, we can write a decoding matrix $\mathbf{D}$ as

$$\mathbf{D} = \begin{bmatrix} d_{11} & \cdots & d_{1M} \\ \vdots & \ddots & \vdots \\ d_{M1} & \cdots & d_{MM} \end{bmatrix}, \tag{5.3}$$

where the diagonal elements are equal to unity, and the remaining elements are Bernoulli distributed, according to (5.1). Note that from internode channel independence, all elements of the $\mathbf{D}$ matrix are also independent. A decoding pattern for node S_i is defined as the i-th row of matrix $\mathbf{D}$.

A simplified case is observed, which assumes network symmetry, meaning that average uplink SNRs are equal, and the same holds for the average internode SNR. This model exposes the fundamental network behaviour while being tractable. With this assumption, the simultaneous outage of *any* n nodes can be assumed to be the same as the simultaneous outage of the *first* n nodes. In this chapter, we first set $n = 2$, and

solve the pairwise case, and provide a method to extend to $n > 2$. Therefore, we reduce the $\mathbf{D}$ matrix by taking its first two rows, obtaining a matrix with size $2 \times M$

$$\hat{\mathbf{D}} = \begin{bmatrix} d_{11} & \cdots & d_{1M} \\ d_{21} & \cdots & d_{2M} \end{bmatrix}. \tag{5.4}$$

Taking the product $\mathbf{Q} = \hat{\mathbf{D}} \times \hat{\mathbf{D}}^{\top}$ we obtain an 2×2 forwarding matrix where the i-th diagonal element, denoted with q_{ii}, corresponds to the number of branches in the MRC output for packets originating from node S_i (i.e., a counter of nodes that have successfully decoded packets arriving from node S_i). The (i, j)-th off-diagonal element, q_{ij}, corresponds to the number of forwarding relays for both node S_i and node S_j. Due to symmetry, it holds that $q_{ij} = q_{ji}$. This forwarding matrix for $n = 2$ can be expressed as

$$\mathbf{Q} = \begin{bmatrix} q_{11} & q_{12} \\ q_{21} & q_{22} \end{bmatrix}. \tag{5.5}$$

The diagonal elements q_{ii} can be determined as

$$q_{ii} = \begin{bmatrix} d_{i1} & \cdots & d_{iM} \end{bmatrix} \times \begin{bmatrix} d_{i1} \\ \vdots \\ d_{iM} \end{bmatrix} = \sum_{j=1}^{M} d_{ij}^2. \tag{5.6}$$

Since d_{ij} is Bernoulli distributed, the square of d_{ij} remains Bernoulli distributed, as the square of a Bernoulli RV maps back to itself [76]. The sum of d_{ij}^2 therefore has a binomial distribution [76]

$$\mathbb{P}[q_{ii}] = \binom{M-1}{q_{ii}-1} p_{\mathrm{dec}}^{q_{ii}-1} (1 - p_{\mathrm{dec}})^{M - q_{ii}}, \quad q_{ii} \in \{1, \ldots, M\}, \tag{5.7}$$

Moreover, the off-diagonal element q_{ij} can be determined as

$$q_{ij} = \begin{bmatrix} d_{i1} & \cdots & d_{iM} \end{bmatrix} \times \begin{bmatrix} d_{j1} \\ \vdots \\ d_{jM} \end{bmatrix} = \sum_{k=1}^{M} d_{ik} d_{jk}. \tag{5.8}$$

The product $d_{ik}d_{jk}$, conditioned on q_{ii} and q_{jj} remains Bernoulli distributed, but with success probability p_{dec}^2, and its PMF is given as

$$\mathbb{P}[q_{ij} | q_{ii}, q_{jj}] = \binom{q_{\min}}{q_{ij}} p_{\mathrm{dec}}^{2q_{ij}} \left(1 - p_{\mathrm{dec}}^2\right)^{q_{\min} - q_{ij}}, \quad q_{ij} \in \{0, \ldots, q_{\min}\}, \tag{5.9}$$

where $q_{\min} = \min(q_{ii}, q_{jj})$, as there cannot be more common terms in the combined signals than $q_{\min}$.

The probability of a specific decoding pattern can be expressed in terms of the elements of the $\mathbf{Q}$ matrix as the joint probability of the diagonal and off-diagonal terms. Combining (5.7) and (5.9), this joint probability is given as

$$\mathbb{P}\left[q_{11}, q_{22}, q_{12}\right] = \mathbb{P}\left[q_{11}\right]\mathbb{P}\left[q_{22}\right]\mathbb{P}\left[q_{12}|q_{11}, q_{22}\right]. \tag{5.10}$$

5.2 Outage analysis

In this section, a brief review the outage probability analysis of one node's packets (denoted as marginal Outage Probability) is presented, and asymptotic expression at high uplink SNR, when $\bar{\gamma} \gg \bar{\gamma}_{\text{int}}$ is given. Afterwards, the analysis extends to the two-node case, and asymptotic expressions for simultaneous outage of two nodes are derived, as well as conditional OP – the probability that one node will be in outage given that the second one is already in outage. Finally, the analysis is concluded by presenting how cases with more than two nodes simultaneously in outage are treated.

5.2.1 Marginal outage probability

First, the OP of just one node's packets is investigated. To obtain this marginal CDF, and therefore the OP, we take the familiar MGF approach [71]. The MGF, assuming i.i.d. uplink SNRs, conditioned on a specific decoding pattern for that node, can be written as the product of the individual MGFs as

$$\mathcal{M}_{\gamma_{\text{mrc}_i}|q_{ii}}\left(s\right) = \prod_{j=1}^{q_{ii}} \mathcal{M}_{\gamma_j}\left(s\right) = \prod_{j=1}^{q_{ii}} \left(1+\bar{\gamma}s\right)^{-1} = \left(1+\bar{\gamma}s\right)^{-q_{ii}}. \tag{5.11}$$

Averaging (5.11) over all possible values of q_{ii} given in (5.7), we obtain the averaged MGF as

$$\mathcal{M}_{\gamma_{\text{mrc}_i}}\left(s\right) = \sum_{q_{ii}=1}^{M} \mathcal{M}_{\gamma_{\text{mrc}_i}|q_{ii}}\left(s\right)\mathbb{P}\left[q_{ii}\right] \tag{5.12}$$

To obtain the marginal CDF, and consequently the marginal OP, we take the inverse Laplace transform $\mathcal{L}^{-1}\left[\mathcal{M}_{\gamma_{\text{mrc}_i}|q_{ii}}\left(s\right)/s\right]$, and apply the linearity property of the inverse Laplace transform, allowing us to take the sum and $\mathbb{P}[q_{ii}]$ in front of the inverse operation. Hence, exact average marginal OP can be expressed as [52, 71]

$$P_O\left(\bar{\gamma};\gamma_0\right) = \sum_{q_{ii}=1}^{M}\left[1-\exp\left(-\frac{\gamma_0}{\bar{\gamma}}\right)\sum_{m=0}^{q_{ii}-1}\frac{1}{m!}\left(\frac{\gamma_0}{\bar{\gamma}}\right)^m\right]\mathbb{P}\left[q_{ii}\right]. \tag{5.13}$$

In the high average uplink SNR regime, we can approximate the denominators in the expression for the conditional MGF by having $1+s\bar{\gamma} \approx s\bar{\gamma}$, and therefore, taking

the same steps as in (5.11)–(5.13), we obtain the approximate expression for marginal OP as

$$\tilde{P}_O\left(\bar{\gamma};\gamma_0\right)=\sum_{q_{ii}=1}^{M}\frac{1}{q_{ii}!}\left(\frac{\gamma_0}{\bar{\gamma}}\right)^{q_{ii}}\mathbb{P}\left[q_{ii}\right]. \tag{5.14}$$

Taking the expansion of (5.14), and letting $\bar{\gamma}\to\infty$, we are left with the first term only, i.e., $q_{ii}=1$, resulting in

$$P_{O_{\text{asy}}}\left(\bar{\gamma};\gamma_0\right)=\left(1-p_{\text{dec}}\right)^{M-1}\left(\frac{\gamma_0}{\bar{\gamma}}\right). \tag{5.15}$$

Furthermore, as the average uplink SNR goes to infinity, the diversity and coding gains are observed, as the asymptotic OP can be written as in (1.4). Directly from (5.15), we can obtain the gains as

$$\mathcal{G}_c=\frac{1}{\gamma_0(1-p_{\text{dec}})^{M-1}},\qquad \mathcal{G}_d=1. \tag{5.16}$$

5.2.2 Simultaneous outage for two source nodes at high SNR

Our goal is to find the simultaneous OP of n nodes (out of M) at high uplink SNR. After the second stage of cooperation, the destination has combined signals carrying packets from each source node using MRC. The combined SNR for node S_k is therefore $\gamma_{\text{mrc}_k}=\sum_{i=1}^{q_{kk}}\gamma_i$. The joint MGF conditioned on the decoding pattern for n source nodes can be written as [76]

$$\begin{aligned}&\mathcal{M}_{\gamma_{\text{mrc}_1},\ldots,\gamma_{\text{mrc}_n}|q_{11}\ldots,q_{nn},q_{12},\ldots,q_{n,n-1}}\left(s_1,\ldots,s_n\right)\\&=\mathrm{E}\left[\exp\left(s_1\gamma_{\text{mrc}_1}+\cdots+\mathrm{s}_n\gamma_{\text{mrc}_n}\right)\right].\end{aligned} \tag{5.17}$$

The following analysis holds for $n=2$ (i.e., two node case), but can be extended for larger values of n, as illustrated in Section 5.2.3.

For $n=2$, we can write the joint MGF as

$$\mathcal{M}_{\gamma_{\text{mrc}_1},\gamma_{\text{mrc}_2}|q_{11},q_{22},q_{12}}\left(s_1,s_2\right)=\mathrm{E}\left[\exp\left(s_1\gamma_{\text{mrc}_1}+s_2\gamma_{\text{mrc}_2}\right)\right]. \tag{5.18}$$

Decomposing the combined SNRs, γ_{mrc_1} and γ_{mrc_2} into its individual components we can re-write (5.18) as

$$\begin{aligned}&\mathcal{M}_{\gamma_i,\gamma_j|q_{11},q_{22},q_{12}}\left(s_1,s_2\right)\\&=\mathrm{E}\left[\exp\left(s_1\sum_{i=1}^{q_{11}}\gamma_i+s_2\sum_{j=1}^{q_{22}}\gamma_j\right)\right].\end{aligned} \tag{5.19}$$

While (5.19) is correct, the right hand side does not take into account how many terms in each sum of γ_{mrc_1} and γ_{mrc_2} are common for both source nodes. Therefore, we re-write

(5.19) as

$$\begin{aligned}&\mathcal{M}_{\gamma_i,\gamma_j,\gamma_k|q_{11},q_{22},q_{12}}(s_1,s_2)\\&=\mathrm{E}\left[\exp\left(s_1\sum_{i=1}^{q_{11}-q_{12}}\gamma_i+s_2\sum_{j=1}^{q_{22}-qq_{12}}\gamma_j+(s_1+s_2)\sum_{k=1}^{q_{12}}\gamma_k\right)\right].\end{aligned}\tag{5.20}$$

For Rayleigh fading, the joint MGF is therefore

$$\begin{aligned}&\mathcal{M}_{\gamma_i,\gamma_j,\gamma_k|q_{11},q_{22},q_{12}}(s_1,s_2)\\&=(1+s_1\bar{\gamma})^{-(q_{11}-q_{12})}(1+s_2\bar{\gamma})^{-(q_{22}-q_{12})}(1+(s_1+s_2)\,\bar{\gamma})^{-q_{12}}.\end{aligned}\tag{5.21}$$

The equation above is an exact expression for the joint MGF. However, for obtaining the two-node simultaneous OP, taking the inverse Laplace transform over both s_1 and s_2 does not yield a closed-form solution.

In the high average uplink SNR regime, taking the same approximation as in the marginal case, $1+s\bar{\gamma}\approx s\bar{\gamma}$, we approximate (5.20) with

$$\begin{aligned}&\mathcal{M}_{\gamma_i,\gamma_j,\gamma_k|q_{11},q_{22},q_{12}}(s_1,s_2)\\&\approx(s_1\bar{\gamma})^{-(q_{11}-q_{12})}(s_2\bar{\gamma})^{-(q_{22}-q_{12})}((s_1+s_2)\,\bar{\gamma})^{-q_{12}}.\end{aligned}\tag{5.22}$$

To obtain the two-node simultaneous OP directly from the joint MGF, we must take the inverse Laplace transform $\mathcal{L}^{-1}\left[\mathcal{M}(s_1,s_2)/(s_1s_2)\right]$. Taking the inverse Laplace transform over s_1, the following expression is obtained

$$\begin{aligned}&\mathcal{L}^{-1}\left[\mathcal{M}_{\gamma_i,\gamma_j,\gamma_k|q_{11},q_{22},q_{12}}(s_1,s_2)/(s_1s_2)\right]\\&=\frac{\gamma_0^{q_{11}}}{\bar{\gamma}^{q_{\mathrm{p}}}}\left(\frac{1}{s_2^{q_{22}-q_{12}+1}}\times{}_1\tilde{F}_1(q_{12};q_{11}+1;-s_2\gamma_0)\right),\end{aligned}\tag{5.23}$$

where $q_{\mathrm{p}}=q_{11}+q_{22}-q_{12}$ and ${}_1\tilde{F}_1(a;b;z)$ is the regularized confluent hypergeometric function, defined in [80, eq. (9.210.1)] as

$${}_1\tilde{F}_1(a;b;z)=\sum_{k=0}^{\infty}\frac{\Gamma(a+k)\,z^k}{\Gamma(a)\,\Gamma(b+k)\,k!}.\tag{5.24}$$

Replacing (5.24) in (5.23) we obtain

$$\begin{aligned}&\mathcal{L}^{-1}\left[\mathcal{M}_{\gamma_i,\gamma_j,\gamma_k|q_{11},q_{22},q_{12}}(s_1,s_2)/(s_1s_2)\right]=\frac{\gamma_0^{q_{11}}}{\bar{\gamma}^{q_{\mathrm{p}}}}\\&\times\left(\frac{1}{s_2^{q_{22}-q_{12}+1}}\times\sum_{k=0}^{\infty}\frac{\Gamma(q_{12}+k)\,(-s_2\gamma_0)^k}{k!\Gamma(q_{12})\,\Gamma(q_{11}+k+1)}\right).\end{aligned}\tag{5.25}$$

Taking the inverse Laplace over the second dimension s_2 in (5.25), we obtain the simultaneous OP, conditioned on the decoding pattern as

$$\begin{aligned}&\tilde{P}_{OJ}(\bar{\gamma};\gamma_0|q_{11},q_{22},q_{12})=\left(\frac{\gamma_0}{\bar{\gamma}}\right)^{q_{\mathrm{p}}}\\&\times\sum_{k=0}^{\infty}(-1)^k\frac{(q_{12})_k}{k!\Gamma(q_{11}+k+1)\,\Gamma(q_{22}-q_{12}-k+1)},\end{aligned}\tag{5.26}$$

with $(q_{12})_k = \Gamma(q_{12}+k)/\Gamma(q_{12})$ denoting the Pochammer symbol [91].

In the equation above, the last term in the denominator goes to infinity when $q_{22} - q_{12} - k + 1 \leq 0$, and the whole fraction equals to zero. Therefore, we can truncate the sum in (5.26) and replace the Gamma functions with factorials, obtaining

$$\begin{aligned}\tilde{P}_{OJ}(\bar{\gamma};\gamma_0|q_{11},q_{22},q_{12}) &= \left(\frac{\gamma_0}{\bar{\gamma}}\right)^{q_{\mathrm{p}}} \\ &\times \sum_{k=0}^{q_{22}-q_{12}+1} (-1)^k \frac{(q_{12})_k}{k!\,(q_{11}+k)!\,(q_{22}-q_{12}-k)!}.\end{aligned} \tag{5.27}$$

Finally, after averaging (5.27) over q_{11}, q_{22} and q_{12} we obtain the approximate two-node simultaneous OP as

$$\begin{aligned}\tilde{P}_{OJ}(\bar{\gamma};\gamma_0) = \sum_{q_{11}=1}^{M}\sum_{q_{22}=1}^{M}\sum_{q_{12}=0}^{q_{\min}} &\mathbb{P}[q_{11},q_{22},q_{12}] \\ &\times P_{OJ_{\mathrm{asy}}}(\bar{\gamma};\gamma_0|q_{11},q_{22},q_{12}),\end{aligned} \tag{5.28}$$

where $\mathbb{P}[q_{11},q_{22},q_{12}]$ is given in (5.10).

Note that in (5.28), the total number of independent paths is $q_{11}+q_{22}-q_{12} \leq M$, while for the special case when only the source nodes send their data the number of common terms is always zero (i.e., for $q_{11}=1$ and $q_{22}=1$, $q_{12}=0$).

As in the marginal case when expanding the sums in (5.28) and $\bar{\gamma}$ goes to infinity, we are left with the terms with the lowest exponent, weighted by their corresponding probabilities of decoding patterns

$$\begin{aligned}P_{OJ_{\mathrm{asy}}}(\bar{\gamma};\gamma_0) &= \left(\frac{\gamma_0}{\bar{\gamma}}\right)^2 \\ &\times \Big((1-p_{\mathrm{dec}})^{2M-2} + (M-1)\,p_{\mathrm{dec}}^3(1-p_{\mathrm{dec}})^{2M-3} \\ &+ 1/2(M-1)^2 p_{\mathrm{dec}}^6(1-p_{\mathrm{dec}})^{2M-4}\Big),\end{aligned} \tag{5.29}$$

The coding and diversity gains are directly obtained from (5.29) as

$$\begin{aligned}\mathcal{G}_c &= {\gamma_0}^{-1} \times \Big((1-p_{\mathrm{dec}})^{2M-2} + (M-1)\,p_{\mathrm{dec}}^3(1-p_{\mathrm{dec}})^{2M-3} \\ &\quad + 1/2(M-1)^2 p_{\mathrm{dec}}^6(1-p_{\mathrm{dec}})^{2M-4}\Big)^{-1/2}, \\ \mathcal{G}_d &= 2.\end{aligned} \tag{5.30}$$

5.2.3 Conditional outage at high SNR

The probability of both nodes are in outage simultaneously, for a specific q_{11}, q_{22} and q_{12} is given in (5.27). This probability can be written as

$$\begin{aligned}&P_{OJ_{\mathrm{asy}}}(\bar{\gamma};\gamma_0|q_{11},q_{22},q_{12}) \\ &= \mathbb{P}[\gamma_{c_1} < \gamma_0, \gamma_{c_2} < \gamma_0 | q_{11},q_{22},q_{12}].\end{aligned} \tag{5.31}$$

We can evaluate the conditional outage of the second source, given the first one is in outage by applying the total probability theorem [76]

$$\begin{aligned}\mathbb{P}\left[\gamma_{c_1} < \gamma_0, \gamma_{c_2} < \gamma_0\right] &= \mathbb{P}\left[\gamma_{c_2} < \gamma_0 | \gamma_{c_1} < \gamma_0\right] \\ &\times \mathbb{P}\left[\gamma_{c_1} < \gamma_0\right],\end{aligned} \tag{5.32}$$

and therefore, from (5.14) and (5.27), obtain the conditional outage of the second source node as

$$\begin{aligned}\tilde{P}_{OC}(\bar{\gamma}; \gamma_0 | q_{11}, q_{22}, q_{12}) &= \frac{\tilde{P}_{OJ}\left(\bar{\gamma}; \gamma_0 | q_{11}, q_{22}, q_{12}\right)}{\tilde{P}_{O}\left(\bar{\gamma}; \gamma_0 | q_{11}\right)} \\ &= \left(\frac{\gamma_0}{\bar{\gamma}}\right)^{q_{22}-q_{12}} \times \frac{{}_2F_1\left(q_{12}, q_{12}-q_{22}; q_{11}+1; 1\right)}{(q_{22}-q_{12})!},\end{aligned} \tag{5.33}$$

where ${}_2F_1\left(a, b; c; z\right)$ is the Gaussian hypergeometric function, defined in [80, eq. (9.14.2)].

Applying [91, eq. (07.23.03.0002.01)], we replace the hypergeometric function with factorials, obtaining

$$\begin{aligned}&\tilde{P}_{OC}\left(\bar{\gamma}; \gamma_0 | \gamma_{c_1} < \gamma_0, q_{11}, q_{22}, q_{12}\right) \\ &= \left(\frac{\gamma_0}{\bar{\gamma}}\right)^{q_{22}-q_{12}} \times \frac{q_{11}!\left(q_{11}+q_{22}-2q_{12}\right)!}{(q_{11}-q_{12})!\left(q_{22}-q_{12}\right)!q_{\mathrm{p}}!}.\end{aligned} \tag{5.34}$$

Averaging (5.34) over q_{11}, q_{22} and q_{12} we obtain the OP of the second node, conditioned on the first one being in outage

$$\begin{aligned}&\tilde{P}_{OC}\left(\bar{\gamma}; \gamma_0 | \gamma_{c_1} < \gamma_0\right) \\ &= \sum_{q_{11}=1}^{M} \sum_{q_{22}=1}^{M} \sum_{q_{12}=0}^{q_{\min}} \mathbb{P}\left[q_{11}, q_{22}, q_{12}\right] \\ &\times \tilde{P}_{OC}\left(\bar{\gamma}; \gamma_0 | \gamma_{c_1} < \gamma_0, q_{11}, q_{22}, q_{12}\right).\end{aligned} \tag{5.35}$$

When expanding (5.35) and letting $\bar{\gamma} \to \infty$, the diversity gain for the conditional outage is zero, as there exist terms for which $q_{22} - q_{12} = 0$, while the coding gain converges to unity with increasing internode SNR.

5.2.4 Simultaneous outage for more than two source nodes at high SNR

Using a similar approach as in the two-node case, we can extend the analysis for OP of n nodes simultaneously. What follows is an example for $n = 3$, and iteratively this can be generalized for arbitrary $n \leq M$. For brevity, the indexes on the left-hand side of equations are omitted. Additionally, the following analysis accounts for a specific decoding pattern, and averaging is performed in the end.

Similar to the two-node case, directly from (5.17) the MGF for the three-node case can be written as [76]

$$\mathcal{M}(s_1, s_2, s_3) = \mathrm{E}\left[\exp\left(s_1\gamma_{\mathrm{mrc}_1} + s_2\gamma_{\mathrm{mrc}_2} + s_3\gamma_{\mathrm{mrc}_3}\right)\right]. \tag{5.36}$$

Replacing all three combined SNRs with their corresponding sums, we can re-write (5.36) as

$$\mathcal{M}(s_1, s_2, s_3) = \mathrm{E}\left[\exp\left(s_1\sum_{i=1}^{q_{11}}\gamma_i + s_2\sum_{j=1}^{q_{22}}\gamma_j + s_3\sum_{k=1}^{q_{33}}\gamma_k\right)\right]. \tag{5.37}$$

Directly decomposing (5.37) into terms which account for all combinations of common SNRs for the three nodes will result in an expression which can be quite cumbersome for further analysis. Namely, we would have to solve

$$\begin{aligned}\mathcal{M}(s_1, s_2, s_3) = \mathrm{E}\big[&\exp\left(s_1\Sigma_1 + s_2\Sigma_2 + s_3\Sigma_3\right.\\ &+ (s_1+s_2)\Sigma_{12} + (s_1+s_3)\Sigma_{13} + (s_2+s_3)\Sigma_{23}\\ &+ \left.(s_1+s_2+s_3)\Sigma_{123}\right)\big],\end{aligned} \tag{5.38}$$

where the SNR terms corresponding to a single source node are

$$\begin{aligned}\Sigma_1 &= \sum\nolimits_{k_1=1}^{q_{11}-(q_{12}+q_{13}-q_{123})}\gamma_{k_1},\\ \Sigma_2 &= \sum\nolimits_{k_2=1}^{q_{22}-(q_{12}+q_{23}-q_{123})}\gamma_{k_2},\\ \Sigma_3 &= \sum\nolimits_{k_3=1}^{q_{33}-(q_{13}+q_{23}-q_{123})}\gamma_{k_3},\end{aligned} \tag{5.39}$$

the terms corresponding to common SNRs per node pair are

$$\begin{aligned}\Sigma_{12} &= \sum\nolimits_{k_4=0}^{q_{12}-q_{123}}\gamma_{k_4},\\ \Sigma_{13} &= \sum\nolimits_{k_5=0}^{q_{13}-q_{123}}\gamma_{k_5},\\ \Sigma_{23} &= \sum\nolimits_{k_6=0}^{q_{23}-q_{123}}\gamma_{k_6},\end{aligned} \tag{5.40}$$

and finally, the terms corresponding to common SNRs for all three nodes is

$$\Sigma_{123} = \sum\nolimits_{k_7=0}^{q_{123}}\gamma_{k_7}. \tag{5.41}$$

For arbitrary n, the joint MGF is expressed in n Laplace dimensions grows with rate $\sum_{k=1}^{n}\binom{n}{k}$. Taking the inverse Laplace transform of (5.38) just over s_1 does not produce a closed-form solution.

Alternatively, we treat the node pair of the first two source nodes as a single, composite node, as shown in Fig 5.2. Given that we already derived the CDF of this

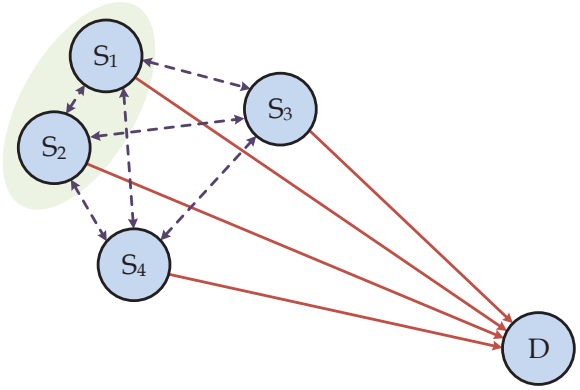

(a) Two nodes are of interest.

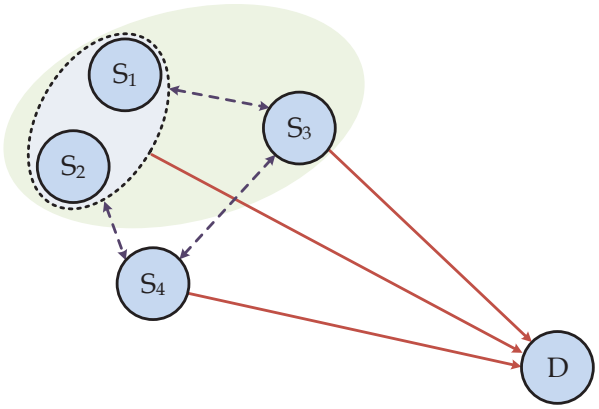

(b) Three nodes are of interest.

Figure 5.2: The composite node is formed by grouping a node pair.

composite node expressed as the simultaneous OP for $n = 2$ in (5.27), we can evaluate the composite MGF as

$$\mathcal{M}\left(s_{\mathrm{p}}\right) = s_{\mathrm{p}}\mathcal{L}\left[P_{OJ}\left(\bar{\gamma};\gamma_0\right)\right]. \tag{5.42}$$

For Rayleigh fading, we have

$$\begin{aligned}\mathcal{M}\left(s_{\mathrm{p}}\right) &= \left(s_{\mathrm{p}}\bar{\gamma}\right)^{-q_{\mathrm{p}}}\frac{q_{\mathrm{p}}!}{\left(q_{22}-q_{12}\right)!}\\ &\times {}_2\tilde{F}_1\left(q_{12}, q_{12}-q_{22}; q_{11}+1; 1\right),\end{aligned} \tag{5.43}$$

where ${}_2\tilde{F}_1\left(a;b;c;z\right)$ is the regularized hypergeometric function, defined in [80, eq. (9.210.2)] as

$${}_2\tilde{F}_1\left(a,b;c;z\right) = \sum_{k=0}^{\infty}\frac{(a)_k(b)_k z^k}{\Gamma\left(c+k\right)k!}. \tag{5.44}$$

Applying [91, eq. (07.24.03.0002.01)], the hypergeometric function is reduced to a fraction of factorials, obtaining

$$\mathcal{M}\left(s_{\mathrm{p}}\right)=\mathcal{A}\times\left(s_{\mathrm{p}}\bar{\gamma}\right)^{-q_{\mathrm{p}}}, \tag{5.45}$$

where

$$\mathcal{A}=\frac{\left(q_{11}+q_{22}-2q_{12}\right)!}{\left(q_{11}-q_{12}\right)!\left(q_{22}-q_{12}\right)!}. \tag{5.46}$$

Keeping in mind the approximation $1+s\bar{\gamma}\approx s\bar{\gamma}$, (5.45) has the same form as the MGF as a sum of exponential RVs [71], just weighted by $\mathcal{A}$. Therefore, we can treat the combined SNR of the node pair as a sum of weighted exponentials, and the MGF of the three node case can be expressed as

$$\begin{aligned}&\mathcal{M}\left(s_{\mathrm{p}},s_3\right)\\&=\mathrm{E}\left[\exp\left(s_{\mathrm{p}}\sum_{i=2}^{q_{\mathrm{p}}-q_{123}}\gamma_i+s_3\sum_{j=1}^{q_{33}-q_{123}}\gamma_j+\left(s_{\mathrm{p}}+s_3\right)\sum_{k=0}^{q_{123}}\gamma_k\right)\right],\end{aligned} \tag{5.47}$$

Following the steps from (5.21) to (5.27), we have

$$\begin{aligned}&\mathcal{M}\left(s_{\mathrm{p}},s_3\right)\approx\mathcal{A}(s_{\mathrm{p}}\bar{\gamma})^{-(q_{\mathrm{p}}-q_{123})}\\&\times\left(s_3\bar{\gamma}\right)^{-(q_{33}-q_{123})}\left(\left(s_{\mathrm{p}}+s_3\right)\bar{\gamma}\right)^{-q_{123}},\end{aligned} \tag{5.48}$$

The inverse Laplace transform of (5.48) over s_{p} evaluated at γ_0 yields

$$\begin{aligned}&\mathcal{L}^{-1}\left[\mathcal{M}\left(s_{\mathrm{p}},s_3\right)/\left(s_{\mathrm{p}}s_3\right)\right]\\&=\frac{\mathcal{A}\gamma_0^{q_{\mathrm{p}}}}{\bar{\gamma}^{q_{\mathrm{p}}+q_{33}-q_{123}}}\times\frac{{}_1\tilde{F}_1\left(q_{123};q_{\mathrm{p}}+1;-s_3\gamma_0\right)}{s_3^{q_{33}-q_{123}+1}}.\end{aligned} \tag{5.49}$$

After re-writing the hypergeometric function as a series, as in the two node case, we take the inverse Laplace transform of (5.49) over s_3 at $\gamma=\gamma_0$. Finally, truncating the series we obtain the conditional simultaneous OP expression for three nodes as

$$\begin{aligned}&\tilde{P}_{OJ_{(3)}}\left(\bar{\gamma};\gamma_0|q_{11},q_{22},q_{33},q_{12},q_{123}\right)=\left(\frac{\gamma_0}{\bar{\gamma}}\right)^{q_{\mathrm{p}}+q_{33}-q_{123}}\\&\times\sum_{k=0}^{q_{33}-q_{123}+1}(-1)^k\frac{\left(q_{123}\right)_k}{k!\left(q_{\mathrm{p}}+k\right)!\left(q_{33}-q_{123}-k\right)!},\end{aligned} \tag{5.50}$$

where q_{33} counts the number of relays for node U_3's packets, and is distributed according to (5.7), and $q_{123}\in\{0,\ldots,\min\left(q_{12},q_{33}\right)\}$ is a Binomial RV counting how many relays are common for all three nodes. Averaging (5.50) over $q_{11},q_{22},q_{33},q_{12}$, and q_{123} we obtain the simultaneous OP for $n=3$ as

$$\begin{aligned}\tilde{P}_{OJ_{(3)}}\left(\bar{\gamma};\gamma_0\right)=&\sum_{q_{11}=1}^{M}\sum_{q_{22}=1}^{M}\sum_{q_{33}=1}^{M}\sum_{q_{12}=0}^{q_{\min}}\sum_{q_{123}=0}^{\min(q_{12},q_{33})}\\&\tilde{P}_{OJ_{(3)}}\left(\bar{\gamma};\gamma_0|q_{11},q_{22},q_{33},q_{12},q_{123}\right)\\&\times\mathbb{P}\left[q_{11},q_{22},q_{33},q_{12},q_{123},\right],\end{aligned} \tag{5.51}$$

where

$$\begin{aligned}\mathbb{P}\left[q_{11},q_{22},q_{33},q_{12},q_{123},\right]&=\mathbb{P}\left[q_{11}\right]\mathbb{P}\left[q_{22}\right]\mathbb{P}\left[q_{33}\right]\\&\times\mathbb{P}\left[q_{12}|q_{11},q_{22}\right]\mathbb{P}\left[q_{123}|q_{12},q_{33}\right].\end{aligned}\tag{5.52}$$

The conditional OP of the third node given that the first two are simultaneously in outage can be obtained by following the same steps as in the two node case.

This probability is expressed as

$$\begin{aligned}P_{OC_{(3)}}&=\mathbb{P}\left[\gamma_{c_3}<\gamma_0|\gamma_{c_1}<\gamma_0,\gamma_{c_2}<\gamma_0\right]\\&=\frac{\mathbb{P}\left[\gamma_{c_1}<\gamma_0,\gamma_{c_2}<\gamma_0,\gamma_{c_3}<\gamma_0\right]}{\mathbb{P}\left[\gamma_{c_1}<\gamma_0,\gamma_{c_2}<\gamma_0\right]}=\frac{P_{OJ_{(3)}}}{P_{OJ_{(2)}}}.\end{aligned}\tag{5.53}$$

Inserting (5.50) and (5.27) in (5.53), this OP is obtained as

$$P_{OC_{(3)}}=\frac{{}_2\tilde{F}_1\left(q_{123},q_{123}-q_{33};q_{\mathrm{p}}+1;1\right)\left(q_{22}-q_{12}\right)!}{{}_2\tilde{F}_1\left(q_{12},q_{12}-q_{22};q_{11}+1;1\right)\left(q_{33}-q_{123}\right)!},\tag{5.54}$$

where ${}_2\tilde{F}_1\left(a,b;c;z\right)$ is the regularized hypergeometric function defined as ${}_2F_1\left(a,b;c;z\right)/\Gamma\left(b\right)$. Applying [91, eq. (07.24.03.0002.01)], we obtain the conditional OP as

$$\begin{aligned}\tilde{P}_{OC_{(3)}}\left(\bar{\gamma};\gamma_0|q_{11},q_{22},q_{33},q_{12},q_{123}\right)&=\left(\frac{\gamma_0}{\bar{\gamma}}\right)^{q_{33}-q_{123}}\\&\times\frac{\left(q_{11}-q_{12}\right)!\left(q_{22}-q_{12}\right)!}{\left(q_{\mathrm{p}}-q_{123}\right)!\left(q_{33}-q_{123}\right)!}\\&\times\frac{\left(q_{\mathrm{p}}+q_{33}-2q_{123}\right)!q_{\mathrm{p}}!}{\left(q_{11}+q_{22}-2q_{12}\right)!\left(q_{\mathrm{p}}+q_{33}-q_{123}\right)!},\end{aligned}\tag{5.55}$$

and when averaged over $q_{11},q_{22},q_{33},q_{12}$, and q_{123}, we obtain

$$\begin{aligned}\tilde{P}_{OC_{(3)}}\left(\bar{\gamma};\gamma_0\right)=&\sum_{q_{11}=1}^{M}\sum_{q_{22}=1}^{M}\sum_{q_{33}=1}^{M}\sum_{q_{12}=0}^{q_{\min}}\sum_{q_{123}=0}^{\min(q_{12},q_{33})}\\&\tilde{P}_{OC_{(3)}}\left(\bar{\gamma};\gamma_0|q_{11},q_{22},q_{33},q_{12},q_{123}\right)\\&\times\mathbb{P}\left[q_{11},q_{22},q_{33},q_{12},q_{123},\right].\end{aligned}\tag{5.56}$$

The evaluation of simultaneous and conditional OP for arbitrary $n\leq M$ nodes can be iteratively extended by repeating the process of forming composite nodes and using the analysis for the two-node case.

5.3 Numerical results

The marginal, two-node simultaneous and conditional OP expressions derived in the previous section are used to efficiently compute numerical values of OP for any practical

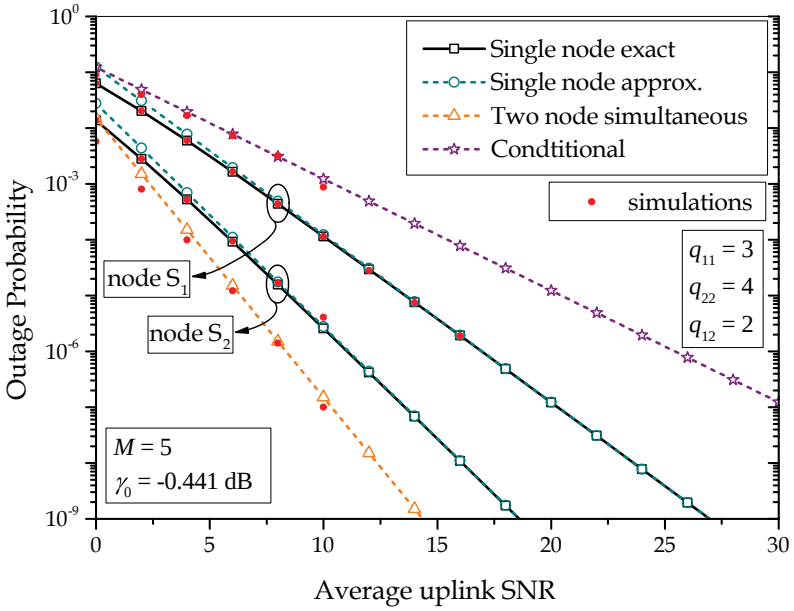

Figure 5.3: Single node, two-node simultaneous and conditional outage probability dependence on average uplink SNR $\bar{\gamma}$ for a specific set of q_{11}, q_{22} and q_{12}.

value of average uplink and internode SNR, network dimension and decoding pattern. The threshold for successfully decoding packets depends on the coding scheme used and on the packet length, as was presented in [52]. We set the optimum threshold to $\gamma_0 = -0.441$ dB, which accounts for network where each node encodes a packet of length 512 bits, using a convolutional coding scheme with one-half code rate with octal generator polynomials (1, 17/15), [52]. All analytical results are confirmed by independent Monte-Carlo simulations.

Figure 5.3 shows outage probability dependence on average uplink SNR for a specific decoding pattern. Marginal outages for both nodes are plotted, as well as the simultaneous two-node outage and the conditional – the probability that the source node S_2 is in outage, given that S_1 is already in outage. As expected, by increasing the average uplink SNR, all outage probabilities decrease. Furthermore, the simultaneous OP cannot be viewed as a product of two marginal outages when there exist common forwarding nodes (i.e., $q_{12} \neq 0$). When one source node is in outage, the outage probability of the second source node greatly increases when common forwarding terms exist. This difference in outage probability is more evident at high uplink SNR. For instance, at $\bar{\gamma} = 6$ dB, the marginal outage of the second source node is 8.78×10^{-5}, but just 7.24×10^{-3} when conditioned on the first source being in outage with two common terms. At $\bar{\gamma} = 16$ dB, the marginal and conditional OPs are 1.07×10^{-8} and 7.87×10^{-5}, respectively, which

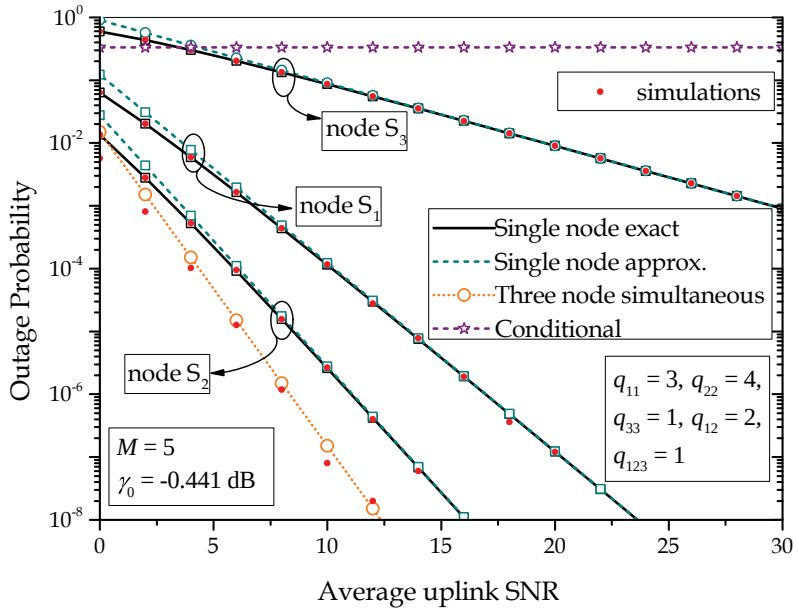

Figure 5.4: Single node, three-node simultaneous and conditional outage probability dependence on average uplink SNR $\bar{\gamma}$ for a specific set of q_{11}, q_{22}, q_{33}, q_{12}, and q_{123} .

is a difference of more than three orders of magnitude.

An extension to the case of three nodes is shown in Fig. 5.4. For this specific decoding pattern, the destination receives S_3's packets only from S_3 directly. Moreover, S_3 is the only node in the network which forwards packets from all three source nodes ($q_{123} = 1$). As a result, when the link from S_3 to D fades and an outage happens, there is a finite probability that the other two nodes will be simultaneously in outage as well, and hence the conditional OP is constant for all values of average uplink SNR.

The exact, approximate and asymptotic OPs of a single source node are shown in Fig. 5.5, for different network size, averaged over all possible decoding patterns. By increasing the number of nodes in the network, only a coding gain can be noticed – the diversity order remains one. The approximate and asymptotic expressions, given in (5.14) and (5.15), respectively, both hold in the high average uplink SNR regime. At low $\bar{\gamma}$ the approximate and asymptotic expressions act as upper and lower bounds, since the difference between the exact and approximative OP expression can be shown to be negative, and the difference between the exact and asymptotic OP can be shown to be positive. While (5.14) remains tight regardless of the number of nodes in the network, (5.15) converges to the exact OP value around $\bar{\gamma} = 16$ dB for $M = 2$, and at $\bar{\gamma} > 25$ dB for $M = 5$.

Asymptotic two-node simultaneous OP dependence on average uplink SNR is shown

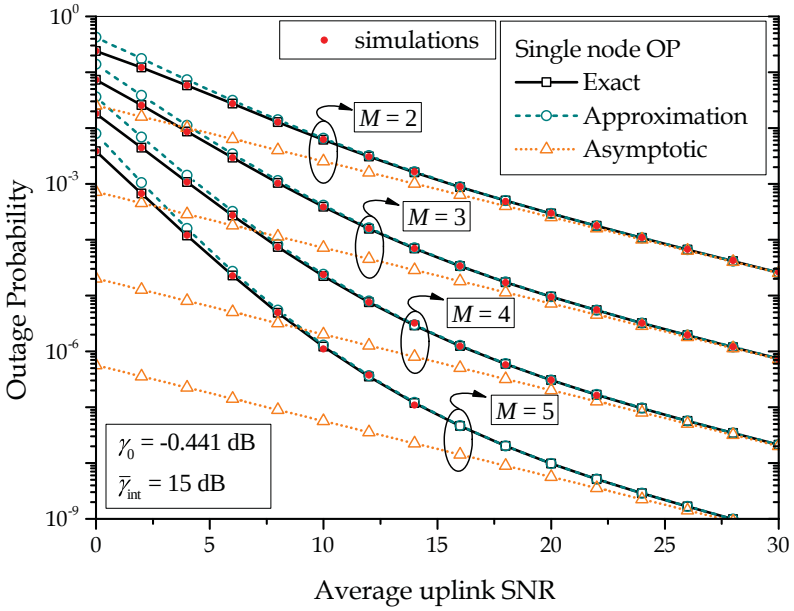

Figure 5.5: Single node outage probability dependence on average uplink SNR $\bar{\gamma}$ for different network dimensions – both exact and asymptotic values are plotted.

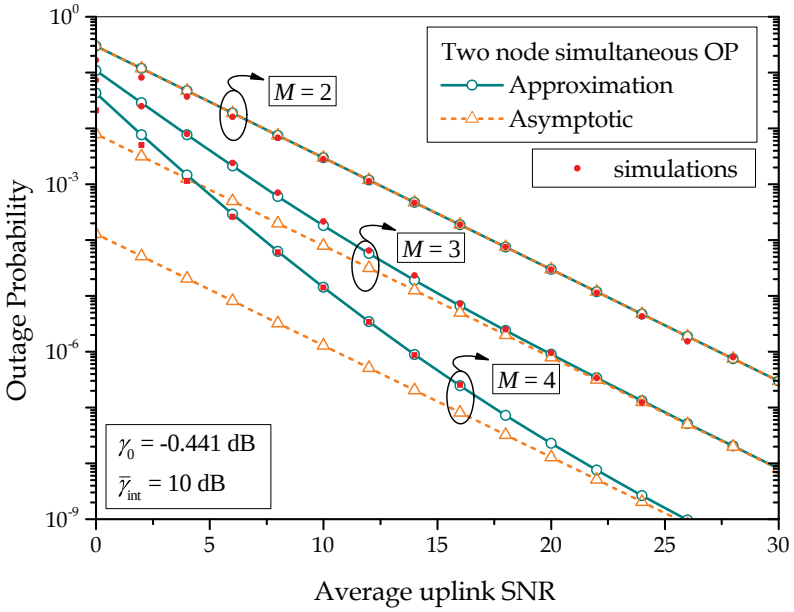

Figure 5.6: Simultaneous two-node outage probability dependence on average uplink SNR $\bar{\gamma}$ for different network dimensions.

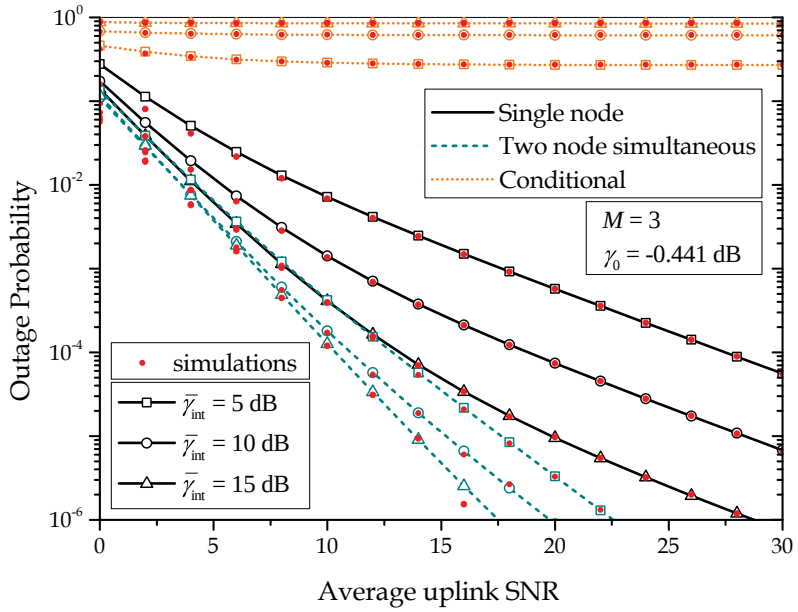

Figure 5.7: Outage probability dependence on average uplink SNR for different values of average internode SNR. Single node, two-node simultaneous and conditional outages are shown.

in Fig. 5.6 for different network size and fixed average internode SNR. As in the marginal case, both asymptotic expressions hold in the high average uplink SNR regime. As we are looking at the simultaneous OP, the diversity order is now two, because even if all internode links fail, the source nodes will send their own data to the destination, as they always have their data. Similar to the marginal case, by adding more nodes in the network, we observe only a coding gain, while the diversity order remains the same. To achieve a OP of $P_{OJ}(\bar{\gamma};\gamma_0) = 10^{-6}$ at $\bar{\gamma}_{\text{int}} = 10$ dB, the average uplink SNR required is 27.4 dB when we only have $M = 2$, and just 13.84 dB when the network dimension increases to $M = 4$.

Figure 5.7 shows marginal, two-node simultaneous, and conditional outage probability dependence on average uplink SNR for different average internode SNR. Here we can observe that whereas the marginal and simultaneous OPs decrease with greater values of average internode SNR, conditional OP increases. Intuitively, this makes sense; namely, when internode channel conditions are favourable, all outage events affecting one data flow will affect the other as well. By knowing the conditional OP of one source node given the other is in outage, we effectively know the correlation of the outage events for the two data flows, as both use same routes to reach the destination.

Finally, this effect can also be seen in Fig. 5.8, where OPs are plotted against average internode SNR. For the marginal and two-node case, we observe an outage floor

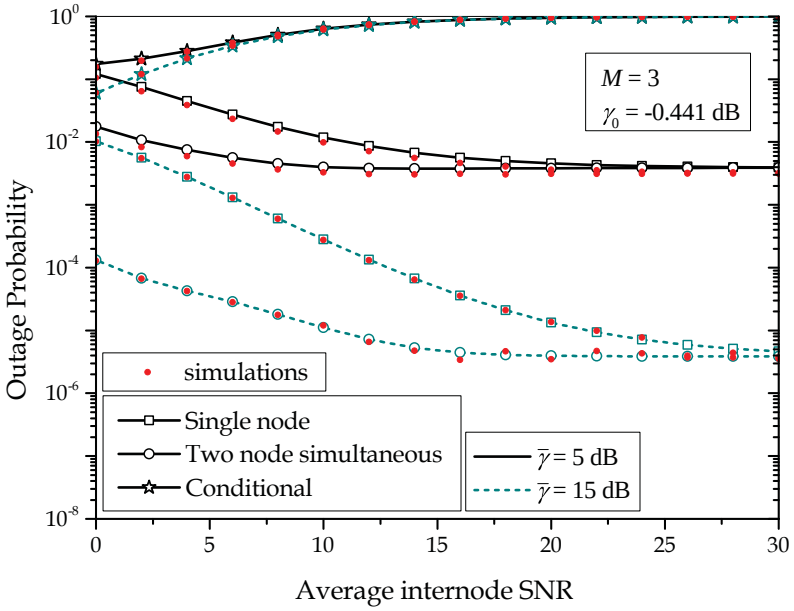

Figure 5.8: Outage probability dependence on average internode SNR for different values of average uplink SNR. Single node, two-node simultaneous and conditional outages are shown.

of 3.11×10^{-3} and 3.89×10^{-6} for $\bar{\gamma} = 5$ dB and $\bar{\gamma} = 15$ dB, respectively. When this floor is reached, improving average internode SNR does not decrease OP, neither marginal or two-node simultaneous. As a result, the conditional OP converges to 1, as it is all but certain that all outage events affecting one data flow will be fully correlated with outage events of the other data flow.

5.4 Conclusion

In the regime of non-perfect decoding at the relays, the results have shown that in the event of simultaneous outage of two nodes, the diversity order of the network is two, because the two source nodes can always send their own data to the destination via their independent uplinks. This is the worst case relay decoding pattern, due to a finite probability that all relays fail to decode data coming from both source nodes. Therefore, by increasing the number of nodes in the network, only a coding gain can be noticed. This coding gain is dependent not only on the network dimension, but also on the probability of successful decoding at the relays.

At fixed average uplink SNR, by increasing the average internode SNR, decoding at the relays becomes perfect, and at this point we can notice an outage floor. Asymptotically, at high average internode SNR, successful decoding is always possible at the

relays, and all relays are forwarding all the data to the destination. As a result, packets from different sources are transmitted through the same uplink channels. Even though performance may be good in terms of OP of a single node, it also means that when the uplink channels simultaneously fade, and when there is an outage, that outage event is experienced by all the data.

Typically in network analysis the assumption is made that errors are independent and uncorrelated. Looking at the results presented in this chapter, we immediately see that multiple data flows, even if going through multiple independent links, have correlated behaviour because of link reuse. As a result, automatic repeat requests and negative acknowledgements become correlated, and multiple links experience poor performance simultaneously. All of this contributes to the network behaving in a correlated way.

Chapter 6

Summary and discussion

With the deployment of wireless networks in industrial systems, improvements can be made in terms of control, robustness, alertness, and better integration in the business process. This thesis is an attempt to address some of the issues that typically arise in industrial wireless network design, such as low-latency and high reliability requirements. Through the utilization of cooperative diversity as one of many emerging wireless technologies, the performance of industrial wireless networks has been analysed. Several analytical and simulation models have been investigated in order to evaluate and predict performance characteristics of DF networks set in an industrial environment.

When considering propagation characteristics that include a shadowing component apart from a multipath fading, results have shown that it is the shadowing effects that are dominating, degrading performance several orders of magnitude compared to the non-shadowing case. In heavy shadowing conditions, performance has not significantly increased even by adding more cooperating nodes in the network.

Existing DF cooperative protocols that could be integrated with existing orthogonal MAC systems have been analysed, and further extended by internode protocols that improved overall network performance. These protocols, although easily implementable have shown to have a half-duplex limitation. Recent developments in wireless network coding [124, 125] have suggested transmission principles that would allow recovering some of the losses associated with half-duplex relays. Current research has pointed to the possibility of full-duplex AF and DF relaying with self-interference mitigation [46, 126]. However, some practical limitations, like errors in the side information prevent complete interference elimination obtainable in the ideal case [46].

The implementation of the internode protocol which delays transmissions to other nodes improves performance in the whole range of average uplink SNR when compared to the non-protocol case. This gain is more noticeable when the time instances of these two transmissions are independently faded. The temporal fading correlation in the internode channels has a stronger effect on performance in the low-internode and high-

uplink SNR regimes. The effects of correlation on OP are greater for larger networks. When there is a finite probability that internode links can be blocked, the diversity order of the network reduces to a single-link case, regardless of the implementation of the threshold-based protocol.

Similar to the threshold-based protocol, by implementing a SR-ARQ mechanism in internode communication, performance is improved as well. However, this mechanism requires more complexity, and each retransmission attempt induces one time-slot delay. Depending on the system design requirements, the selection of the internode protocols use can be considered as a trade-off between low-latency and communication with no data loss, depending on the data traffic type. As a consequence, a need for wireless-adapted protocols that support multimedia data types arise, which would not degrade the quality of service compared to the control traffic. By allocating equal time periods for transmission and reception, end-to-end performance is limited by the weakest hop, and therefore one can consider relaying solutions which implement buffering and/or different time-shares for data transmission and reception.

Single-node performance may not be a correct network-wise performance indicator when uplink channel is reused by multiple data flows, especially with the assumption of equal average uplink and/or internode SNRs. By having common relays, the outage events for the data coming from multiple source nodes, even if going through multiple independent paths, are correlated. Even though single-node performance can be good, it also means that when shared uplink channels simultaneously fade, and when an outage event occurs, that outage event is experienced by all the data.

Finally, the analysis presented in this thesis was limited to a small-to-medium sized network cluster with one destination node. As industrial wireless networks can have a large number of nodes, interference problems that may arise cannot be addressed solely with cooperative protocols, which have their fundamental limits, as pointed out in [127].

The benefits of cooperation can be exploited by finite-sized and partially connected network clusters, but large-scale networks cannot. Receivers can only focus on a small number of strong nearby transmitters, ignoring distant ones, leading to receiver near-sightedness and a clustered network structure. In other words, cooperation cannot change an interference-limited network to a noise-limited one [127]. Therefore, the analysis of cooperative networks should be limited to a small-to-medium sized network, which can then be considered clustered and hence noise-limited.

Other open issues include optimal node deployment, localization, security, and interoperability between different manufacturers. Furthermore, from a practical point of view, engineers need software tools for planning, configuration, and maintenance of wireless industrial networks. Opportunity for further areas of research and performance evaluation of industrial wireless networks may involve using more complex collaborative

protocols, or different technology, such as ultra wideband, MIMO techniques, cognitive radio. These are experientially significant as communication systems move towards 5G and beyond.

Appendix A

Simulation tools

Throughout the thesis, derived analytical results are confirmed by running independent simulations. This Appendix presents unified simulation tools for modelling single link wireless channels subject to fading, shadowing and AWGN. These simulators only consider first order statistics. Samples which are distributed according to a certain PDF are generated independently. Over a significantly large time period or for a large number of samples generated, these simulators produce values for average OP.

Firstly, MATLAB code is presented for plotting a histogram of the desired fading channel at normalized SNR, given in codes **A.1** and **A.2**. Afterwards, the code for OP at different average SNR values is given in **A.3** and **A.4**. When no shadowing is present, the RV which follows the Nakagami-m distribution is generated as the square root value of a Gamma-distributed RV, with fading parameter m. For the special case of $m = 1$, Rayleigh fading channel is obtained. When the channel is subject to both multipath fading and shadowing, i.e., generalized-$\mathcal{K}$ fading, the $\mathcal{K}_G$ RV is generated as a product of the square root of two independent Gamma-distributed RVs with fading and shadowing parameters given as m and k, respectively.

When plotting the histogram for the envelope and the SNR, an analytical expression is plotted for comparison as well. For OP evaluation, the generated RV is compared to a predetermined threshold, and OP is finally obtained by counting how many times the generated RV is less than the threshold.

Note that single link cases are presented in the following codes. When applying MRC, the SNR RVs are generated separately for each independent branch, and are summed afterwards, forming the combined SNR. Only then the combined SNR is compared to the threshold to obtain OP values.

All commands for generating RVs are built-in into MATLAB, and by exploiting MATLABs parallel computation over matrices, the simulation time for one point is significantly reduced when compared to a loop for all generated samples. In the thesis, simulations were performed by using a faculty computer equipped with a third genera-

tion Intel Core-i7 processor with eight threads and 32 gigabytes of RAM. For each point 10^7 RVs we generated, and the output per point is obtained on average for less than a minute.

Figure A.1 shows the PDFs of the signal envelope and received SNR, obtained analytically and with simulations (histogram), for the Nakagami-m channel for different values of the fading parameter m. In Fig. A.2, the envelope and SNR PDFs for the Generalized-$\mathcal{K}$ channel are shown, for fixed fading parameter m but different shadowing sharpness, expressed in terms of the shadowing spread σ_{SH}.

Code A.1: Histogram simulation for Nakagami-m fading channels.

```
% Nakagami-m channel - histogram
N_samp = 10^5;                              % Number of generated samples
m = 1;                                      % Fading parameter
omega = 1;                                  % Normalized power
Xsim = sqrt(gamrnd(m,omega./m,N_samp,1)); % Generating samples
% Histogram - Envelope
step = 0.1;
range = 10;
x = 0 : step : range;
[xhist,rhist] = hist(Xsim,x);               % Building histogram
xhist_norm = xhist/(step*N_samp);           % Normalizing histogram
% Plot envelope histogram
bar(rhist, xhist/((step*N_samp)), 'b', 'LineWidth', 1);
hold on
% Analytical expression
naka_en = ...
    (2*m^m.*x.^(2*m-1)/(omega^m*gamma(m))).*exp(-(m.*x.^2)/omega);
% Plot envelope analytical
plot(x,naka_en,'r-', 'LineWidth',4);
% Export
fileID = fopen('Histogram_Envelope.txt','w');
fprintf(fileID,'%6.2f %12.8f\n',[rhist; xhist_norm]);
fclose(fileID);
% Histogram - SNR
g = 0 : step : range;
SNR = omega * 1;                            % Normalized SNR
[ghist,shist] = hist(Xsim.^2,x);            % Building histogram
ghist_norm = ghist/(step*N_samp);           % Normalizing histogram
% Plot SNR histogram
figure(2)
bar(shist, ghist/((step*N_samp)), 'b', 'LineWidth', 1);
hold on
% Analytical expression
naka_snr = 1/gamma(m)*(m/SNR)^m.*g.^(m-1).*exp(-(m.*g)/SNR);
% Plot SNR analytical
plot(g,naka_snr,'r-', 'LineWidth',4);
% Export to file
fileID = fopen('Histogram_SNR.txt','w');
fprintf(fileID,'%6.2f %12.8f\n',[shist; ghist_norm]);
fclose(fileID);
```

Code A.2: Histogram simulation for Generalized-$\mathcal{K}$ fading channels.

```
% Generalized-K channel - histogram
N_samp = 10^5;                              % Number of generated samples
m = 1;                                      % Fading parameter
k = 2.557359;                               % Shadowing parameter
omega = 1;                                  % Normalized power
Xmp = sqrt(gamrnd(m,omega./m,N_samp,1)); % Generating multipath samples
Xsh = sqrt(gamrnd(k,omega./k,N_samp,1)); % Generating shadowing samples
Xsim = Xmp.*Xsh;                            % Composite envelope
% Histogram - Envelope
step = 0.1;
range = 10;
x = 0 : step : range;
[xhist,rhist] = hist(Xsim,x);               % Building histogram
xhist_norm = xhist/(step*N_samp);           % Normalizing histogram
% Plot envelope histogram
bar(rhist, xhist/((step*N_samp)), 'b', 'LineWidth', 1);
hold on
% Analytical expression
kg_en = 4.*x.^(k+m-1)*(m*k/omega)^((k+m)/2)/(gamma(m)*gamma(k)).*...
    besselk(k-m,2*sqrt(m*k/omega).*x);
% Plot envelope analytical
plot(x,kg_en,'r-', 'LineWidth',4);
% Export
fileID = fopen('Histogram_Envelope.txt','w');
fprintf(fileID,'%6.2f %12.8f\n',[rhist; xhist_norm]);
fclose(fileID);
% Histogram - SNR
g = 0 : step : range;
SNR = omega * 1;                            % Normalized SNR
[ghist,shist] = hist(Xsim.^2,x);            % Building histogram
ghist_norm = ghist/(step*N_samp);           % Normalizing histogram
% Plot SNR histogram
figure(2)
bar(shist, ghist/((step*N_samp)), 'b', 'LineWidth', 1);
hold on
% Analytical expression
kg_snr = 2*(k*m/SNR)^((k+m)/2)/(gamma(m)*gamma(k)).*g.^((k+m)/2-1).*...
    besselk(k-m,2*sqrt(k*m/SNR.*g));
% Plot SNR analytical
plot(g,kg_snr,'r-', 'LineWidth',4);
% Export
fileID = fopen('Histogram_SNR.txt','w');
fprintf(fileID,'%6.2f %12.8f\n',[shist; ghist_norm]);
fclose(fileID);
```

Code A.3: Outage probability simulatior for Nakagami-m fading channels.

```
% Nakagami-m outage probability simulator
N_samp = 10^7;                              % Number of generated samples
SNRdB = 0 : 2 : 30;                         % Values of SNR in [dB]
gTHdB = 0;                                  % Outage Threshold in [dB]
gTH = 10^(gTHdB/10);                        % Outage Threshold [linear]
% Preallocation for speed
ii_end = length(SNRdB);
nErr=zeros(1,ii_end);
op=zeros(1,ii_end);
% Fading and Shadowing parameters
m = 1;                                      % Fading parameter
omega = 1;                                  % Normalized power
for ii = 1 : ii_end                         % Length SNR vector
    SNR = 10^(SNRdB(ii)/10);                % Average SNR [linear]
    % Generating Nakagami-m fading envelope
    X = sqrt(gamrnd(m,omega./m,N_samp,1));
    g=SNR.*(X.^2);                          % SNR
    % Counting Errors
    nErr(ii) = sum(real(g < gTH) > 0);
    % Evaluation outage probability
    op(ii)=nErr(ii)/N_samp;
    % Export
    r1=fopen('SIM_OP_naka_m1.txt','at');
    fprintf(r1,'%.16g\t %.16g\n',SNRdB(ii), op(ii));
    fclose(r1);
end
% Plot outage dependence on SNR
semilogy(SNRdB, op, 'g-+', 'LineWidth', 2)
axis([0 30 1e-6 1e0])
```

Code A.4: Outage probability simulatior for Generalized-$\mathcal{K}$ fading channels.

```
% Generalized-K outage probability simulator
N_samp = 10^7;                              % Number of generated samples
SNRdB = 0 : 2 : 30;                         % Values of SNR in [dB]
gTHdB = 0;                                  % Outage Threshold in [dB]
gTH = 10^(gTHdB/10);                        % Outage Threshold [linear]
% Preallocation for speed
ii_end = length(SNRdB);
nErr=zeros(1,ii_end);
op=zeros(1,ii_end);
% Fading and Shadowing parameters
m = 1;                                      % Fading parameter
k = 2.557359;                               % Shadowing parameter
omega = 1;                                  % Normalized power
for ii = 1 : ii_end                         % Length SNR vector
    SNR = 10^(SNRdB(ii)/10);                % Average SNR [linear]
    % Generating Generalized-K fading envelope
    Xmp = sqrt(gamrnd(m,omega./m,N_samp,1));
    Xsh = sqrt(gamrnd(k,omega./k,N_samp,1));
    X = Xmp.*Xsh;
    g=SNR.*(X.^2);                          % SNR
    % Counting Errors
    nErr(ii) = sum(real(g < gTH) > 0);
    % Evaluation outage probability
    op(ii)=nErr(ii)/N_samp;
    % Export
    r1=fopen('SIM_OP_KG_m1_k255.txt','at');
    fprintf(r1,'%.16g\t %.16g\n',SNRdB(ii), op(ii));
    fclose(r1);
end
% Plot outage dependence on SNR
semilogy(SNRdB, op, 'g-+', 'LineWidth', 2)
axis([0 30 1e-6 1e0])
```

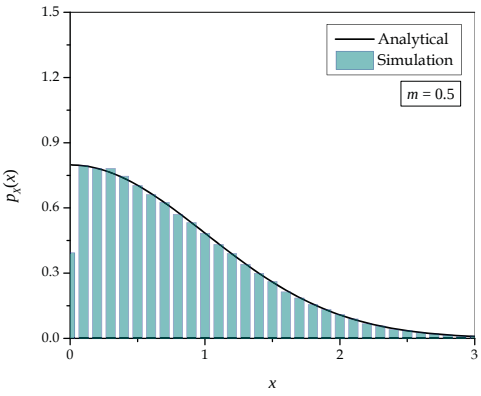

(a) Envelope histogram for $m = 0.5$.

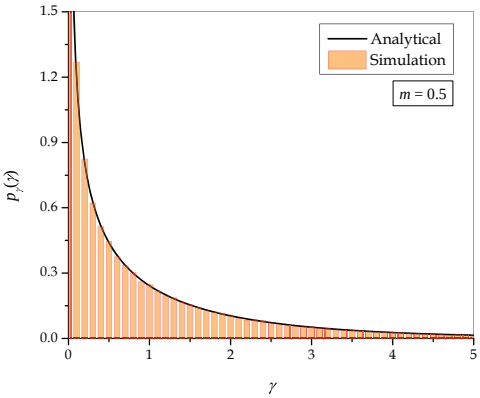

(b) SNR histogram for $m = 0.5$.

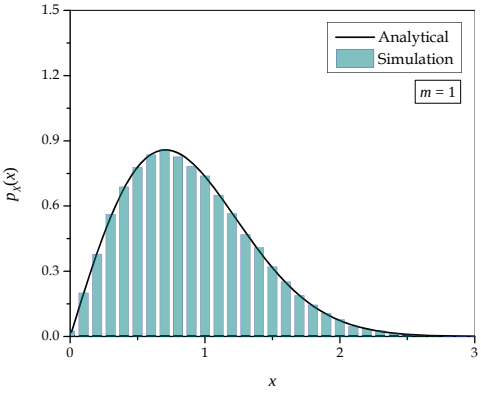

(c) Envelope histogram for $m = 1$.

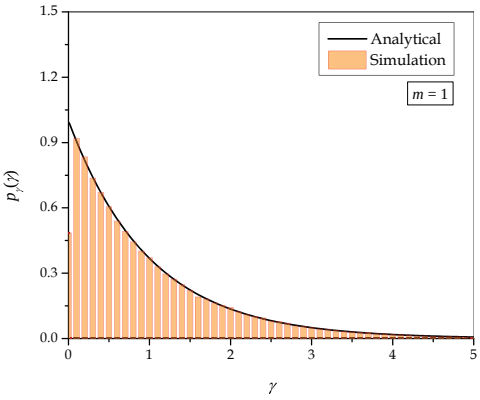

(d) SNR histogram for $m = 1$.

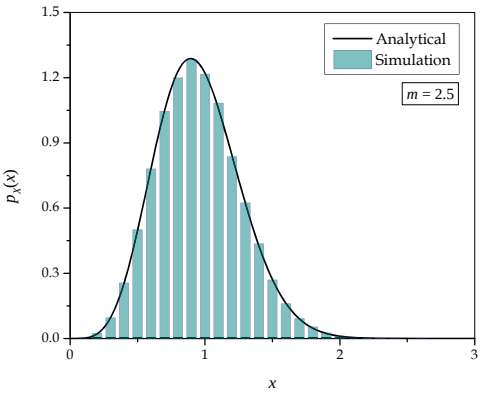

(e) Envelope histogram for $m = 2.5$.

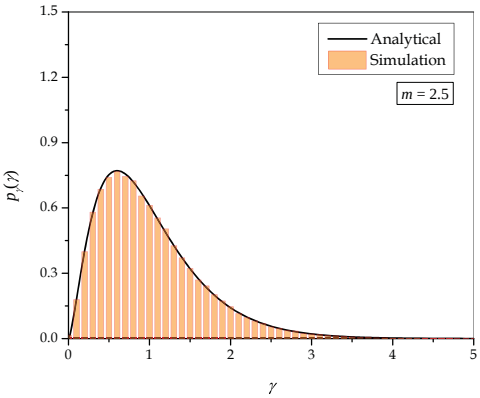

(f) SNR histogram for $m = 2.5$.

Figure A.1: Nakagami-m envelope and normalized SNR histograms.

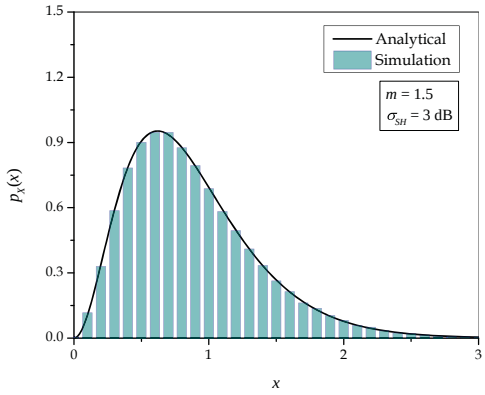

(a) Envelope histogram for $m = 1.5$ and $\sigma_{SH} = 3$ dB.

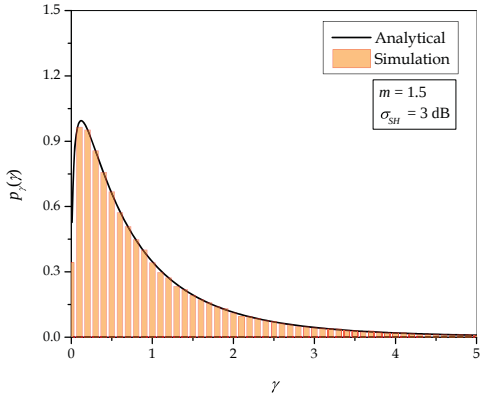

(b) SNR histogram for $m = 1.5$ and $\sigma_{SH} = 3$ dB.

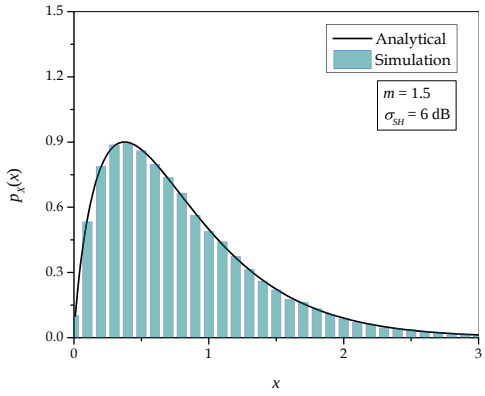

(c) Envelope histogram for $m = 1.5$ and $\sigma_{SH} = 6$ dB.

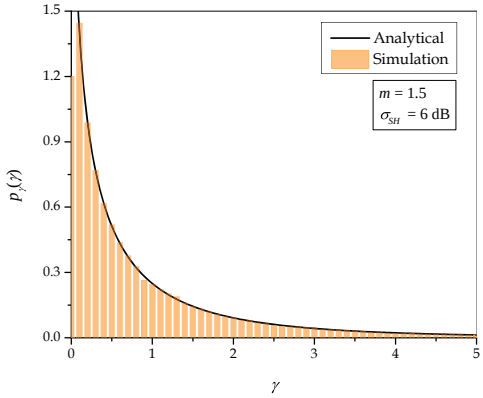

(d) SNR histogram for $m = 1.5$ and $\sigma_{SH} = 6$ dB.

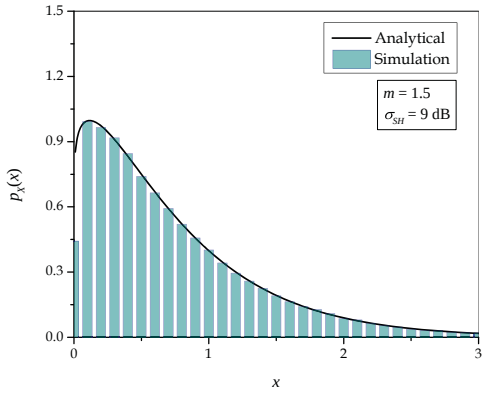

(e) Envelope histogram for $m = 1.5$ and $\sigma_{SH} = 9$ dB.

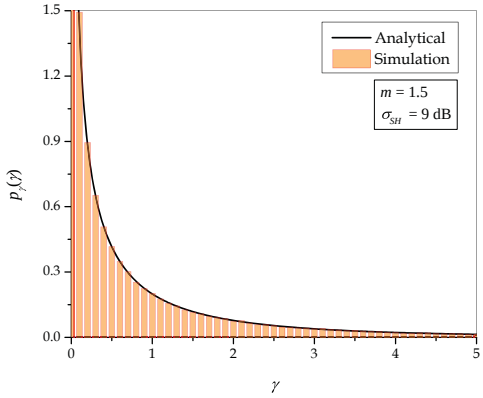

(f) SNR histogram for $m = 1.5$ and $\sigma_{SH} = 9$ dB.

Figure A.2: Generalized-$\mathcal{K}$ envelope and normalized SNR histograms.

References

[1] E. Tanghe, W. Joseph, L. Verloock, L. Martens, H. Capoen, K. V. Herwegen, and W. Vantomme, "The industrial indoor channel: large-scale and temporal fading at 900, 2400, and 5200 MHz," *IEEE Transactions on Wireless Communications*, vol. 7, no. 7, pp. 2740–2751, Jul. 2008.

[2] V. C. Gungor and G. P. Hancke, "Industrial wireless sensor networks: Challenges, design principles, and technical approaches," *IEEE Transactions on Industrial Electronics*, vol. 56, no. 10, pp. 4258–4265, Oct. 2009.

[3] V. Gungor and F. Lambert, "A survey on communication networks for electric system automation," *Computer Networks*, vol. 50, no. 7, pp. 877 – 897, May 2006.

[4] ZigBee Alliance. [Online]. Available: http://www.zigbee.org/

[5] Wireless HART. [Online]. Available: http://en.hartcomm.org/hcp/tech/wihart/wireless_overview.html

[6] S. Han, X. Zhu, A. K. Mok, D. Chen, and M. Nixon, "Reliable and real-time communication in industrial wireless mesh networks," in *Proceedings of the 17th IEEE Real-Time and Embedded Technology and Applications Symposium (RTAS)*, Chicago, IL, USA, Apr. 2011, pp. 3–12.

[7] Q. Braet, D. Plets, W. Joseph, and L. Martens, "Real-time path loss modelling for a more robust wireless performance," in *Proccidings of the 8th European Conference on Antennas and Propagation (EuCAP)*, The Hague, Netherlands, Apr. 2014, pp. 2109–2113.

[8] S. Ivanov and E. Nett, "Localization-based radio model calibration for fault-tolerant wireless mesh networks," *IEEE Transactions on Industrial Informatics*, vol. 9, no. 1, pp. 246–253, Feb. 2013.

[9] G. T. Đorđević, K. Kansanen, and A. Cvetković, "Outage performance of decode-and-forward cooperative networks over Nakagami-m fading with node blockage,"

IEEE Transactions on Wireless Communications, vol. 15, no. 9, pp. 5848–5860, Sep. 2016.

[10] P. S. Bithas, N. C. Sagias, P. T. Mathiopoulos, G. K. Karagiannidis, and A. A. Rontogiannis, "On the performance analysis of digital communications over generalized-k fading channels," *IEEE Communications Letters*, vol. 10, no. 5, pp. 353–355, May 2006.

[11] P. Shankar, "Error rates in generalized shadowed fading channels," *Wireless Personal Communications*, vol. 28, no. 3, pp. 233–238, Feb. 2004.

[12] I. M. Kostić, "Analytical approach to performance analysis for channel subject to shadowing and fading," *IEE Proceedings - Communications*, vol. 152, no. 6, pp. 821–827, Dec. 2005.

[13] B. H. Walke, S. Mangold, and L. Berlemann, *IEEE 802 wireless systems: protocols, multi-hop mesh/relaying, performance and spectrum coexistence*. John Wiley & Sons, 2007.

[14] Kateyeva, "Report on television satellite relay," *Radio Technika (in Russian)*, vol. 14, p. 67, Jan. 1959.

[15] M. Handelsman, "Performance equations for a "stationary" passive satellite relay (22,000-mile altitude) for communication," *IRE Transactions on Communications Systems*, vol. 7, pp. 31–37, May 1959.

[16] S. P. Brown and G. F. Senn, "Project score," *Proceedings of the IRE*, vol. 48, pp. 624–630, Apr. 1960.

[17] W. Hagan, "Communication by polar-orbit satellite relay," *IRE Transactions on Communications Systems*, vol. 8, pp. 250–254, Dec. 1960.

[18] F. E. Bond, C. R. Cahn, and H. F. Meyer, "Interference and channel allocation problems associated with orbiting satellite communication relays," *Proceedings of the IRE*, vol. 48, pp. 608–612, Apr. 1960.

[19] M. Dohler and Y. Li, *Cooperative communications: hardware, channel and PHY*. John Wiley & Sons, 2010.

[20] E. van der Meulen, "Transmission of information in a t-terminal discrete memoryless channel," Department of Statistics, University of California, Berkeley, CA, USA, Tech. Rep., 1968.

[21] E. van der Meulen, "Three-terminal communication channels," *Advances in applied Probability*, pp. 120–154, 1971.

[22] H. Sato, "Information transmission through a channel with Relay," The Aloha System, University of Hawaii, Honolulu, HI, USA, Tech. Rep., 1976.

[23] T. Cover and A. E. Gamal, "Capacity theorems for the relay channel," *IEEE Transactions on Information Theory*, vol. 25, no. 5, pp. 572–584, Sep. 1979.

[24] T. Cover and J. Thomas, *Elements of Information Theory*, 2nd ed. John Wiley & Sons, 2012.

[25] 3rd Generation Partnership Project, "Technical specification group radio access network; opportunity driven multiple access," 3G, Tech. Rep. 25.924 V1.0.0, 1999.

[26] T. J. Harrold and A. R. Nix, "Intelligent relaying for future personal communication systems," in *IEE Colloquium on Capacity and Range Enhancement Techniques for the Third Generation Mobile Communications and Beyond (Ref. No. 2000/003)*, Feb. 2000, pp. 9–1.

[27] T. J. Harrold and A. R. Nix, "Capacity enhancement using intelligent relaying for future personal communication systems," in *Proceeding of the 52nd IEEE Vehicular Technology Conference (VTC 2000-Fall)*, Boston, MA, USA, Sep. 2000, pp. 2115–2120.

[28] R. Wang and D. C. Cox, "A step toward ad hoc networks: can relays really improve the performance of cellular networks?" in *Proceeding of the 37th Asilomar Conference on Signals, Systems and Computers*, Pacific Grove, CA, USA, Nov. 2003, pp. 1743–1747.

[29] R. Pabst, B. H. Walke, D. C. Schultz, P. Herhold, H. Yanikomeroglu, S. Mukherjee, H. Viswanathan, M. Lott, W. Zirwas, M. Dohler, H. Aghvami, D. D. Falconer, and G. P. Fettweis, "Relay-based deployment concepts for wireless and mobile broadband radio," *IEEE Communications Magazine*, vol. 42, no. 9, pp. 80–89, Sep. 2004.

[30] A. Sendonaris, E. Erkip, and B. Aazhang, "Increasing uplink capacity via user cooperation diversity," in *Proceedings of the 1998 IEEE International Symposium on Information Theory (ISIT)*, Cambridge, MA, USA, Aug. 1998, p. 156.

[31] A. Sendonaris, E. Erkip, and B. Aazhang, "User cooperation diversity. Part I. system description," *IEEE Transactions on Communications*, vol. 51, no. 11, pp. 1927–1938, Nov. 2003.

[32] A. Sendonaris, E. Erkip, and B. Aazhang, "User cooperation diversity. Part II. implementation aspects and performance analysis," *IEEE Transactions on Communications*, vol. 51, no. 11, pp. 1939–1948, Nov. 2003.

[33] J. N. Laneman and G. W. Wornell, "Energy-efficient antenna sharing and relaying for wireless networks," in *Proceeding of the 2000 IEEE Wireless Communications and Networking Confernce (WCNC)*, Chicago, IL, USA, Sep. 2000, pp. 7–12.

[34] J. N. Laneman, G. W. Wornell, and D. Tse, "An efficient protocol for realizing cooperative diversity in wireless networks," in *Proceedings of the 2001 IEEE International Symposium on Information Theory (ISIT)*, Washington, D.C., USA, Jun. 2001, p. 294.

[35] J. Laneman, "Cooperative diversity in wireless networks: Algorithms and architectures," Ph.D. dissertation, MIT, 2002.

[36] J. Laneman, D. Tse, and G. W. Wornell, "Cooperative diversity in wireless networks: Efficient protocols and outage behavior," *IEEE Transactions on Information Theory*, vol. 50, no. 12, pp. 3062–3080, Dec. 2004.

[37] X. Li, Y. C. Wu, and E. Serpedin, "Timing synchronization in decode-and-forward cooperative communication systems," *IEEE Transactions on Signal Processing*, vol. 57, no. 4, pp. 1444–1455, Apr. 2009.

[38] Y. Yao and X. Dong, "Low-complexity timing synchronization for decode-and-forward cooperative communication systems with multiple relays," *IEEE Transactions on Vehicular Technology*, vol. 62, no. 6, pp. 2865–2871, Jul. 2013.

[39] L. Zheng and D. N. C. Tse, "Diversity and multiplexing: a fundamental tradeoff in multiple-antenna channels," *IEEE Transactions on Information Theory*, vol. 49, no. 5, pp. 1073–1096, May 2003.

[40] X. Bao and J. Li, "Decode-amplify-forward (DAF): a new class of forwarding strategy for wireless relay channels," in *Proceedings of the 6th IEEE Workshop on Signal Processing Advances in Wireless Communications (SPAWC)*, New York, NY, USA, Jun. 2005, pp. 816–820.

[41] X. Bao and J. Li, "Efficient message relaying for wireless user cooperation: Decode-amplify-forward (DAF) and hybrid DAF and coded-cooperation," *IEEE Transactions on Wireless Communications*, vol. 6, no. 11, pp. 3975–3984, Nov. 2007.

[42] B. Nazer and M. Gastpar, "Compute-and-forward: Harnessing interference through structured codes," *IEEE Transactions on Information Theory*, vol. 57, no. 10, pp. 6463–6486, Oct. 2011.

[43] S. N. Hong and G. Caire, "Compute-and-forward strategies for cooperative distributed antenna systems," *IEEE Transactions on Information Theory*, vol. 59, no. 9, pp. 5227–5243, Sep. 2013.

[44] T. Riihonen, S. Werner, and R. Wichman, "Hybrid full-duplex/half-duplex relaying with transmit power adaptation," *IEEE Transactions on Wireless Communications*, vol. 10, no. 9, pp. 3074–3085, Jul. 2011.

[45] H. Ju, E. Oh, and D. Hong, "Improving efficiency of resource usage in two-hop full duplex relay systems based on resource sharing and interference cancellation," *IEEE Transactions on Wireless Communications*, vol. 8, no. 8, pp. 3933–3938, Aug. 2009.

[46] T. Riihonen, S. Werner, and R. Wichman, "Mitigation of loopback self-interference in full-duplex MIMO relays," *IEEE Transactions on Signal Processing*, vol. 59, no. 12, pp. 5983–5993, Dec 2011.

[47] I. Krikidis, H. A. Suraweera, P. J. Smith, and C. Yuen, "Full-duplex relay selection for amplify-and-forward cooperative networks," *IEEE Transactions on Wireless Communications*, vol. 11, no. 12, pp. 4381–4393, Dec. 2012.

[48] M. Khafagy, A. Ismail, M.-S. Alouini, and S. Aissa, "On the outage performance of full-duplex selective decode-and-forward relaying," *IEEE Communications Letters*, vol. 17, no. 6, pp. 1180–1183, Jun. 2013.

[49] E. Antonio-Rodríguez, R. López-Valcarce, T. Riihonen, S. Werner, and R. Wichman, "Adaptive self-interference cancellation in wideband full-duplex decode-and-forward MIMO relays," in *Proceeding of the 14th IEEE Workshop on Signal Processing Advances in Wireless Communications (SPAWC)*, Darmstadt, Germany, Jun. 2013, pp. 370–374.

[50] I. Chatzigeorgiou, W. Guo, I. J. Wassell, and R. Carrasco, "Packet error probability for decode-and-forward cooperative networks of selfish users," in *Proceedings of the 10th International Symposium on Communication Theory and Applications (ISCTA)*, Ambleside, UK, Jul. 2009, pp. –.

[51] I. Chatzigeorgiou, W. Guo, I. J. Wassell, and R. Carrasco, "Error probability analysis of unselfish cooperation over quasi-static fading channels," in *Proceedings*

of the 71st IEEE Vehicular Technology Conference (VTC 2010-Spring), Taipei, Taiwan, May 2010, pp. 1–5.

[52] I. Chatzigeorgiou, W. Guo, I. J. Wassell, and R. Carrasco, "Exact and asymptotic outage probability analysis for decode-and-forward networks," *IEEE Transactions on Communications*, vol. 59, no. 2, pp. 376–381, Feb. 2011.

[53] A. Cvetković, K. Kansanen, and G. T. Đorđević, "Outage analysis for uncoordinated decode-and-forward networks over Nakagami-m channels," in *Proceedings of the 20th Telecommunications Forum (TELFOR)*, Belgrade, Serbia, Nov. 2012, pp. 490–493.

[54] S. S. Ikki and M. H. Ahmed, "Performance analysis of adaptive decode-and-forward cooperative diversity networks with best-relay selection," *IEEE Transactions on Communications*, vol. 58, no. 1, pp. 68–72, Jan. 2010.

[55] S. S. Ikki and M. H. Ahmed, "Performance analysis of cooperative diversity with incremental-best-relay technique over Rayleigh fading channels," *IEEE Transactions on Communications*, vol. 59, no. 8, pp. 2152–2161, Aug. 2011.

[56] G. Yu, Z. Zhang, and P. Qiu, "Cooperative ARQ in wireless networks: Protocols description and performance analysis," in *Proceedings of the 2006 IEEE International Conference on Communications (ICC 2006)*, Istanbul, Turkey, Jun. 2006, pp. 3608–3614.

[57] S. Atan and U. Aygölü, "Novel protocols for cooperative wireless networks with common destination," in *Proceedings of the 2015 European Conference on Networks and Communications (EuCNC)*, Paris, France, Jun. 2015, pp. 67–71.

[58] A. S. Salim, H. Ali, and M. Kousa, "ARQ-based scheme for coded wireless cooperative communications," in *Proceedings of the 9th International Wireless Communications and Mobile Computing Conference (IWCMC)*, Sardinia, Italy, Jul. 2013, pp. 355–360.

[59] V. Stanković, A. Host-Madsen, and Z. Xiong, "Cooperative diversity for wireless ad hoc networks," *IEEE Signal Processing Magazine*, vol. 23, no. 5, pp. 37–49, Sep. 2006.

[60] X. Yang, L. Liu, N. H. Vaidya, and F. Zhao, "A vehicle-to-vehicle communication protocol for cooperative collision warning," in *Proceedings of the First Annual International Conference on Mobile and Ubiquitous Systems: Networking and Services (MOBIQUITOUS)*, Cambridge, MA, USA, Aug. 2004, pp. 114–123.

[61] M. Guo, M. H. Ammar, and E. W. Zegura, "V3: a vehicle-to-vehicle live video streaming architecture," in *Proceedings of the Third IEEE International Conference on Pervasive Computing and Communications (PerCom)*, Los Alamitos, CA, USA, Mar. 2005, pp. 171–180.

[62] L. Weixin, W. Ning, Z. Zhongpei, L. Shaoqian, and J. Na, "The differential detection OFDM cooperative diversity system in vehicle-to-vehicle communications," in *Proceedings of the 6th International Conference on ITS Telecommunications*, Chengdu, China, Jun. 2006, pp. 1118–1121.

[63] F. Ye, M. Adams, and S. Roy, "V2V wireless communication protocol for rear-end collision avoidance on highways," in *Proceedings of the 2008 IEEE ICC Workshops*, Beijing, China, May 2008, pp. 375–379.

[64] H. Ilhan, I. Altunbas, and M. Uysal, "Performance analysis and optimization of relay-assisted vehicle-to-vehicle (V2V) cooperative communication," in *Proceedings of the 16th IEEE Signal Processing, Communication and Applications Conference (SIU)*, Aydın, Turkey, Apr. 2008, pp. 1–4.

[65] M. Uysal, Z. Ghassemlooy, A. Bekkali, A. Kadri, and H. Menouar, "Visible light communication for vehicular networking: Performance study of a V2V system using a measured headlamp beam pattern model," *IEEE Vehicular Technology Magazine*, vol. 10, no. 4, pp. 45–53, Dec. 2015.

[66] I. F. Akyildiz, W. Su, Y. Sankarasubramaniam, and E. Cayirci, "A survey on sensor networks," *IEEE Communications Magazine*, vol. 40, no. 8, pp. 102–114, Aug. 2002.

[67] K. S. J. Pister, "Smart dust-hardware limits to wireless sensor networks," in *Proceedings of the 23rd Conference on Distributed Computing Systems, (ICDCS)*, Providence, RI, USA, May 2003, p. 2.

[68] K. Xu, H. Hassanein, G. Takahara, and Q. Wang, "Relay node deployment strategies in heterogeneous wireless sensor networks: single-hop communication case," in *Proceedings of the 2005 IEEE Global Telecommunications Conference (GLOBECOM)*, St. Louis, MO, USA, Nov. 2005.

[69] M. Dohler, A. Gkelias, and A. H. Aghvami, "Capacity of distributed PHY-layer sensor networks," *IEEE Transactions on Vehicular Technology*, vol. 55, no. 2, pp. 622–639, Mar. 2006.

[70] J. Kim and W. Lee, "Cooperative relaying strategies for multi-hop wireless sensor networks," in *Procedding of the 3rd Internation Conference on Communication Systems Software and Middleware and Workshops*, Bangalore, India, Jan. 2008, pp. 103–106.

[71] M. K. Simon and M.-S. Alouini, *Digital communication over fading channels*, 2nd ed. John Wiley & Sons, 2005.

[72] D. Tse and P. Viswanath, *Fundamentals of wireless communication*. Cambridge University Press, 2005.

[73] A. Aragon-Zavala, *Antennas and propagation for wireless communication systems*. John Wiley & Sons, 2008.

[74] T. Bai, R. Vaze, and R. W. Heath, "Using random shape theory to model blockage in random cellular networks," in *Proceedings of the 2012 International Conference on Signal Processing and Communications (SPCOM)*, Bangalore, India, Jul. 2012, pp. 1–5.

[75] J. Choi, "On the macro diversity with multiple BSs to mitigate blockage in millimeter-Wave communications," *IEEE Communications Letters*, vol. 18, no. 9, pp. 1653–1656, Sep. 2014.

[76] A. Papoulis and S. U. Pillai, *Probability, random variables, and stochastic processes*. McGraw-Hill, 2002.

[77] Z. Wang and G. B. Giannakis, "A simple and general parameterization quantifying performance in fading channels," *IEEE Transactions on Communications*, vol. 51, no. 8, pp. 1389–1398, Aug. 2003.

[78] G. L. Stüber, *Principles of mobile communication*. Springer, 2011.

[79] M. Nakagami, "The m-distribution – A general formula of intensity distribution of rapid fading," *Statistical Method of Radio Propagation*, 1960.

[80] I. Gradshteyn and I. Ryzhik, *Table of Integrals, Series, and Products*, 5th ed. Academic Press, 1994.

[81] F. Hansen and F. I. Meno, "Mobile fading – rayleigh and lognormal superimposed," *IEEE Transactions on Vehicular Technology*, vol. 26, no. 4, pp. 332–335, Nov. 1977.

[82] H. Suzuki, "A statistical model for urban multipath channels with random delay," *IEEE Transactions on Communications*, vol. 25, pp. 673–680, Jul. 1977.

[83] G. L. Turin, F. D. Clapp, T. L. Johnston, S. B. Fine, and D. Lavry, "A statistical model of urban multipath propagation," *IEEE Transactions on Vehicular Technology*, vol. 21, no. 1, pp. 1–9, Feb. 1972.

[84] H. Hashemi, "Simulation of the urban radio propagation channel," *IEEE Transactions on Vehicular Technology*, vol. 28, no. 3, pp. 213–225, Aug. 1979.

[85] T. S. Rappaport, S. Y. Seidel, and K. Takamizawa, "Statistical channel impulse response models for factory and open plan building radio communicate system design," *IEEE Transactions on Communications*, vol. 39, no. 5, pp. 794–807, May 1991.

[86] P. Yegani and C. D. McGillem, "A statistical model for the factory radio channel," *IEEE Transactions on Communications*, vol. 39, no. 10, pp. 1445–1454, Oct. 1991.

[87] H. Hashemi, "Impulse response modeling of indoor radio propagation channels," *IEEE journal on selected areas in communications*, vol. 11, no. 7, pp. 967–978, Sep. 1993.

[88] A. Abdi and M. Kaveh, "K distribution: an appropriate substitute for Rayleigh-lognormal distribution in fading-shadowing wireless channels," *Electronics Letters*, vol. 34, no. 9, pp. 851–852, Apr. 1998.

[89] P. M. Shankar, "Outage probabilities of a MIMO scheme in shadowed fading channels with micro- and macrodiversity reception," *IEEE Transactions on Wireless Communications*, vol. 7, no. 6, pp. 2015–2019, Jun. 2008.

[90] N. D. Chatzidiamantis and G. K. Karagiannidis, "On the distribution of the sum of gamma-gamma variates and applications in RF and optical wireless communications," *IEEE Transactions on Communications*, vol. 59, no. 5, pp. 1298–1308, May 2011.

[91] The wolfarm functions site. [Online]. Available: http://functions.wolfram.com/

[92] I. M. Kostić, "A method for error rate analysis in the presence of rapid and slow fading," in *Proceedings of th 46th Conference on electronic engineering, Telecommunications, Computer Science, Automation and Nuclear Technology (ETRAN)*, Banja Vrućica - Teslić, Bosnia and Herzegovina, Jun. 2002, pp. 62–64.

[93] N. Zdravković, J. Anastasov, and G. T. Đorđević, "Outage capacity analysis of Generalized-$\mathcal{K}$ fading channels," in *Proceedings of th 58th Conference on electronic engineering, Telecommunications, Computer Science, Automation and Nuclear Technology (ETRAN)*, Vrnjačka Banja, Serbia, Jun. 2014, pp. TE1.8 1–4.

[94] C. Xiao, Y. R. Zheng, and N. C. Beaulieu, "Novel sum-of-sinusoids simulation models for Rayleigh and Rician fading channels," *IEEE Transactions on Wireless Communications*, vol. 5, no. 12, pp. 3667–3679, Dec. 2006.

[95] D. D. Patil, "On the simulations of correlated Nakagami-m fading channels using sum-of-sinusoids method," Ph.D. dissertation, University of Missouri–Columbia, 2006.

[96] F. Yilmaz and M.-S. Alouini, "A new simple model for composite fading channels: Second order statistics and channel capacity," in *Proceedings of 7th International Symposium on Wireless Communication Systems (ISWCS)*, York, England, Sep. 2010, pp. 676–680.

[97] H. Soury, F. Yilmaz, and M.-S. Alouini, "Average bit error probability of binary coherent signaling over generalized fading channels subject to additive generalized gaussian noise," *IEEE Communications Letters*, vol. 16, no. 6, pp. 785–788, Jun. 2012.

[98] J. Anastasov, N. Zdravković, and G. T. Đorđević, "Outage capacity evaluation of extended generalized-$\mathcal{K}$ fading channel in the presence of random blockage," *Journal of the Franklin Institute*, vol. 352, no. 10, pp. 4610–4623, Oct. 2015.

[99] M. A. Chaudhry and S. M. Zubair, *On a class of incomplete Gamma functions with applications*. CRC Press, 2001.

[100] N. Zdravković, "Packet error rate of decode-and-forward cooperative wireless networks over composite fading channels," in *Proceedings of th 12th International Conference on Applied Electromagnetics (PES)*, Niš, Serbia, Aug. 2015, pp. –.

[101] N. Zdravković, "Outage analysis in clustered cooperative networks over $\mathcal{K}$ fading channels," in *Proceedings of the 23rd Telecommunications Forum (TELFOR)*, Belgrade, Serbia, Nov. 2015, pp. 95–98.

[102] N. Zdravković, "Outage analysis of clustered cooperative networks in generalized fading and shadowing," *TELFOR Journal*, vol. 8, no. 2, pp. 81–86, 2016.

[103] N. Zdravković, A. Cvetković, G. T. Đorđević, and K. Kansanen, "Outage probability of decode-and-forward network with threshold based protocol over Rayleigh fading," in *Proceedings of the 21st Telecommunications Forum (TELFOR)*, Belgrade, Serbia, Nov. 2013, pp. 315–318.

[104] N. Zdravković, A. Cvetković, K. Kansanen, and G. T. Đorđević, "Outage performance of low-latency decode-and-forward cooperative wireless networks,"

EURASIP Journal on Wireless Communications and Networking, vol. 2016, no. 1, pp. 1–10, 2016.

[105] N. Zdravković and A. Cvetković, "Packet error rate analysis of decode-and-forward wireless networks with internode SR-ARQ protocols," in *Proceedings of 12th International Conference on Telecommunication in Modern Satellite, Cable and Broadcasting Services (TELSIKS)*, Niš, Serbia, Oct. 2015, pp. 39–42.

[106] N. Zdravković, K. Kansanen, and G. T. Đorđević, "On the outage correlation analysis of decode-and-forward cooperative wireless networks," *IEEE Transactions on Wireless Communications (under review)*, 2016.

[107] N. Zdravković, "Outage analysis of low-latency cooperative wireless networks with threshold-based protocol over composite fading," *Facta Universitatis, series Automatic Control and Robotics*, vol. 16, no. 1, pp. 37–48, 2017.

[108] N. Zdravković, M. Petković, G. T. Đorđević, and K. Kansanen, "Outage analysis of mixed FSO/WiMAX link," *IEEE Photonics Journal*, vol. 8, no. 1, pp. 1–14, Feb. 2016.

[109] N. Zdravković, A. Cvetković, D. Milić, and G. T. Đorđević, "Packet error rate analysis of decode-and-forward free-space optical cooperative networks in the presence of random link blockage," *Journal of Modern Optics (Accepted, available online)*, 2017.

[110] A. Cvetković, J. Anastasov, and N. Zdravković, "Outage performance of satellite-terrestrial multiuser networks with fixed gain AF relay," in *Proceedings of LI International Scientific Conference on Information, Communication and Energy Systems and Technologies (ICEST)*, Ohrid, FYR of Macedonia, Jun. 2016, pp. 131–134.

[111] I. Chatzigeorgiou, I. J. Wassell, and R. Carrasco, "On the frame error rate of transmission schemes on quasi-static fading channels," in *Proceedings of the 42nd Annual Conference on Information Sciences and Systems, (CISS)*, Princeton, NJ, USA, Mar. 2008, pp. 577–581.

[112] I. Chatzigeorgiou, I. J. Wassell, and R. Carrasco, "Threshold-based frame error rate analysis of mimo systems over quasistatic fading channels," *Electronics Letters*, vol. 45, no. 4, pp. 216–217, Feb. 2009.

[113] A. A. Abu-Dayya and N. C. Beaulieu, "Analysis of switched diversity systems on generalized-fading channels," *IEEE Transactions on Communications*, vol. 42, no. 11, pp. 2959–2966, Nov. 1994.

[114] J. Proakis, *Digital Communications*, 4th ed. McGraw-Hill, 2001.

[115] T. S. Rappaport, *Wireless communications: principles and practice*. Prentice Hall, 1996.

[116] T.-D. Chiueh and P.-Y. Tsai, *OFDM baseband receiver design for wireless communications*. John Wiley & Sons, 2008.

[117] Q. Liu, S. Zhou, and G. B. Giannakis, "Cross-layer combining of adaptive modulation and coding with truncated arq over wireless links," *IEEE Transactions on Wireless Communications*, vol. 3, no. 5, pp. 1746–1755, Sep. 2004.

[118] Y. Xi, A. Burr, J. Wei, and D. Grace, "A general upper bound to evaluate packet error rate over quasi-static fading channels," *IEEE Transactions on Wireless Communications*, vol. 10, no. 5, pp. 1373–1377, May 2011.

[119] P. Ferrand, J.-M. Gorce, and C. Goursaud, "Approximations of the packet error rate under quasi-static fading in direct and relayed links," *EURASIP Journal on Wireless Communications and Networking*, vol. 2015, no. 1, pp. 1–12, Jan. 2015.

[120] M. R. D. Rodrigues, I. Chatzgeorgiou, I. J. Wassell, and R. Carrasco, "On the performance of turbo codes in quasi-static fading channels," in *Proceedings of the 2005 International Symposium on Information Theory (ISIT)*, Adelaide, Australia, Sep. 2005, pp. 622–626.

[121] K. Wu and J. Harms, "Performance study of a multipath routing method for wireless mobile ad hoc networks," in *Proceedings of the 9th International Symposium on Modeling, Analysis and Simulation of Computer and Telecommunication Systems (MASCOTS)*, Cincinnati, OH, USA, Aug. 2001, pp. 99–107.

[122] E. P. C. Jones, M. Karsten, and P. A. S. Ward, "Multipath load balancing in multihop wireless networks," in *Proceedings of the 2005 IEEE International Conference on Wireless And Mobile Computing, Networking And Communications (WiMob)*, vol. 2, Montreal, Canada, Aug. 2005, pp. 158–166.

[123] D. E. Quevedo, A. Ahlen, and K. H. Johansson, "State estimation over sensor networks with correlated wireless fading channels," *IEEE Transactions on Automatic Control*, vol. 58, no. 3, pp. 581–593, Mar. 2013.

[124] S. Katti, H. Rahul, W. Hu, D. Katabi, M. Medard, and J. Crowcroft, "Xors in the air: Practical wireless network coding," *IEEE/ACM Transactions on Networking*, vol. 16, no. 3, pp. 497–510, Jun. 2008.

[125] C. D. T. Thai, P. Popovski, M. Kaneko, and E. de Carvalho, "Multi-flow scheduling for coordinated direct and relayed users in cellular systems," *IEEE Transactions on Communications*, vol. 61, no. 2, pp. 669–678, Feb. 2013.

[126] F. Boccardi, R. W. Heath, A. Lozano, T. L. Marzetta, and P. Popovski, "Five disruptive technology directions for 5G," *IEEE Communications Magazine*, vol. 52, no. 2, pp. 74–80, Feb. 2014.

[127] A. Lozano, R. W. Heath, and J. G. Andrews, "Fundamental limits of cooperation," *IEEE Transactions on Information Theory*, vol. 59, no. 9, pp. 5213–5226, Sep. 2013.